5-2018

Understanding the Evolution of Surface Texture Under Boundary Lubrication

Salil T. Bapat
University of Arkansas, Fayetteville

Understanding the Evolution of Surface Texture Under Boundary Lubrication

A dissertation submitted in partial fulfillment
of the requirements for the degree of
Doctor of Philosophy in Microelectronics-Photonics

by

Salil Bapat
Indian Institute of Technology, Kanpur
Bachelor of Technology in Materials and Metallurgical Engineering, 2007
University of Minnesota
Master of Science in Materials Science and Engineering, 2011

May 2018
University of Arkansas

This dissertation is approved for recommendation to the Graduate Council.

Ajay P. Malshe, PhD
Dissertation Director

Greg Salamo, PhD
Committee Member

Douglas Spearot, PhD
Committee Member

Z. Ryan Tian, PhD
Committee Member

Arun Nair, PhD
Committee Member

Rick Wise, PhD
Ex-Officio Member

The following signatories attest that all software used in this dissertation was legally licensed for use by Salil Bapat for research purposes and publication.

_____ _____

Salil Bapat, Student Dr. Ajay P. Malshe, Dissertation Director

This dissertation was submitted to http://www.turnitin.com for plagiarism review by the TurnItIn company's software. The signatories have examined the report on this dissertation that was returned by TurnItIn and attest that, in their opinion, the items highlighted by the software are incidental to common usage and are not plagiarized material.

_____ _____

Dr. Rick Wise, Program Director Dr. Ajay P. Malshe, Dissertation Director

Abstract

The objective of this research was to understand the evolution of surface texture under boundary/mixed lubrication (BL). Significant material/energy losses occur during BL because of direct contact between the two surfaces. Traditionally, tribofilms have been studied extensively for BL while textures have been used as a static engineering design parameter to enhance lubricant film properties. However, texture is dynamic at the tribological mating interface, where both physical and chemical interactions are continuously modulated. The evolution and the interplay between the tribofilm and texture is least studied in the literature, which is the focus of this research.

MoS_2-based lubricants, known for their excellent anti-friction and anti-wear performance [1]–[3], were used during the experiments. The experiments were divided into two parts; 1) polished steel discs were used to study directed organization/re-organization of surface asperities in correlation with tribofilm; 2) textured discs were used to study the effect of artificial texture on manipulation of tribofilm properties. Three stages of lubrication evolution, namely break-in, development, and steady-state, were discovered and studied experimentally. Surface texture was characterized using laser scanning microscope. Tribofilm morphology and chemistry was studied using scanning and transmission electron microscopy and Raman spectroscopy.

The results showed that the surface roughness increases during break-in period and then stabilizes. Addition of directional texture results in early onset and stabilization of tribo-chemical reactions. Raman spectra confirmed presence of MoS_2, FeS_2, Fe_2O_3, and molybdate compounds, consistent with previous studies. [3] Cross-sectional TEM images revealed presence of stored lubricant in valleys while delivering lamellar tribo-layer on asperities.

From the results, the following lubrication mechanism was discussed. Initially, during the break-in period, contact between mating surfaces results in re-organization/re-alignment surface asperities under the applied load and directional motion. Creation of fresh asperities in the presence of lubricant along with energy dissipation is responsible for the onset of tribo-chemical reactions. Subsequently, during the development stage, progressing reactions between surface asperities and lubricant lead to formation and stabilization of tribofilm. Eventually, in the steady-state, stabilized texture and tribofilm results in stable lubrication response. The findings of this research will benefit heavy-duty industrial applications involving low-speed, high-load conditions.

Acknowledgements

First, I would like to thank my adviser Dr. Ajay P. Malshe for giving me the opportunity to work on this project. I also want to acknowledge the support and valuable guidance he provided at each stage of this research experience as well for the mentorship in making me a well-rounded researcher, teacher, and a better person. I also want to acknowledge the help and support provided by Dr. Greg Salamo, Dr. Doug Spearot, Dr. Ryan Tian and Dr. Arun Nair as part of my dissertation committee.

I want to thank my wife Vaibhavi for her love and support, tolerating me through my idiosyncrasies absent-minded behavior and for being a continuous motivator. I also want to thank my parents, my sister, my in-laws, my extended family, and relatives for their impactful role in my life, continuous support, and for being a constant source of motivation. I could not have done it without their love and guidance all through this eventful journey.

I am grateful to have some wonderful friends throughout my academic journey. I want to acknowledge their contributions in making me the person I am today. Thank you so much Gayatri, Anand, Charu, Shashank, and the whole IIT Kanpur friends circle. Before I came to the University of Arkansas for my doctoral studies, I was fortunate enough to spend some wonderful years in company and support of my friends in Minnesota. I want to thank Dk, Ajay, Nikhil, Sudarshan, Madhura, Salil, Purva, Esha, Rahul, Sajal, Neha, Raghav, Siddharth, Erika, Nachiket, and others for getting me acclimatized to the US culture and pulling me through all the snow-filled winters. I want to thank and acknowledge my friends and MicroEP colleagues at Arkansas including Shilpi, Cedric, and Hulusi for all their help. I also would like to thank all the members of ICT at the International Students and Scholar office especially Cynthia Smith for giving me the opportunity to be a part of a multi-cultural team.

I want to acknowledge the continuous support and guidance of MicroEP community especially Ms. Renee Jones-Hearon, Prof. Ken Vickers and Dr. Rick Wise for their valuable help. I want to thank the administrative help and assistance from Nano Institute and Mechanical Engineering staff including Ms. Melynda Hart, Ms. Sunny Robinson, and Ms. Kathy Kirk. I also want to thank Mr. Ben Fleming from the mechanical engineering machine shop for his help in preparation and processing of materials/tools used in the experiments during this research.

Last but not the least, I want to thank my colleagues and co-workers at Materials and Manufacturing Research Labs for their valuable inputs through the research work. I want to specifically thank Dr. Wenyang Zhang and Dr. Parash Kalita for tremendous help and support, not only for helping with my research but also for all the help provided during last five years outside of the lab in Fayetteville.

I want to acknowledge support from Arkansas Nano-Bio Characterization facility for the characterization equipment used for this research. I want to thank Dr. Mourad Benamara for training, support, and help with TEM sample preparation and imaging. This research would not have been complete without the equipment and facilities at University of Arkansas. I would like to thank Dr. Min Zou for access to the Keyence VK-X 250 laser microscope used in this research.

Funding for this research was provided by the Center for Advanced Surface Engineering, under the National Science Foundation Grant No. OIA-1457888 and the Arkansas EPSCoR Program, ASSET III. Any opinions, findings, and conclusions or recommendations expressed in this material are those of the author(s) and do not necessarily reflect the views of the National Science Foundation

Table of Contents

List of Figures

List of Tables

1. INTRODUCTION AND BACKGROUND

A. Industrial Importance of Friction and Lubrication

Machines are a critical part of modern technological life cycle from mining, manufacturing, transportation, operation and up to the disposal stage. Most machines rely on moving parts necessary to transfer input energy to productive output. However, part of the input energy is consumed in overcoming the friction between the moving parts. It was estimated that friction related losses consume about 33% of fuel in a passenger car and about 38% of input energy in mining equipment. [4], [5] In addition to frictional losses, undesirable material losses (called wear), and in some cases corrosion, also occur due to repeated contact between the mating surfaces and improper lubrication. Significant wear or corrosive damage to the parts can lead to premature failure, production downtime, and additional repair and replacement costs. A recent report estimates that friction and wear losses in tribological contacts consume about 23% of world's total energy. [6] With advancement in technology, increasing global demands, and limited fossil resources, reducing frictional losses can thus be regarded as a key step in conserving energy and efficient use of resources. Designing better and more effective lubrication strategies is thus critical to reduce frictional and material losses in industrial machinery.

Over the last few decades, effective lubrication strategies have been proposed and developed by using advanced lubricants as well as by using textured surfaces. However, the role and evolution of surface texture in conjunction with advanced lubricants is yet to be studied. This research was aimed toward providing fundamental understanding of evolution of surface texture and its role in governing and manipulating the lubricant film dynamics. Following subsections provide brief introduction of lubrication regimes, boundary lubrication challenges, surface modifications, and research hypotheses.

B. Fundamentals of Lubrication

Lubricants are substances introduced between moving components to reduce friction. Typically, the lubricants (solid, liquid or gaseous layers) have low shear strength that facilitates smooth sliding motion. [7] Both natural and synthetic oils are used as lubricants in a variety of industrial applications. The efficiency of such fluid lubricants typically depends on rheological properties of lubricants (viscosity, η) and operating conditions including load (N), speed (P_{av}) and temperature. With variations in operating conditions, the thickness of fluid film (h) also changes resulting in alteration of the associated frictional response which is represented by different lubrication regimes as shown in Figure 1.1 (Stribeck curve). A Stribeck curve is typically divided into following three main lubrication regimes:

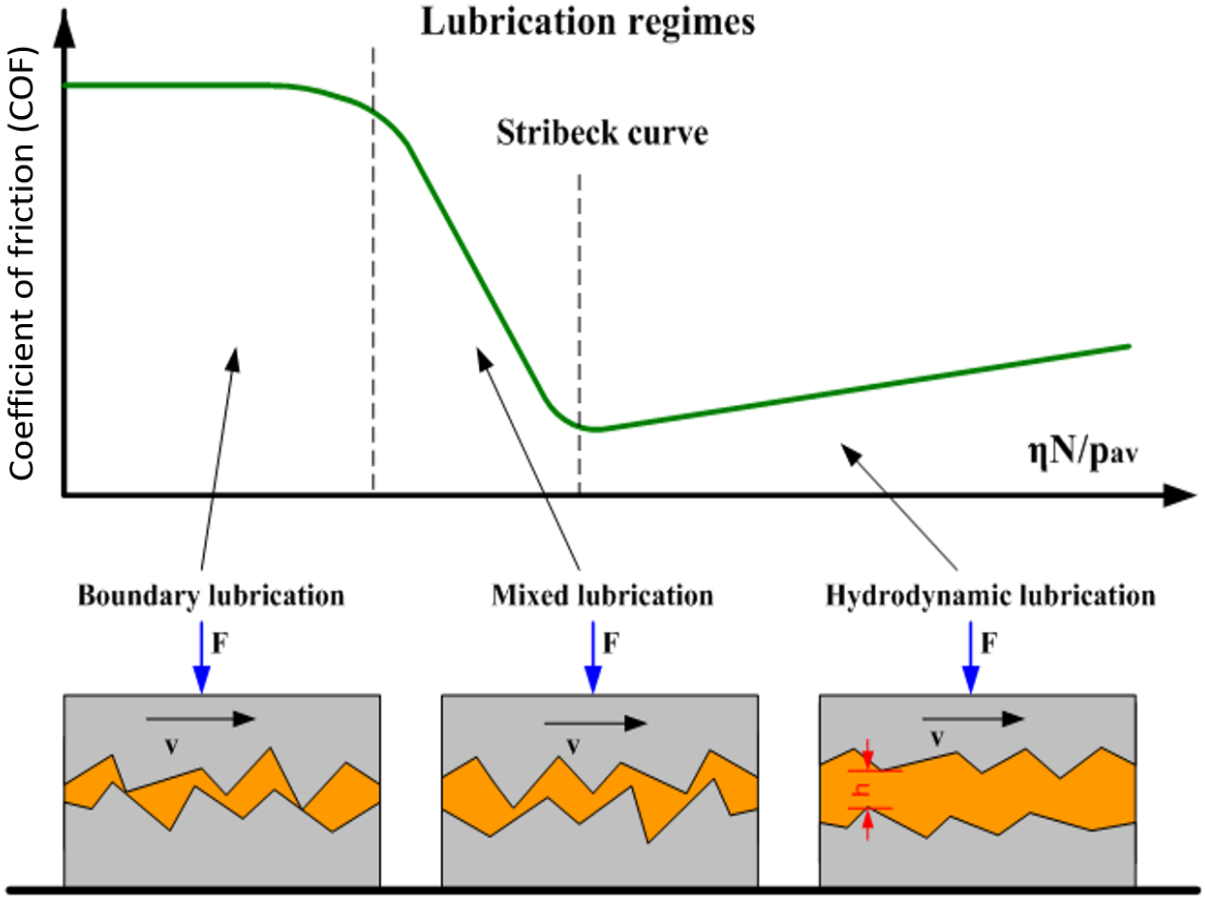

Figure 1.1 Lubrication regimes. [8]

i. Hydrodynamic (HD) lubrication,

ii. Mixed lubrication, and

iii. Boundary lubrication (BL).

In HD lubrication, mating surfaces are completely separated by a thick fluid film with negligible asperity contact present between the two surfaces. [9] This fluid film supports the applied load and the tribological response is solely dependent on the material properties of the lubricant. As the thickness of fluid film decreases, the system starts operating in a mixed lubrication regime. In mixed lubrication, the load is partly supported by the fluid film between the contacts and partly by the asperities in contact. As the contact between surface asperities increases, the coefficient of friction (COF) also increases. Finally, under extreme conditions, when the thickness of fluid film drops below average roughness of the mating surfaces, boundary lubrication (BL) regime is observed. Under BL, there is direct asperity-to-asperity contact and, as a result, the friction increases. Physical and chemical properties of mating surfaces along with molecular adsorbed films and lubricant additives dominate the frictional response. [10] BL is a result of extreme operating conditions that include high load, low speed, and low viscosity. Such conditions are inevitably encountered in practice especially during start-up, low speed/severe loading operation. Several engineering applications are affected by boundary lubrication such as piston-piston rings, bearings, gears, and cam-tappet contacts. [11], [12] Direct asperity-to-asperity contact under BL can also lead to of adhesion/welding between the surface asperities. During repeated sliding motion, such welded asperities can shear off leading to removal of material, also known as wear. These generated wear particles can get trapped within the contact region and lead to abrasive wear leading to further damage of the surface. [13] BL represents the harshest operating conditions and biggest challenge for friction management and effective

lubrication strategies. [13]

Typical boundary lubrication strategies include use of anti-friction and/or anti-wear additives in oil. [11] These additives function by forming a thin protective coating or sacrificial layers on the surface and prevent further damage. [14], [15] The protective films can either be in the form of a physisorbed molecular layer or in the form of a chemically adsorbed/reacted coating. Lamellar solid lubricants and such as graphite and molybdenum disulfide (MoS_2) are also commonly used as effective boundary lubricants. [16] Lamellar solid lubricants have weak inter-layer bonding between the planes allowing them to shear easily under application of load. Under the severe operating conditions, where local flash temperatures can be significantly high, these additives chemically react with the surface forming glassy films that carry the load and minimize wear. [14], [17] Since the films are formed as a result of rubbing between the two surfaces and chemical reactions, they are called tribo-chemical films or tribofilms as referred from here onwards (tribos - rubbing, from Greek). Due to the continuous motion of two mating surfaces, the interaction between the two surfaces and lubricants under BL is a stochastic and evolving process and is explored further in the next subsection.

C. Tribological Surface Modifications:

Under BL regime, where surface asperities are not separated by oil film, the surface modifications become even more prominent. Tribological surface interactions are a complex set of events where both physical and chemical interactions at micron and sub-micron scales dictate the response of a system under applied load. Apart from the two mating surfaces and their surface features, presence of lubricant particles and wear debris cannot be ignored. Figure 1.2 depicts four types of tribological surface modification expected during boundary lubrication:

i. Surface modification without material transfer (work hardening, plastic

deformation, fatigue, cracking etc.),

ii. Surface modifications accompanied by material transfer (diffusion and chemical reactions at the surface, tribo-oxidation),

iii. Formation of tribo-film (via transfer of atoms from mating surfaces, debris particles and adsorption and chemical reaction of lubricant molecules), and

iv. Wear (loss of material from surface). [18]

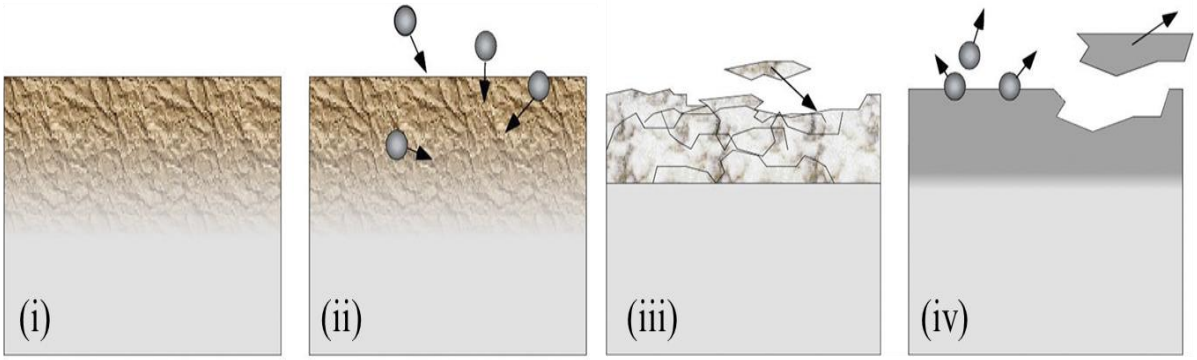

Figure 1.2 Tribological events and surface modifications. [18]

Primarily, the interaction of lubricant molecules and formation of tribo-chemical films is expected at the sub-micron to molecular level. Contact and deformation of micro-asperities will affect the surface at the micro to sub-micron level. These events are governed by the contact mechanics and driven by energetics of the tribo-system. Under repetitive motion between the two surfaces, continuous reorganization and re-alignment of surface features is expected along with the development, wear-off, and replenishment of lubricant tribofilm. The organization of surface features is nothing but surface texture and, thus, forms an inherent part of a tribological system. The synergistic evolution of surface texture and tribofilm to deliver effective lubrication is the key research hypothesis of this research work. The tribological events described above and their correlation with tribofilm properties to deliver effective boundary lubrication is summarized in Figure 1.3 below with the help of a schematic. As shown, the surface texture and tribofilm

evolve concurrently as illustrated by interlocking gears (suggesting their behavior is synergistic) as a result of various physical and chemical tribological events at microscopic and sub-microscopic scales.

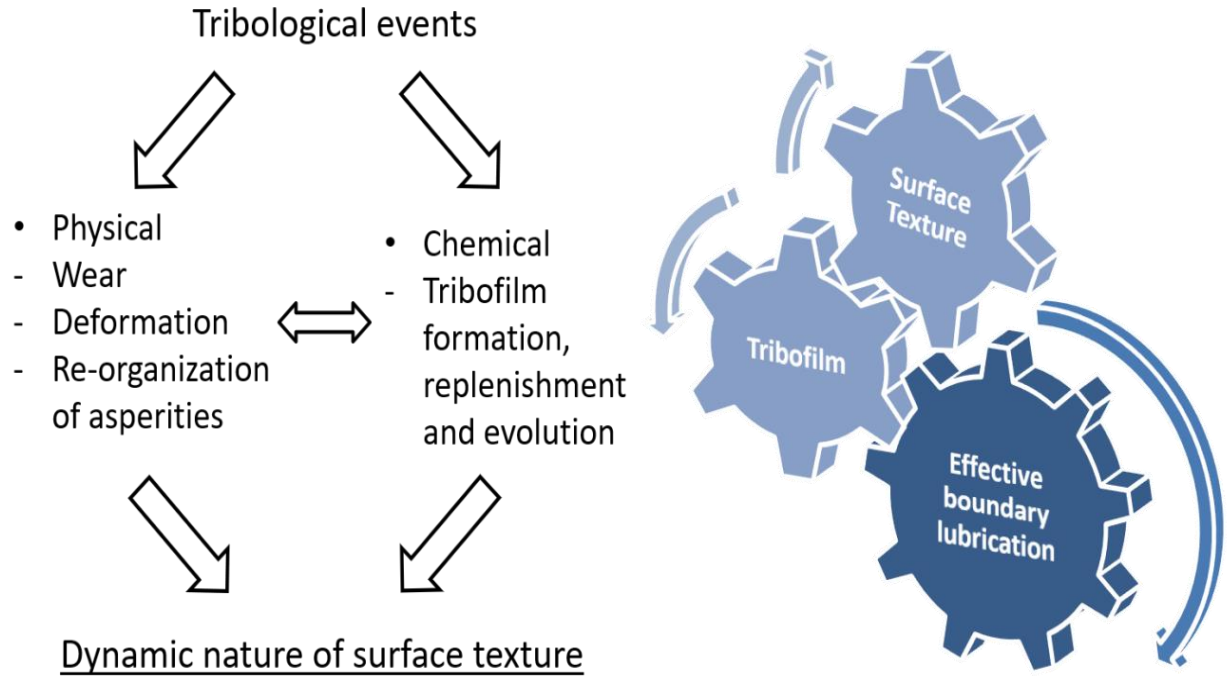

Figure 1.3 Synergistic evolution of surface texture and tribofilm for boundary lubrication.

From previous work, tribofilms formed by advanced nano-engineered lubricants (NL) have been shown to form, wear off, and replenish themselves to deliver a steady-state, low-friction response. [19] Studying the role of texture and its evolution in tribofilm dynamics is thus very fundamental and complementary to the previous studies and scientific understanding. The evolution of texture is dependent on several tribological variables as depicted in Figure 1.4. For this research work, as highlighted by red outline in Figure 1.4, only time was chosen as a controlling variable during the experiments. The tribological parameters (load and speed) were chosen to simulate boundary/mixed lubrication conditions while the lubricant chemistry was chosen based on a previous optimization study. [3]

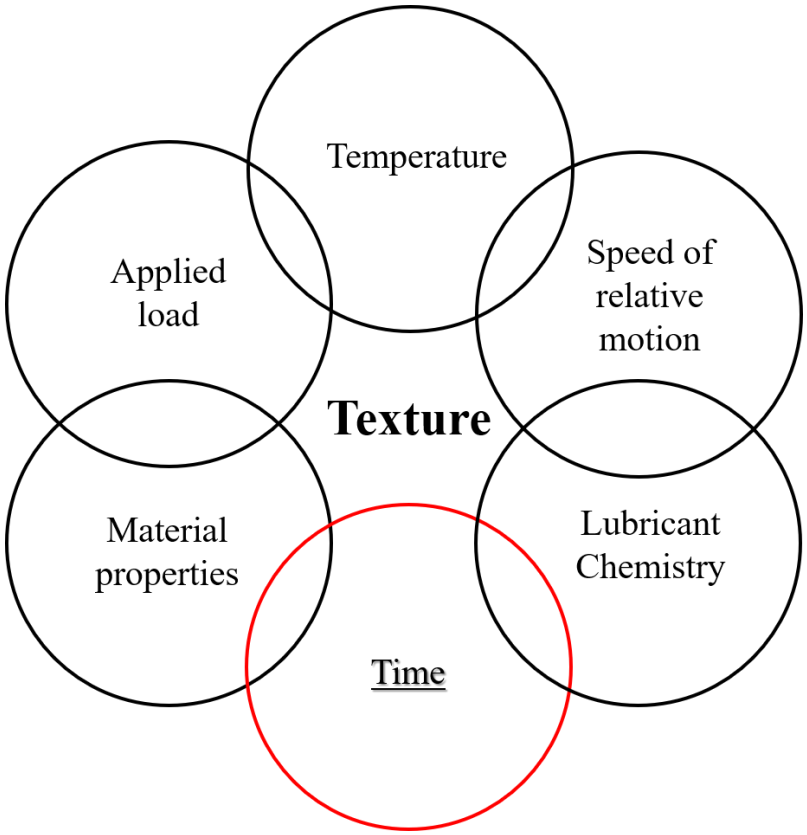

Figure 1.4 Experimental variables controlling texture evolution during boundary lubrication.

D. Research Hypothesis

As noted above, the primary hypothesis of this research is that texture manages and manipulates tribofilm formation and evolution. Both the tribofilm and texture are dynamic due to continuous physical and chemical interactions in a tribo-system. They evolve over time under the applied load to deliver effective lubrication. The following points capture the hypothesis of the events and were systematically investigated during the research performed:

i. The micron and sub-micron level interaction between mating surface asperities and lubricant particles is a stochastic process.

ii. Valleys on the textured surface act as reservoir for lubricant while the peaks serve as contact points for energy dissipation and supporting the load.

iii. The direct asperity-to-asperity contact under boundary lubrication leads to local

increase in flash temperatures and pressure which facilitates the tribo-chemical reactions forming stable tribofilm.

iv. As time progresses, the breakdown, replenishment, and reformation of tribofilm is dictated by complementary changes in surface texture.

E. Outline of Dissertation

The following chapters discuss the literature review and fundamentals of surface texturing in lubrication, experimental tools techniques, details of experiments and parameter matrix, results and discussion followed by conclusion and future directions for this work.

2. REVIEW OF CONCEPTS, LITERATURE AND MOTIVATION

A. Surface Texture as Design Tool

Surface texture can be defined as a repetitive arrangement of features of various shapes and sizes over a surface along three dimensions. [20] The Encyclopedia of Production Engineering defines surface texture as follows [21]:

> "Surface texture is the geometrical irregularities present at a surface. Surface texture does not include those geometrical irregularities contributing to the form or shape of the surface."

Surface texture or texture is one of the most important tools in nature's tool-box (shown in Figure 2.1) to design and develop functional surfaces such as a superhydrophobic lotus leaf, drag reducing shark skin, and many others as depicted in Figure 2.1. [22] Similarly, textures are also utilized in many common applications such as treads on car tires and dimples on a golf ball or on roadside reflectors. Since texture and its evolution are a key part of this research, it is important to understand how texture enables different functionalities.

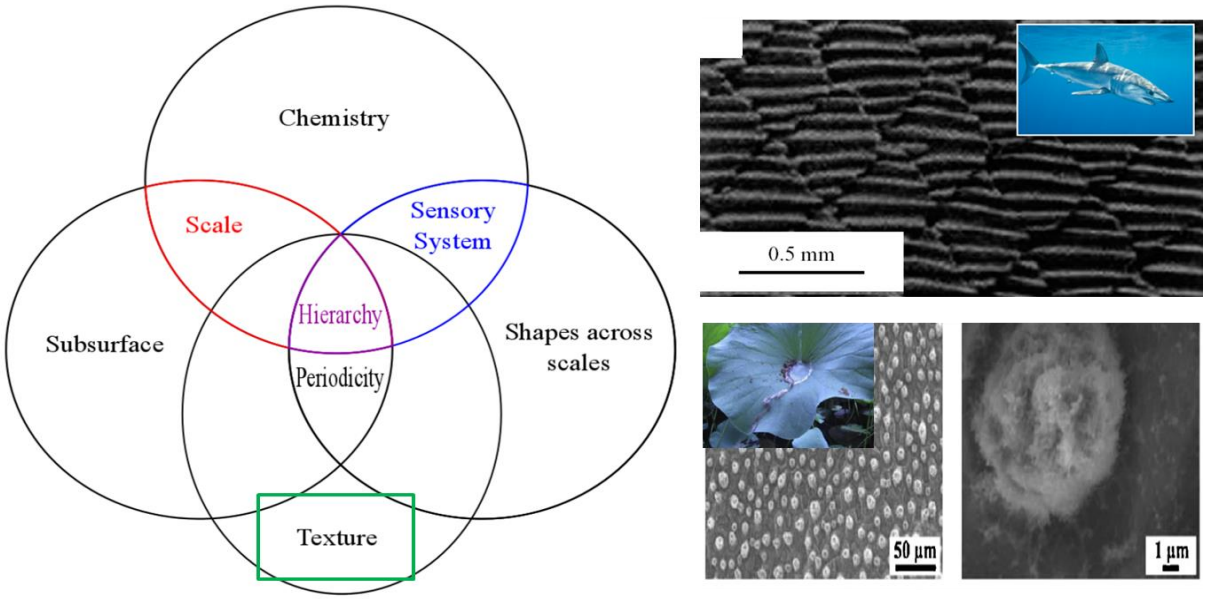

Figure 2.1 Nature's design tool-box and example of functional surfaces in nature. [22]–[24]

Textures are an inherent and important part of the interface that interacts with the environment to deliver the desired function. This interaction can be viewed as a physical effect, chemical effect, or combination of both. The physical effects of surface texture are attributed to the geometry of the surface features and their arrangement. Physical effect is observed in shark-skin (Figure 2.1- top right) or on a golf ball where the surface patterns maneuver the surrounding water/air flow to reduce the frictional drag. [22] Chemical effects can be attributed to the manipulation of surface energy and/or chemical reactions at the interface controlled by surface features. As an illustrative example, lotus leaves have hierarchical textures (Figure 2.1- bottom right) made from hydrophobic wax that enables superhydrophobicity or 'lotus-leaf' effect. Fog basking desert beetles are another example of chemical texture where the alternating hydrophobic-hydrophilic arrangement of micro-domains enable water capture and channeling of water droplets into a beetle's mouth. [25] Both physical and chemical effects of surface texture are important in context of friction and lubrication. Mating surfaces (textured or untextured), lubricant, and wear debris form a multi-body, complex tribological system that includes various physiochemical interactions at the interface as described in Section 1-C.

It is important to note that many of these biological functional surfaces have survived, adapted, and evolved through continuous interaction with the surrounding environmental changes.[22] Engineering systems and artificial textures, on the other hand, have not yet adapted to capture the evolution of surface texture over time due to continuous interaction with the environment. In tribological systems, texture is often viewed as 'static' design parameter instead of dynamic parameter as a case in point. This is further highlighted in Section 2-D where role of textures in lubrication is reviewed. The following section provides a brief overview of measurement and characterization of surface texture.

B. Measurement of Surface Texture

For studying the evolution of texture, it is important to understand the measurement techniques and conventional approaches to characterize textured surfaces. Texture can be viewed as a deviation from an ideally flat surface resulting from the distribution of surface features. Thus, commonly utilized texture characterization tools measure the height variations on the sample either along a linear profile (2-D measurement, height (z) variation measured along line f(x)) or within the area of interest (3-D measurement, z- f(x,y)). Conventionally, surface texture characterization has been performed by using profile methods (2D) such as stylus tip profilometer. The resulting measurement is usually a linear profile of a surface along a scanning direction. A majority of functional surfaces rely on how the areal surface features collectively interact with the environment. Hence, profile measurement and profile roughness parameters may be inadequate to fully describe the functional nature of a surface. [26] Figure 2.2 illustrates some of the limitations of profile measurements compared to areal (3-D) measurements.

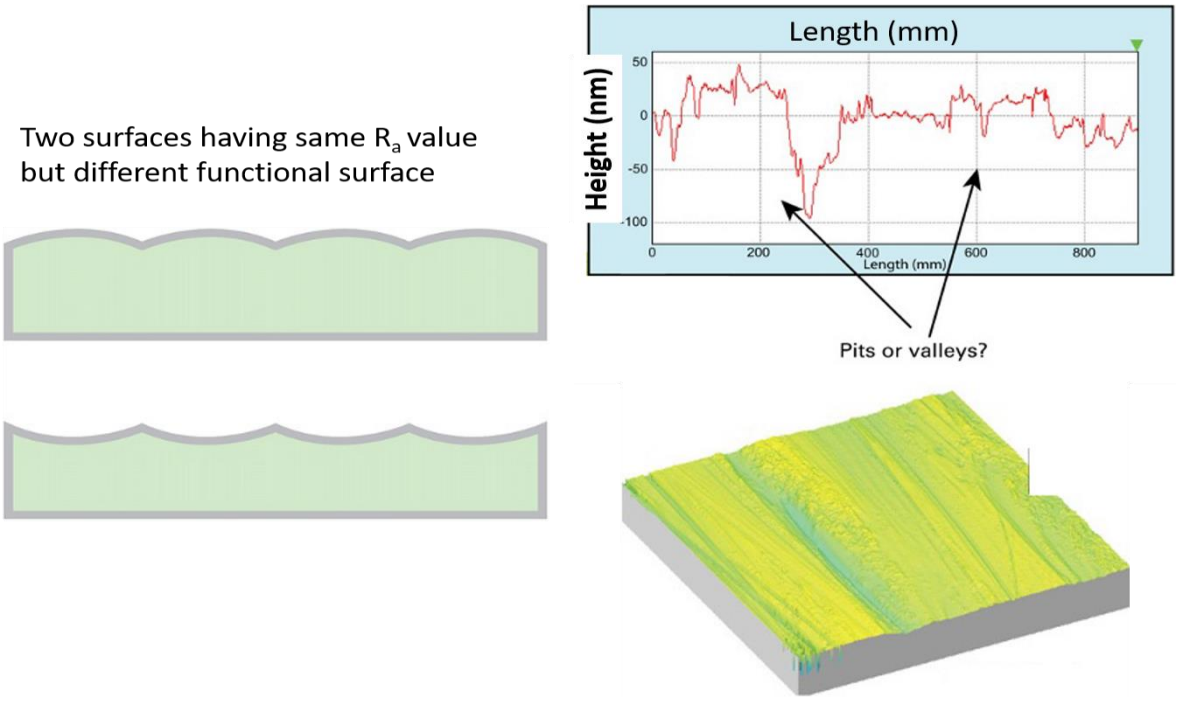

Figure 2.2 Profile vs. areal texture characterization. [26]

Surface roughness (R_a) is a commonly used profile parameter to specify the surface finish. However, Figure 2.2 shows two surface profiles with different functional features but having the same surface roughness (R_a) value. Similarly, functional features such as valleys vs. pits can be analyzed and differentiated in areal measurement unlike profile measurement as illustrated in Figure 2.2. With this shift from conventional profile measurement to areal texture characterization, International Standards Organization (ISO) has developed new standard for areal measurements. Building up on the conventional roughness and bearing ratio parameters, ISO 25178: Part 2 defines a set of 3D texture parameters. [27] The description of texture parameters relevant to this research and their interpretation is discussed further in Section 3-B.

C. Nano-engineered Lubricants (NL) - Prior Work

As summarized in Chapter 1, operating under BL leads to undesirable consequences. However, maintaining full fluid film lubrication at all the times and avoiding the BL regime is not practical in majority of engineering applications. To avoid detrimental effects, lubrication solutions specifically targeted at the BL regime must be considered along with a better understanding of modifications in underlying surface texture. Nanoparticle-based lubricant formulations using lamellar solid lubricant MoS_2 offer an attractive strategy to provide effective boundary lubrication with superior anti-friction and anti-wear properties. Previous research at Materials and Manufacturing Research Lab (MMRL) at the University of Arkansas was focused on synthesis, development, and process optimization of MoS_2-based advanced nano-engineered lubricant (NL). [1] The optimized process led to formation deagglomerated organic-inorganic nanoparticles (Figure 2.3 (a)) which showed excellent tribological properties under boundary lubrication. [28] Delivery mechanism, frictional response, and tribofilm properties of advanced nano-engineered lubricant were studied during the grinding process under the Minimum

Quantity Lubrication (MQL) method (Figure 2.3 (b)). [2], [29] In addition, the tribofilm properties and its evolution were studied as a function of load and lubricant chemistry (Figure 2.3 (c)).[3], [30] The research work reported in this dissertation was aimed toward understanding the complementary role of texture (isotropic and anisotropic) in boundary lubrication. The lubricant preparation and composition (highlighted by red box in Figure 2.3 (c)) used in this research was based on the prior optimization work and their details can be found in previous reports. [1], [3]

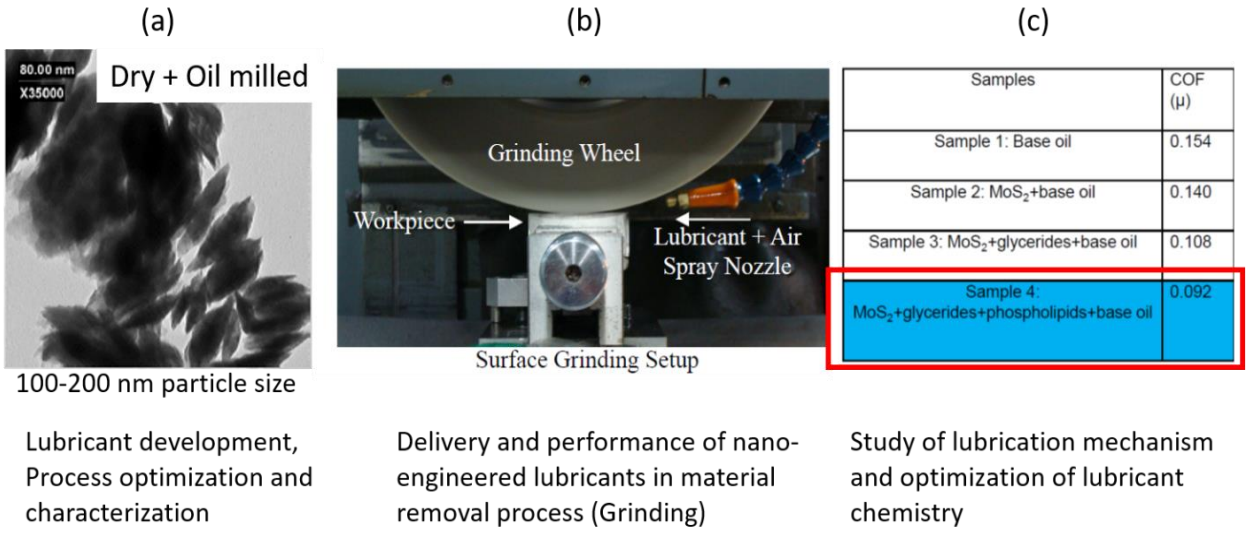

Figure 2.3 Summary of previous research work on MoS_2 based nano-engineered lubricants (NL) at the University of Arkansas.

The MoS_2 nano-engineered lubricant was chosen for this study because of its superior boundary lubrication properties and as a continuation of prior work. It should be noted that other nanoparticle-based lubricants can also be utilized for effective lubrication. These lubricants can be made up of other lamellar solid lubricants such as hexagonal boron nitride [31], [32] (h-BN), graphite and graphene, and tungsten disulfide (WS_2) [33]. Additionally, soft metals (such as copper [34] and silver [35], [36]) and metal oxides (such as CuO, ZnO and TiO_2 [37]–[40]), have also been demonstrated. Diverse types of nano-additives for tribological applications have been

studied and reported. More detailed description of various nanoparticles as lubricant additives can be found in review articles referenced here. [41]–[46]

The following sections summarize the current understanding of role of surface texture in lubrication and provides a brief overview of literature. The gaps in current understanding and novelty of this research are highlighted along with the research objectives and driving questions.

D. Textures in Lubrication - Review of Literature

Surface textures or surface patterns have been commonly employed for developing lubricant strategies over the last few decades. Primarily, the focus has been on developing textures that manipulate the fluid film thickness in hydrodynamic regime. [47] The hydrodynamic lift generated at each individual texture feature (e.g. dimple, chevron, ellipsoid) was studied theoretically and experimentally [48]–[51] in order to optimize the effect of feature shape, size, and orientation. Additionally, textured surfaces were also studied in context of solid lubricant powders and coatings. Particularly, texture patterns such as regular and zig-zag grooves [52], [53], dimples [54]–[56], and bio-inspired lotus-leaf like texture [57] were examined and showed promising results with burnished, pressed, or coated MoS_2 solid lubricants. It was reported that the valleys in the developed textures act as a micro-reservoir to store the solid lubricant particles as well as trap wear-debris. Similarly, numerous research efforts report effect of surface texture with pure base oil without additives (no tribo-chemical film). Table 2.1 enlists some of the representative reports that use textured ferrous materials with base oils. The table includes the materials used, design attributes of applied surface texture, and important results and conclusions.

It is important to note that evolution of surface texture was not studied systematically in conjunction with the friction and wear properties in these reports. As listed in the table, the

Table 2.1 Summary of selected research papers for use of surface texturing in presence of pure base oils without additives for friction management.

Ref.	Materials, lubricants	Texture details	Results	Other comments	Texture evolution
[58], [59]	H-13 steel-52100 steel balls, PAO base oils of different viscosities	Dimples: 58-80 µm range, 7-15% areal density	Texture expands the HD lubrication regime, shows lower COF, lower dimple density preferred	lapping of bulges formed after LST is essential for positive effect	Not studied
[60]–[62]	52100 steel pin and disc, PAO oil	Combination of multiple shapes in various arrays, 40-120 µm size, 7-20 % areal density, ≈6 µm depth	Low COF values attributed to effective hydrodynamic effect	Textured pockets help storing the wear debris	Not studied
[63]	52100 Steel disc and pin, PAO 8 base oil	Dimples: 60 µm size, Grooves: 40-120 µm width, 125-500 µm spacing	Skewness and kurtosis were considered as important parameters for effective lubrication	Different speeds-starved, BL and mixed lubrication. ST increases friction in starved case	Not studied
[64], [65]	Textured AISI 304 stainless steel discs, Al_2O_3 balls, PAO 4 and PAO 40 base oil	Dimples: 100-200 µm size, 25-100 µm depth, 10-30 % dimple density	All textured samples show lower COF for up to 0.5 cm/s sliding velocity, for higher speeds samples with lower density and depths show lower COF	Textured surfaces have lower wear volume than untextured; up to 100 times reduction for PAO 40 oil reported	Not studied
[66]	Textured 52100 steel discs, polished C85 steel pins, PAO 18 base oil	Dimples: 40-200 µm size, 2-8 µm depth, 5-30 % dimple density; hexagonal, cubic and random arrangement of dimples	Optimization of dimple parameters conducted to get lower COF values	Dimple aspect ratio of 0.1 shows the best results; 10% packing density if optimum; hexagonal arrangement is better	Not studied
[67]	Textured cast iron, 42CrMo6 steel counter-face, PAO 8 base oil	Dimples - Elongated and circular, 100-500 µm feature size, 10-50 µm depth, 5-10 % areal density; different arrangements and orientations examined	DOE results show diameter and area fraction as dominant dimple design parameters for low COF values, Other parameters affect the lifetime of tests	Optimization of dimple parameters and sliding angle w.r.t. direction of features was reported	Not studied
[68]	AISI 316L steel disc, sapphire balls, 4 different halogen free room temperature ionic liquids (RTILs)	Random texture: 2 different textures with different surface roughness R_a = 24.5 nm and R_a = 4.5 nm	Higher roughness discs show lower COF and wear rate with all ionic liquids tested	Lubricant layer on surface detected without tribo-corrosion	Not studied
[69]	52100 steel discs and balls, pure paraffin white oil	Droplet shapes, parallelogram shape, their mixture and overlap (small deep droplet in large shallow parallelogram) in size range 10-200 µm and up to 3 µm depth with different areal densities	As high as 80% friction reduction was achieved for >100MPa contact pressures, higher areal density shows better result than lower density of overlapped features	Overlapping feature design was aimed towards maximizing their benefits under different loading conditions	Not studied

majority of reported research on texturing is based on trial-and-error approach where features of various shapes and sizes with variable feature density are tested and optimized in the presence of lubricant. It should, however, be noted that the observations made from the above-mentioned research on the use of textured surfaces with base oils or solid lubricants are certainly helpful in terms of understanding possible mechanisms of tribofilm formation and surface protection. It is widely recognized that surface texture aids lubrication via the following key attributes [70]:

i. manipulating lubricant film formation and aid the fluid flow through the channels;
ii. serving as a reservoir for lubricant and prevent seizures under severe conditions;
iii. trapping the formed debris within the pockets and prevent their further contact with the rubbing surfaces to reduce subsequent wear; and,
iv. changing the pressure distribution across the mating surfaces, both locally and globally, as a result of surface asperities and local contact. [70]

As seen in Section 1-B, commonly used boundary lubrication strategies involve use of additives that can chemically react with the surface and from a protective tribofilm. Typically, commercially formulated oils utilize different additive molecules that serve distinct functions such as modifying viscosity, inhibiting corrosion, friction modifiers, anti- wear/extreme pressure (EP), reducing foam, etc. However, in the context of this research, anti-friction/wear and extreme pressure additives are more important. Both nanoparticle additives and additive compounds such as zinc dithiophosphate (ZDDP), molybdenum dialkyldithiocarbamate (MoDTC), and molybdenum dialkyldithiophosphate (MoDDP) are commonly researched for their boundary lubrication properties as a result of formation of tribofilm. Table 2.2 summarizes representative reports targeted on studying frictional properties of additives in the presence of surface texture. The summary includes the materials used, design attributes of applied surface texture, and

important results and conclusions from the papers.

Table 2.2 Summary of selected research papers on the use of surface texturing in presence of base oils containing additives for friction management.

Ref.	Materials, lubricants	Texture details	Results	Other comments	Texture evolution
[71]	52100 steel ball and textured plate; base oil with MoDDP additive	Dimples :45-50 µm dia. and 0.56-4.4 µm depth; Grooves: 30 µm width and 2.5–12.2 µm depth	Optimized surface texture shows better frictional response under BL with MoDDP additive	Under BL, MoDDP forms oxidized anti-wear tribofilm	Not studied
[72]	Textured H-11 steel plate, Al-4Mg pin, engine oil with ZDDP additive	Directional grinding with emery paper and cross-pattern formed by 90° polishing, R_a: 0.1-0.5 µm	Surface slope of asperities (Δ_a) parameter correlated well with COF trend	Lower asperity slope also means lower shear stress and less transferred material to the counterpart	Not studied
[73]	Cast iron (cut from commercial engine), Diesel engine oil lubricant	Grooves: Different orientations, 100 µm width, 10% density, 7 and 19 µm depths	For different groove depths, different orientations show best results	Hydrodynamic effect - Low loads; Lubricant supply effect - High loads	Not studied
[74]	Grey cast iron- Steel ball, 5W30 diesel engine oil	Honed grooves: 25 µm width, 3-6 µm depth, 300-1200 µm pitch	Smoother surfaces and widely spaced grooves work better in BL	Rpk values correlate to tribofilm formation	Not studied
[75]	H-13 textured tool steel, 52100 steel pins, PAO4 and PAO4 + 2.5% ZDDP + 2.5% MoDTC additive	Dimples: 100 µm dia., 10 µm depth, 240 µm pitch	LST was detrimental to protective tribofilm formation with additives	LST also produced more wear for both lubricants with and without additive	Not studied
[76]	Al alloy piston skirt - Grey cast iron liner, PAO, PAO oil mixed with BN and MoS_2 NPs and surfactants	Random roughness: S_a=0.62 µm, S_q=0.84 µm, S_{sk}= -0.46, S_{ku}=17.4 (Topographical parameters)	PAO- MoS_2 combination shows lowest COF, MoS_2 formulations show reduced wear owing to tribofilm formation	Chlorinated hydrocarbons provide extreme pressure (EP) resistance, BN does not show significant improvement	Not studied
[77]	Textured 65Mn steel plate, GCr15 steel ball, PAO4 + nano diesel soot particles	Dimples: dia.- 150µm, depth -30µm, density - 19.6-44.2%	44.2% density dimples showed lowest wear rate	Dimples store lubricant and wear debris	Not studied
[78]	AISI D2 steel ring, AISI 1018 steel block, PAO2 + TiO_2 nanoparticles of different sizes	R_a values: 0.3 µm, 0.7 µm, and 1.4 µm obtained by machining and polishing	Particle size of 0.165 µm showed lowest friction and wear	smaller particles were stored in valleys to show friction reduction by mending effect	Not studied
[79]	Rough copper surface, Steel ball, Dry, base oil (dodacane) and base oil+ZnS nanowires	Random roughness: Thermally evaporated Cu film with different surface roughness; R_q:0.94-4.15 nm	Avg COF for base oil+ZnS mixture is lowest; raw friction force is also lower for composite lubricant	Friction tests performed using nano-tribometer, Surface topography plays crucial role in deciding frictional response at higher loads	Not studied

Table 2.2 (Cont.)

Ref.	Materials, lubricants	Texture details	Results	Other comments	Texture evolution
This work	Textured 52100 steel discs, 52100 steel ball, PAO10 base oil with and without MoS_2 based NL	Directional concentric texture applied using P1200 SiC grinding paper	Textured discs manage and manipulate tribo-chemical reaction and film formation and show early onset of steady-state friction	Valleys act as reservoir those are filled with reacted and stored lubricant and show self-assembled tribofilm	**YES**

Similar to reports listed in Table 2.1, the reports involving additives listed in Table 2.2 are also focused on trial-and-error based methods with the goal of optimizing texture features (such as size, shape, and areal density) for better anti-friction/anti-wear characteristics. Evolution of surface texture remains largely ignored even though it is of utmost and inherent importance in boundary lubrication and, thus, is the motivation behind this research. It is also interesting to note that in some cases, textured surfaces even show detrimental effects and result in a high coefficient of friction (COF) and/or more wear.

Table 2.3 lists a compilation of research efforts that report studies of changing surface texture. The table summarizes materials and lubricants used, details of surface texture, texture characterization method (profile or areal), along with brief remarks on reported results. As listed in the table, the research involving evolution of areal surface texture has mostly been focused on monitoring and analyzing wear. Other reports investigated used profile parameters which may not be sufficient to describe the functional nature of the surfaces as seen in Section 2-B. Furthermore, study of tribofilm properties formed by using nano-engineered lubricant additives in correlation with texture evolution has not been studied. Thus, novelty of this research is highlighted with help of Table 2.3 where the study of evolution of areal surface texture by using relevant parameters and its correlation with tribofilm evolution by using nano-engineered lubricant additives is reported for the first time in this research.

Table 2.3 Comparison of reports studying change in texture during tribological/wear tests.

Ref.	Material and surface preparation	Lubricants used	Comments	Profile or Areal parameters	Evolution Study
This work	52100 steel disc and ball, directional concentric texture applied by P1200 grit size SiC paper	PAO10 base oil with and without MoS_2 based NL	Textured discs show early onset of steady-state friction; variation of surface texture parameters can be correlated to observed frictional response and tribofilm properties	Both areal and profile	Evolution of relevant surface texture parameters was studied in context of tribofilm formation and frictional response
[80]	EN-32 steel, polished substrates	Micro and nano MoS_2 suspension	Correlation of particle size with tribo-layer formation and coverage was studied	Profile	Z height profiles were analyzed
[81]	Bearing steel, R_q=200nm and 50nm with longitudinal roughness lay	PAO base oil	Micro pitting rig (MPR) tester, wear model was developed and studied experimentally	Profile	Only R_q roughness values was reported
[82], [83]	Case carburized 16MnCr5 steel rollers, rings had different surface roughness	Base oil + ZDDP additive	Micro pitting rig (MPR) tester, hardness evolution was studied in correlation with tribofilm properties	Profile	Only R_a, R_z and R_q roughness values were reported
[84]	Machined 1045 steel discs, 52100 steel balls	SAE 40 and N16 oils	Loads changed to sample BL and full film lubrication, focus on wear particles and wear volume progression	Areal	Only S_a, S_q roughness values reported
[85]	AISI 1045 steel-52100 ball pair and Ti6Al4V-Al_2O_3 ball pair, polished with different grit sizes Sa~0.035 to 6.73 µm	None	Fretting wear test tribometer, evolution of roughness was analyzed and compared for surfaces with different starting surface roughness	Areal	Various surface texture parameters were studied in context of material wear with no lubricant

E. Motivation and Research Objectives

It is clear from the above discussion that modification of mechanical surfaces via inclusion of various surface textures is a useful approach for effective lubrication. However, it also highlights some of the shortcomings of the current understanding of the evolution of surface

texture and tribofilm under boundary lubrication. Based on the research hypotheses discussed in Chapter 1, the following research goals were set for this research:

i. Study of evolution of isotropic surface texture on mating polished surfaces: physical, chemical, and functional analysis
   - aimed towards understanding the self-organization of surface features without any directionality (referred to as 'untextured' discs from here onwards).

ii. Study of evolution of fabricated/synthetic surface texture pattern: physical, chemical, and functional analysis
   - aimed towards understanding how partially directional texture affects and manipulates tribofilm properties and frictional response (referred to as 'textured' discs from here onwards).

The first part of the research was devoted to fundamental understanding of dynamic nature of 'non-intentional' or 'natural' surface texture and benefit to lubrication in presence of nano-engineered lubricants. This was followed by research aimed towards understanding the effect of 'intentional' texture patterns on effective tribofilm formation and lubrication. The driving questions for this research are listed below:

i. How does the surface texture change dynamically during boundary lubrication?

ii. How do the nano-engineered lubricants interact with surface asperities under the applied load?

iii. What role does time plays in terms of achieving a certain physical and chemical topography under boundary lubrication conditions?
   - Which surface features are critical? How do they evolve/dissolve over time? How is the periodicity and directionality of features affected?

iv. What length scales (micro, sub-micron) are primarily affected?

- How does this co-relate to tribofilm formation and frictional response?

Evolution of texture was analyzed using areal as well as profile texture characterization methods according to the ISO guidelines, [27], [86], [87] while the tribofilm properties were characterized using SEM, TEM, and Raman spectroscopy. The following chapter details the experimental tools and techniques used in this research and a brief description of testing methods and relevant texture parameters. Description of preliminary experiments, feasibility tests, and identification of parameter matrix is included in Chapter 4. Chapters 5-7 include discussion and interpretation of experimental results and future directions for the research.

3. EXPERIMENTAL TECHNIQUES AND DETAILS

This section provides a brief description of experimental techniques and characterization tools used during this research for experiments and analysis followed by experimental details and parameter matrix. The functional characteristics of texture and lubricant were tested with a tribometer setup. Surface texture was measured using a Keyence VK-X 250 laser microscope, [88] while SEM/EDS, FIB/TEM, and Raman techniques were used for chemical characterization. A brief working mechanism of these tools and their setup for the experimental characterization is described below.

A. Description of Experimental Tools and Techniques

I. Tribological testing (COF- Coefficient of Friction measurement)

The tribological tests were performed using the CSM pin-on-disc tribometer (model-TRB) [89] under ambient conditions. Pin-on-disc tribometers are commonly used for fundamental research experiments because of their simplicity and robustness. The open loop system allows for effective control of test variables such as load and speed making this setup suitable for fundamental studies involving experiments with sliding point contact. The tribometer can be used in a reciprocating mode (linear motion) by attaching a linear module or under a rotational mode (circular motion). Both modes were tested during the feasibility tests and rotational setup was finalized for experiments (see Appendix A for additional details). Figure 3.1 shows a photograph of the pin-on-disc tribometer used for the experiments in rotational mode. The pin consists of a ball which was held stationary during the test with the help of ball holder. The sample disc was mounted with the help of rotary clamp which either rotated at a constant speed (rotational mode) or reciprocated back and forth with a fixed amplitude (reciprocating mode) at a chosen speed during the test with the help of motor.

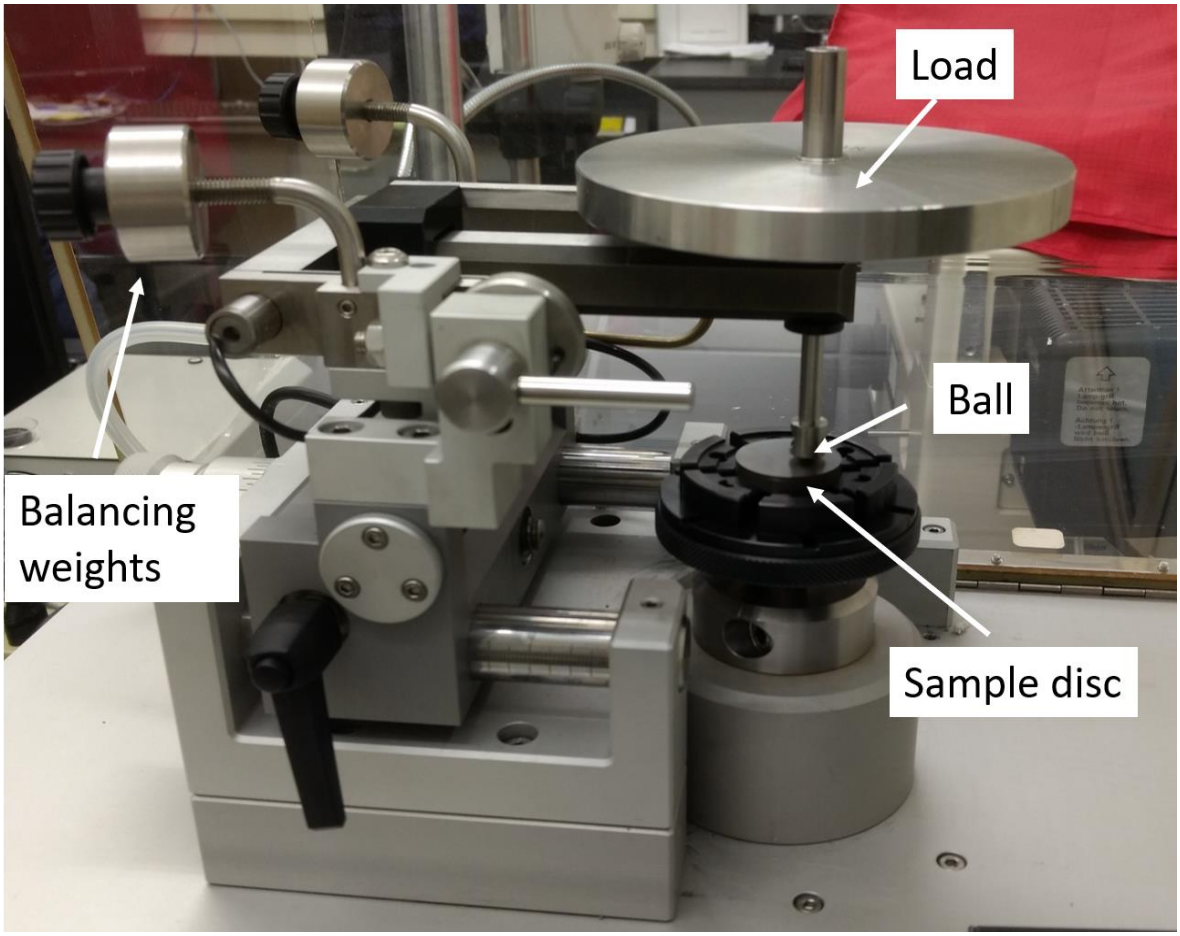

Figure 3.1 CSM pin-on-disc tribometer (photo by author).

Normal loads from 1 N up to 20 N could be applied from top after balancing the arm to zero-load condition with the help of balancing weights. Lubricant was applied between the ball and disc before the test. The experiments were controlled by using computer user interface with TriboX software. The test parameters such as rotational speed and test duration were input in the software (as discussed in detail in Section 4-A) and the test was automatically stopped after a set time interval/distance travelled. Friction force was measured with the help of LVDT sensor and coefficient of friction (COF) values were recorded after every 0.5 sec. The data acquired by the software was then exported and the frictional response (COF vs. time) was plotted. The detailed experimental procedure is further described Section 3-C under experimental details.

II. Scanning electron microscope (SEM) and energy dispersive spectroscopy (EDS)

Scanning Electron Microscopy (SEM) equipped with an Energy Dispersive Spectroscopy (EDS) tool [90] was used to characterize surface morphology and tribofilm coverage. FEI Nova Nanolab 200 SEM equipment (shown in Figure 3.2) was used during this research. [91]

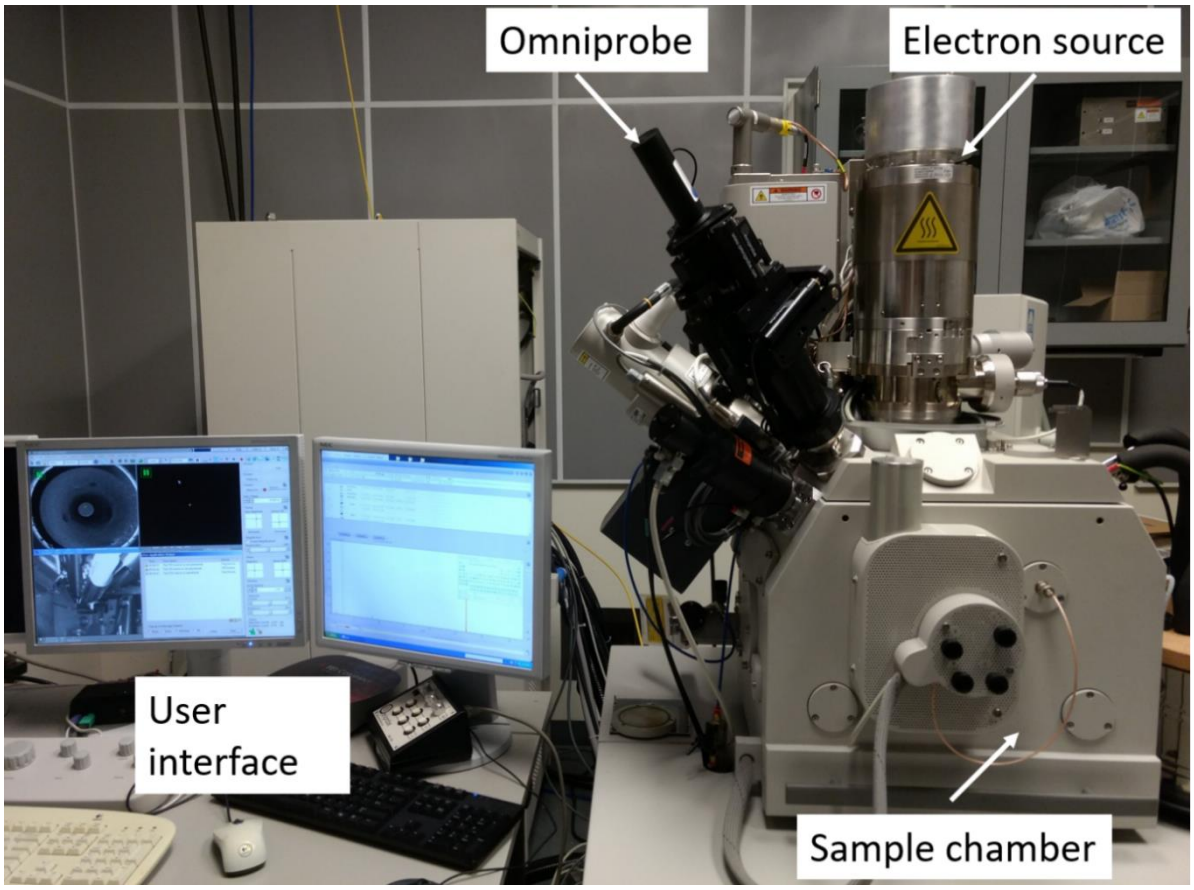

Figure 3.2 Nova Nanolab 200 SEM equipment (photo by author).

This instrument is equipped with a Focused Ion Beam (FIB) machining accessory for in-situ machining and cutting. The equipment also has a provision for a gas nozzle inlet which can be used for fabricating oxide films and depositing platinum metal contacts and an Omniprobe [92] micro manipulator used for TEM sample preparation. SEM uses a high energy electron beam to characterize and image the sample surface. A collimated beam of electrons is incident on the sample surface that emits electrons and x-rays as a result of surface interactions.

The electron beam is rastered across the sample surface to generate the image with the help of backscattered or secondary electrons. Elemental analysis (EDS) is carried out by collecting x-ray radiation emitted from sample surface. The emitted x-rays are the result of atomic level interaction and each element has a characteristic x-ray emission wavelength. This is used to generate elemental mapping of the sample surface. The images were taken at 15 kV, 2.2 nA electron beam settings. A working distance of 5 mm (eucentric height) was maintained to get best quality micrographs for magnifications up to 35000X. Elemental maps were created and saved with the help of elemental mapping software on the user interface computer. [93]

III. Focused ion beam (FIB) sample preparation

After the tribological tests, tribofilm cross-section was studied with the help of transmission electron microscope (TEM). Focused ion beam (FIB) utility that is a part of Nova Nanolab 200 SEM, was utilized for cross-sectional TEM sample preparation. Figure 3.3 shows the detailed step-by-step procedure for cutting a cross-section of the tribofilm sample. After the area of interest was selected (Figure 3.3 (a)) using the EDS mapping tool, the tribofilm surface was first protected using a 1-2 μm thick platinum layer (Figure 3.3 (b)). The protective coating was applied to prevent damage to the tribofilm and surface during ion milling. During operation, the ion beam was focused on the selected area of sample to etch the material surface. Alternatively, the ion beam could also be used to deposit oxides or platinum on the selected area of the sample when used with appropriate gas injectors. Since there is a competition between etching and deposition at the material interface in presence of ions, the TEM sample preparation process requires careful operation and continuous monitoring. Higher ion beam currents (0.3 nA to 1 nA) are used to cut the trenches during step (b), while the polishing of the interface and slice (step (h)) was performed at 30 pA beam current in order to ensure that the sliced interface is not

destroyed with high energy Ga ions. After the cross-section of the sample was cut, the sample slice was transferred on to the Omniprobe micro-manipulator [92] and then on to the TEM grid (from steps (d) to (g)) for TEM observation.

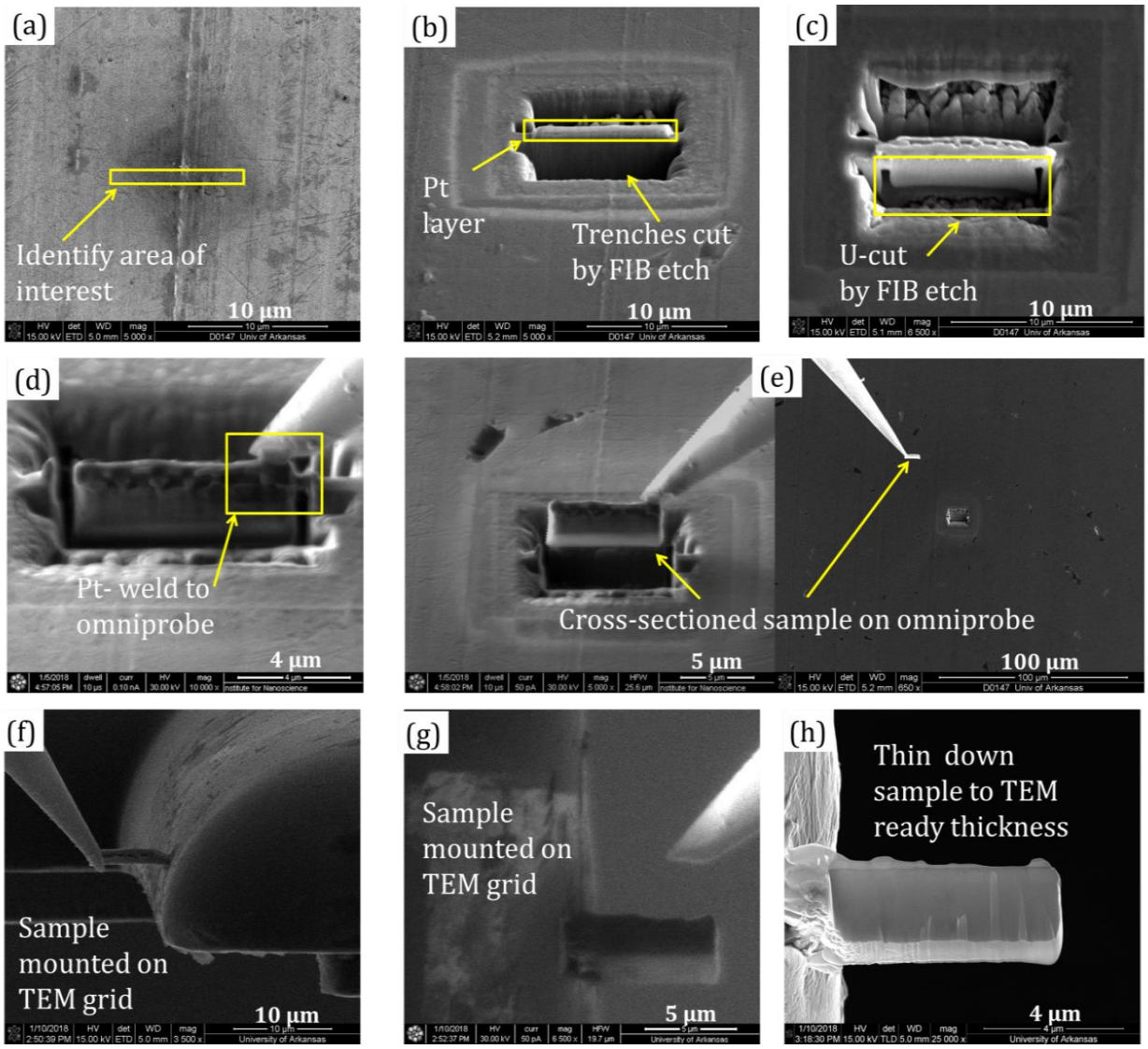

Figure 3.3 TEM sample preparation steps using FIB and Omniprobe.

IV. Transmission electron microscope (TEM)

The sample prepared with FIB described above was characterized using a FEI Titan 80-300 [94] (shown in Figure 3.4) TEM microscope to study cross-sections of the tribofilm samples. Similar to SEM, TEM also uses a beam of high energy electrons to characterize the sample.

However, unlike SEM, electrons that are transmitted through the sample are detected as compared to secondary and backscattered electrons to gather valuable information from the sample. Transmitted electrons are then focused and projected on the fluorescent screen/ photographic plate by using a set of objective and projection lenses to capture the image.

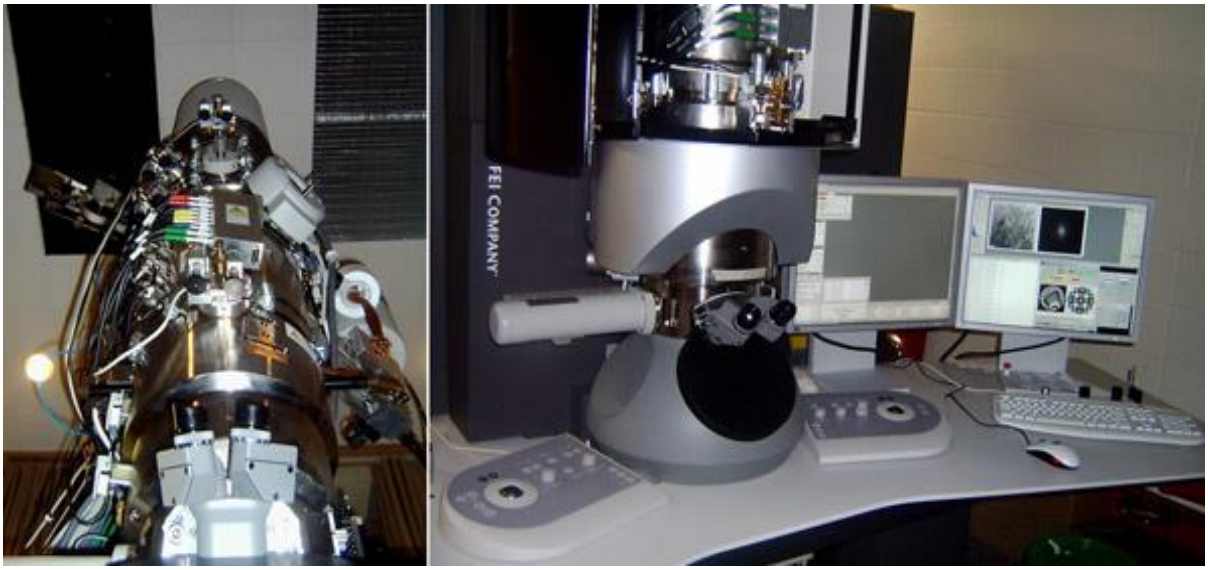

Figure 3.4 FEI Titan 80-300 TEM setup. [94]

The operating voltage of TEM is higher (few hundred keV as compared to 10-50 keV) than SEM as higher operating voltage corresponds to higher energy electrons that can transmit through the sample. For the electrons to transmit through the sample, the sample thickness should be less than 500 nm making step 'h' from the FIB sample preparation procedure vital. TEM is a very versatile and powerful tool in terms of characterizing different types of materials in various ways in order to obtain useful information about a particular sample. Apart from micro- and nano-structural imaging and morphological study at very high magnification (300,000X and more), TEM microscope is also equipped with the EDS detector for elemental maps (line scans) as well as X-ray diffraction analysis. For tribofilm characterization, magnifications up to 300,000X were used along with EDS point and line scan to identify the

distribution of phases within the cross-section.

V. Raman microscope

Chemical analysis of tribofilms was performed using Renishaw InVia Raman spectrometer [95] shown in Figure 3.5. The equipment uses a 765 nm, 150 mW laser to probe molecular vibration modes on the sample surface. When the input radiation frequency matches with the characteristic vibrational frequency modes within a molecule, the vibrations are resonated into an excited state. The excited resonance state, when relaxed down to the ground state, results in an output radiation signal. The interaction between the input radiation and the molecule is typically inelastic and, hence, the output radiation usually has less energy (larger wavelength) than the input. This 'shift' between the input wavelength and output wavelength is known as 'Stokes shift' and is measured. Stokes shift is characteristic of a molecular vibrational signal and, thus, the material surface can be analyzed for its molecular structure by comparing the measured Stokes shift with the known values for previously identified samples within the database. The measurements were performed using 20X objective, 20% laser power, 60 sec acquisition time and three integrations.

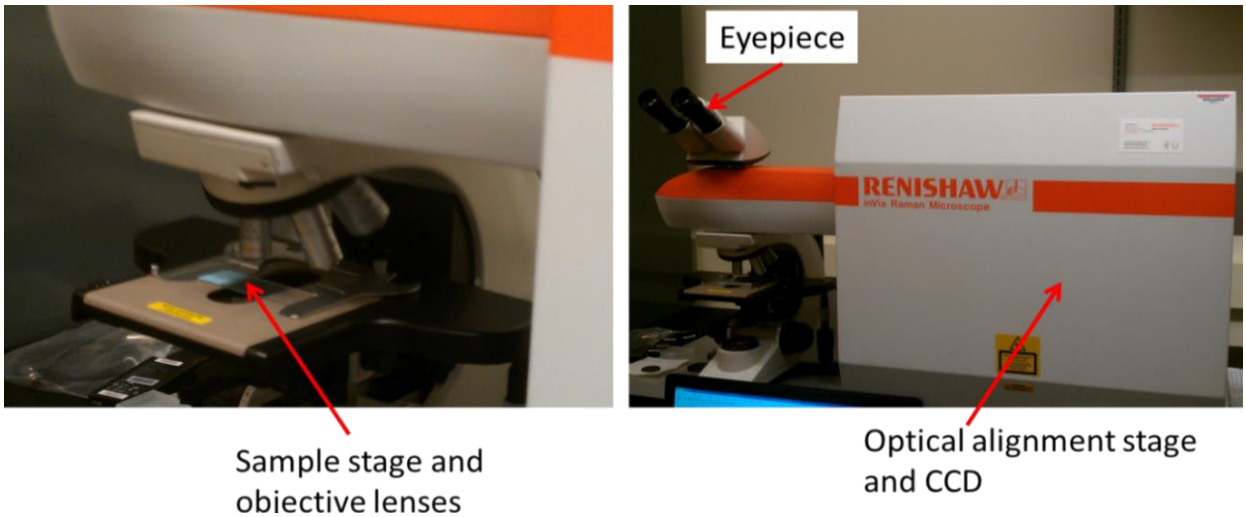

Figure 3.5 Renishaw InVia Raman microscope setup (photo by author).

VI. Laser scanning microscope

As mentioned in Chapter 2, surface texture measurement and analysis were the key aspects of this research. A non-contact laser scanning microscope (Keyence VK-X 250) [88] was used to measure the areal surface texture. Figure 3.6 shows the laser microscope setup.

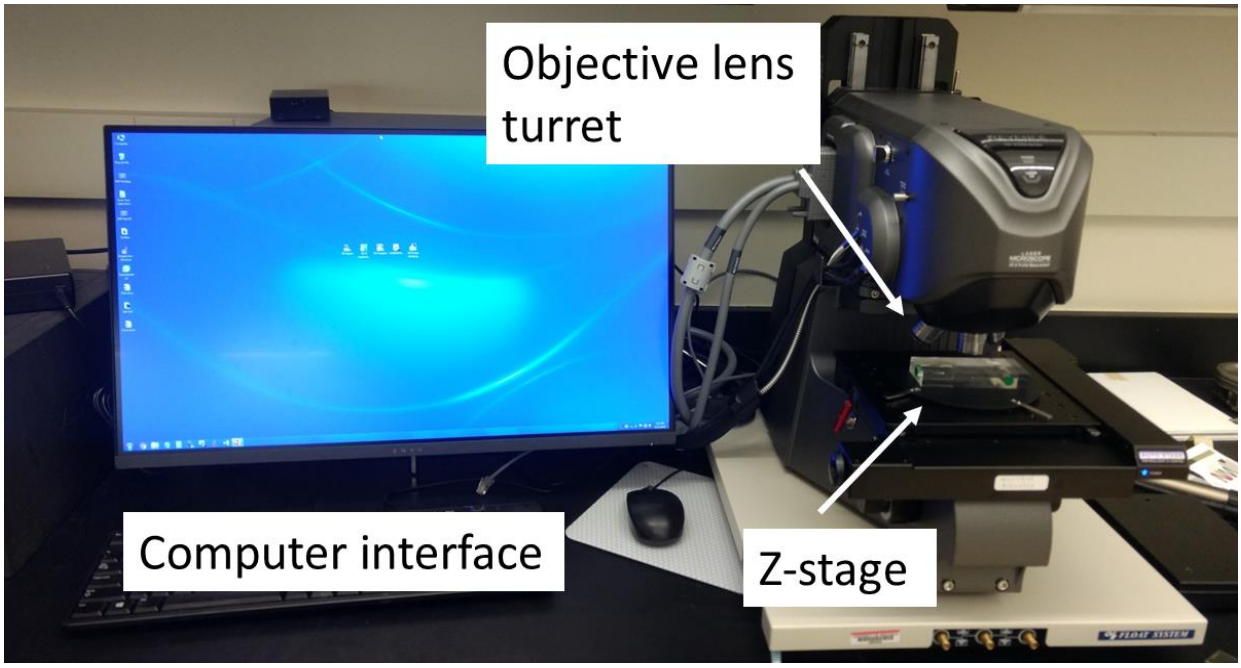

Figure 3.6 Keyence VK-X 250 laser scanning microscope (photo by author).

The laser microscope was used with 20X magnification lens, areal surface profile mode, and 2048 X 1536 pixels measurement size (super fine measurement setting). The laser beam was focused on a sample surface and rastered the measurement area during the measurement operation. The reflected laser intensity from each pixel was recorded through a confocal lens by a photoreceptor. Confocal collection ensured that reflected intensity (and height information) from only the points under focus got recorded. The sample stage was then moved in the Z-direction and the scanning procedure was repeated within the selected Z-axis measurement range. The reflected laser intensity values from each step collectively then produced a 3-D height image of the measurement area. [96] The laser microscope was operated under a fully automated

mode with the help of VK-X software control. The measurement details (such as scan size and Z-range) were specified by the user and final raw data file was saved at the end of the measurement scan. The raw data file was then opened with the help of multifile analyzer software to select the region of interest and calculate the texture parameters as per user specifications. Additionally, this microscope was also used as an optical microscope for measuring wear scar diameter (WSD, measured on the ball counter-surface) and wear track widths, which are typically used to assess the degree of wear in tribological contacts. The next section describes the methodology to calculate surface texture parameters with the help of multifile analyzer software and a brief overview of texture parameters of interest that were used during the analysis.

B. Description and Calculation of Surface Texture Parameters

The raw data measured from VK-X 250 laser microscope was analyzed using multi-file analyzer as discussed in this section. The raw data was first imported into the software and nominal shape correction filter was applied. This removed the form of the surface profile (by correcting the tilt) before it was further analyzed. The roughness profile was obtained by filtering out the long wavelength components (waviness). Filter values were chosen based on the measurement area/profile of interest in accordance with the ISO 25178:3 and ISO 4288:3 guidelines. [86], [87] Surface texture measurements were taken at four locations of the wear track at 20X magnification. Final calculated texture parameters values were averaged for texture evolution study. Both areal and profile parameters were calculated using the software as illustrated by screenshots shown in Figure 3.7 and Figure 3.8. As depicted in these figures, the parameters were only calculated on the wear track by choosing the area or line across the wear track while appropriate filter settings were chosen using the filter settings options.

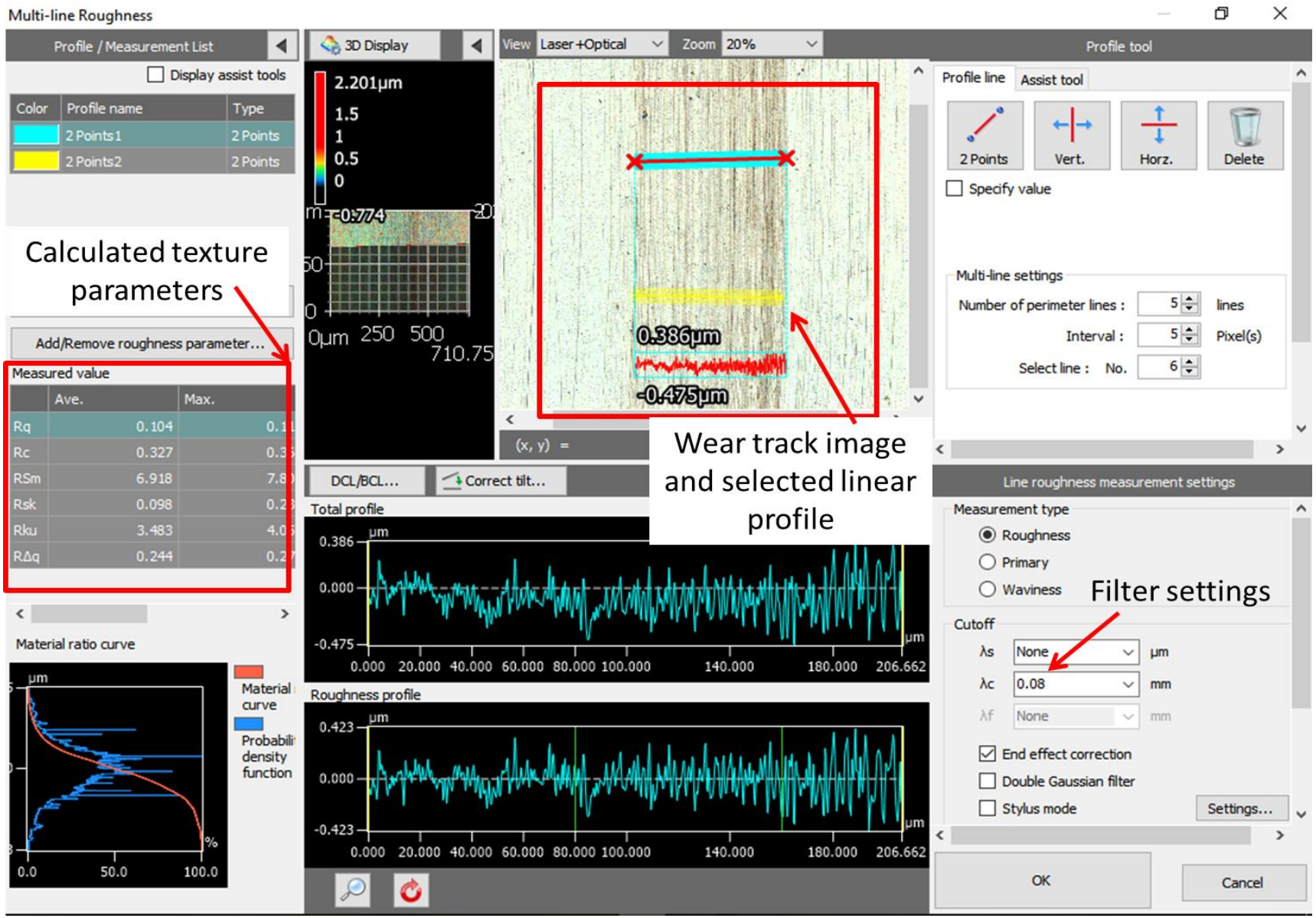

Figure 3.7 Calculation of profile texture parameters on the wear track using multifile analyzer software interface.

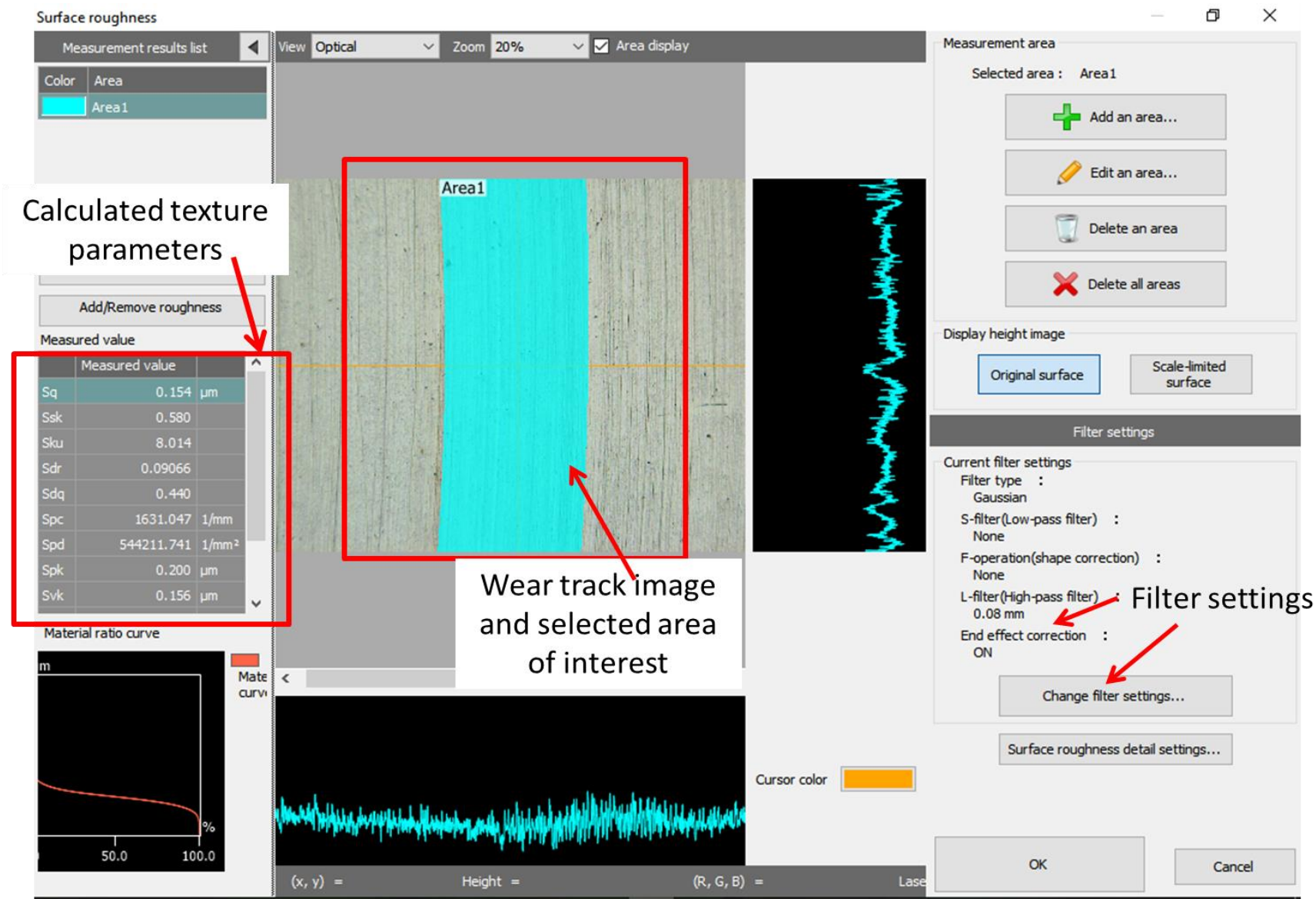

Figure 3.8 Calculation of areal texture parameters on the wear track using multifile analyzer software interface.

From a set of parameters defined in ISO standards [27], [87], tier I parameters were identified and used to study the evolution of surface texture. Table 3.1 lists the parameters of interest extracted from a multi-line roughness measurement shown in Figure 3.7 along with their description and interpretation in context of tribological properties.

Table 3.1 Description of profile parameters of interest (images from Keyence line roughness parameter guide available online [97]).

Profile parameters of interest			
Parameter	Meaning	Visual Description (illustration)	Interpretation
R_c (Mean height of profile elements) [98]	Average value of the height of the curve element along the sampling length	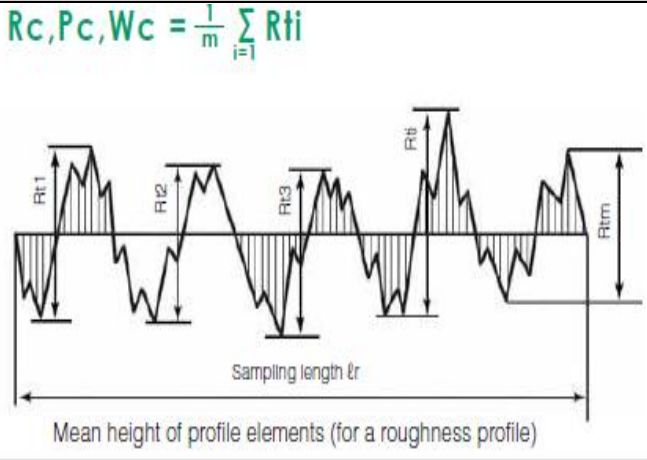	Indicates the average distance between peak and valley
R_{sm} (Mean width of the profile elements) [99]	Average value of the length of the profile element along the sampling length	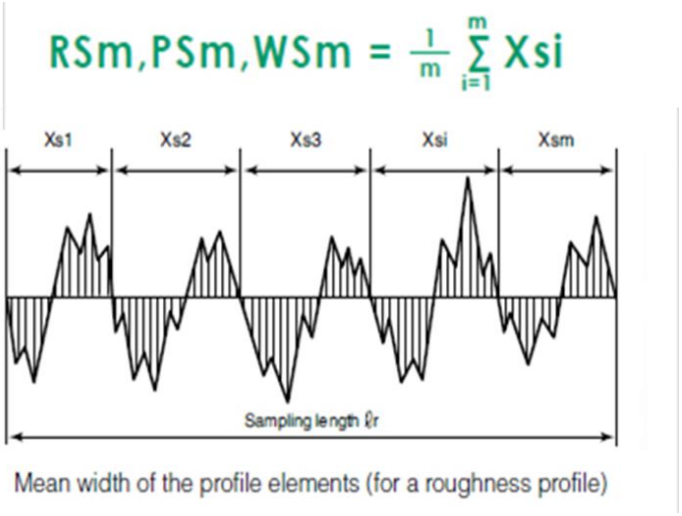	Indicates the periodicity of features (or presence of lay) in sampling direction

Table 3.2 provides description and interpretation of key areal parameters extracted by the process described in Figure 3.8, which were used for texture evolution study.

Table 3.2 Brief description of areal parameters of interest (images from Keyence areal roughness parameter guide available online [100]).

Areal parameters of interest			
Parameter	Meaning	Visual description (illustration)	Interpretation
S_q (Root mean square height) [101]	Areal surface roughness	$Sq = \sqrt{\frac{1}{A}\iint_A Z^2(x,y)dxdy}$ 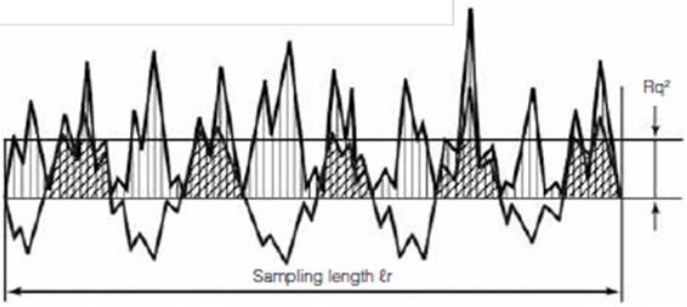 The figure is an example of Rq (root mean square deviation of a line). Sq is an areal extension of Rq.	Indicates the rms deviation of surface heights over the calculation area w.r.t mean plane
S_{pd} (Density of peaks) [102]	No. of peaks per unit area	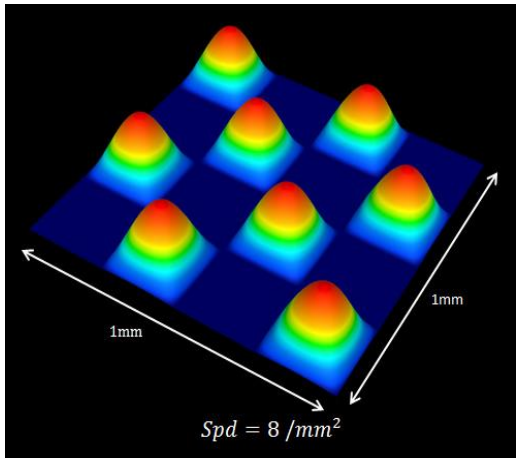	No. of contact points available on defined area
S_{pc} (Arithmetic mean peak curvature) [103]	Arithmetic mean of the principal curvature of the peaks	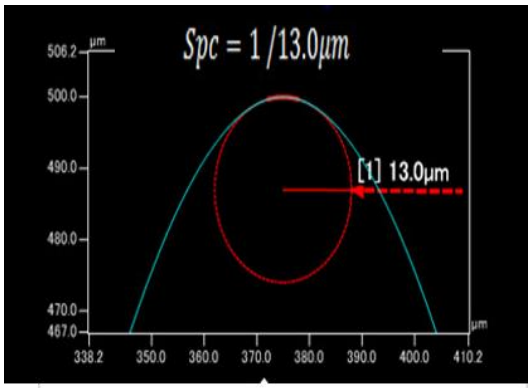 $S_{pc} = -\frac{1}{2}\frac{1}{n}\sum_{k=1}^{n}\left(\frac{\partial^2 z(x,y)}{\partial x^2} + \frac{\partial^2 z(x,y)}{\partial y^2}\right)$	Indicates sharpness of the peaks; Lower values suggest more rounded peaks

Above parameters were chosen from a set of height and feature parameters defined in ISO standards. These parameters carry information about the spatial height distribution of features along with the functional attributes of the features. [104], [105]

In addition to above height and feature parameters, functional, and functional volume parameters are also defined in ISO 25178. [27] These parameters are useful in determining the volumetric information about peaks and valleys on the surface extracted from area materials ratio curve (described in Appendix B). [106] Table 3.3 lists and describes functional and volumetric parameters and their interpretation in context of comparative analysis/interpretation of results for textured and untextured discs presented later. Even though these parameters carry valuable information about the bearing properties of materials, they were not considered for evolution study. Since the definition of core volume (volume of material between 10% and 80% materials ratio) was different for each sample, a comparison between sample surfaces at different time intervals was not meaningful. However, they were used to compare between raw textured and untextured discs (before tribotesting) to gain more insights on possible lubrication mechanisms.

Table 3.3 Description of selected functional and volumetric parameters from ISO set (images from Keyence areal roughness parameter guide available online [100]).

Parameter	Meaning	Visual Description (illustration)	Interpretation
S_{pk} (Reduced peak height) [107]	Mean height of peaks above the core surface	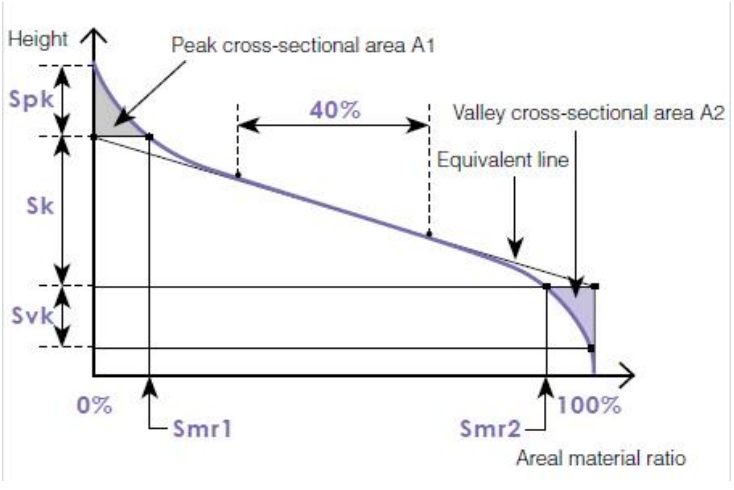	Indicates the nominal height of material peaks that are worn off during break-in stage

Table 3.3 (Cont.)

Parameter	Meaning	Visual Description (illustration)	Interpretation
S_{vk} (Reduced valley depth) [108]	Arithmetical mean of the reduced valley depth	See above for illustration of materials ratio curve 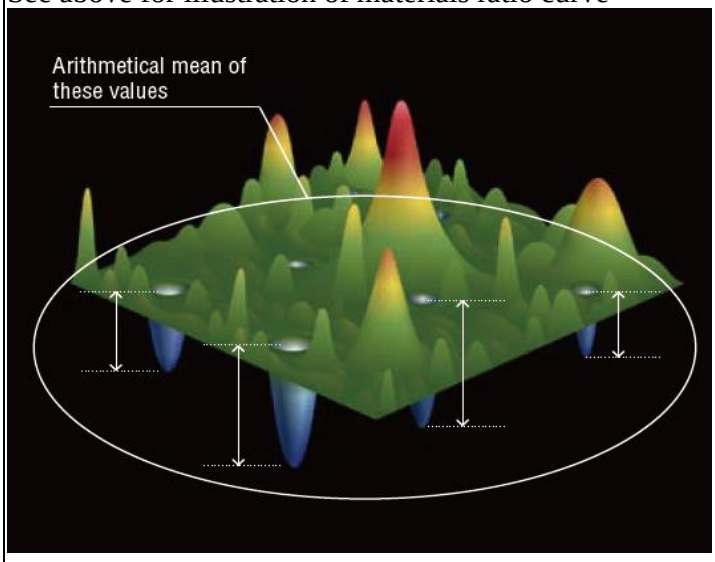	Indicates the nominal depth of valleys below core surface where lubricant or wear debris may get stored
V_{vv} (Dale void volume) [109]	Volume of voids at 80% material ratio curve (80% is default value according to ISO 25178 standard)	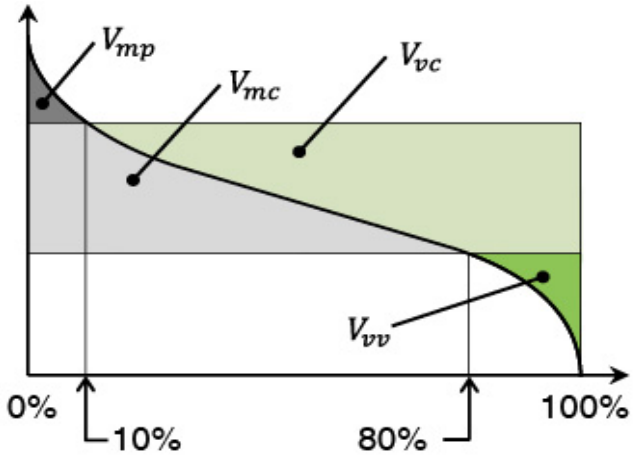	Used to identify the total volume of deepest valleys (lubricant retention) on the surface that are not affected by material wear
V_{mp} (Peak material volume) [110]	Volume of peaks at 10% (ISO default value) material ratio curve	See illustration of materials ratio curve and V_{mp} above	Used to identify the total volume of tallest peaks that get worn off during operation

As shown and discussed in the above table, these parameters were helpful in terms of comparing the functional nature of surfaces. Higher S_{pk} value indicates the presence of high

peaks above the core material surface and V_{mp} characterizes their volume. In tribological contact, these high peaks provide initial contact with smaller contact area (high stress) and thus get worn off. [104] Similarly, higher S_{vk} and V_{vv} values indicate presence of deeper valleys on the surface that may be useful for better lubricant retention and better entrapment of wear debris. [106]

Surface texture parameters described above were used to characterize the evolution of texture as a function of time specific to the height and spatial distribution of features. Apart from specific information assessed using individual texture parameters, collective analysis of all the texture parameters is also discussed in context of lubrication mechanism and tribofilm evolution in Chapters 5 and 6.

The next chapter discusses the details of tribological experiments and feasibility tests, identification of texturing technique, planning experiments, and identification of parameter matrix. This is followed by discussion and interpretations of the results and future directions.

4. EXPERIMENTAL DETAILS AND TECHNICAL APPROACH

This chapter discusses the feasibility and planning experiments along with the details of the experimental procedure and parameter matrix used for tribological testing. As a part of the feasibility studies, different texturing methods were explored as discussed below.

Two research objectives that were identified in Chapter 2, and the corresponding theme of the experiments, are schematically represented in Figure 4.1.

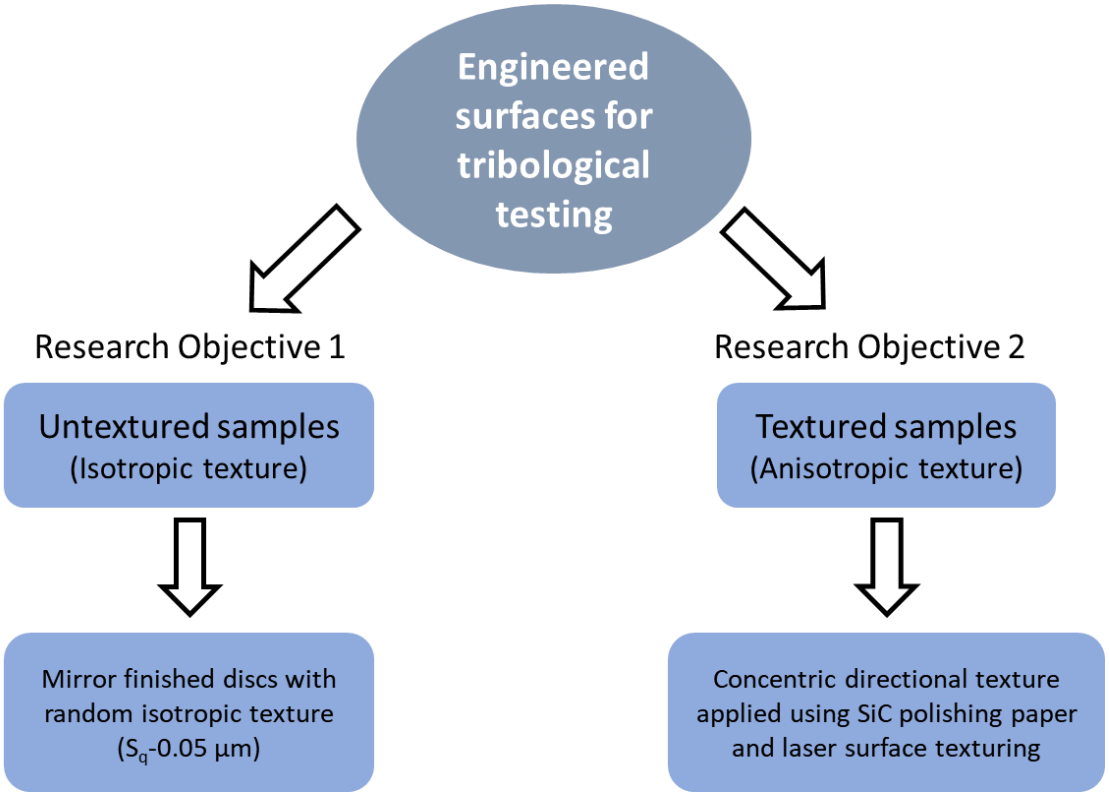

Figure 4.1 Outline for the experiments.

As depicted in Figure 4.1, two types of textures were studied:

i. Research objective 1 (Untextured discs): Starting surface texture was isotropic with no previous directionality of surface asperities.
ii. Research objective 2 (Textured discs): Directional concentric texture was applied to the steel discs using laser texturing and mechanical polishing with SiC abrasive paper. The

resultant texture had surface asperities directionally oriented with respect to the circular motion in a pin-on-disc rotational setup used for the experiments.

For each starting texture, controlled tests were performed to study the trend of frictional response. From the observed trends, different time intervals were chosen for studying the evolution of texture in correlation with the tribofilm and frictional response.

A. Research Objective 1 - Planning Experiments with Untextured Discs

For studying the evolution of isotropic starting surface texture on the mating of untextured surfaces, a pin-on-disc tribometer setup was used. The rotational setup was chosen because it allowed testing at constant linear speed and provided an advantage when studying texture evolution (see Appendix A for details). The experiments were performed using hardened 52100 steel balls and discs (both ball and disc hardness ~ 60 HRC). Hardened steel was chosen for experiments because it is widely used in many industrial applications [111] involving harsh lubrication conditions. The disc surface was polished to a mirror finish (S_q ~ 0.04 µm) using a commercial contract lapping service. This polishing process ensured that there was no previous directionality to surface asperities. The mirror finished discs were used as received without any additional surface treatment. Hardened mirror finished 52100 steel balls (S_q~0.04 µm) were purchased commercially and were used as received.

Nano-engineered lubricant (NL) formulation used during this research was prepared using the methods described in previous studies. [1], [3] Commercially available micron-sized MoS_2 powder (Alfa Aesar) was chemo-mechanically processed under dry and oil milling conditions in a high energy ball mill, resulting in the formation of intercalated MoS_2 nanoparticles capped with hydrocarbon chains. The nanoparticles had an ellipsoid shape with an average particle size of 100-200 nm. A detailed description of the processing steps and

characterization is described in previous reports. [1]–[3] The lubricant formulation used during the experiments was prepared by adding 1% by weight solid MoS_2, 1.5% by weight canola oil (ADM), and 0.5% by weight phospholipid (lecithin, Alcolec-S) to a poly alpha olefin (PAO) base oil. The base oil had a kinematic viscosity of 10cSt at 100 °C. Functional organic additives (canola oil and lecithin) provided suspension stability and extreme pressure (EP) properties to the lubricant mixture.

The time intervals of interest for studying the evolution of an isotropic texture were identified from planning experiments. The trend in the coefficient of friction (COF) vs. time was observed to create an experimental parameter map for further experimental study. Table 4.1 lists the experimental parameters that were used during planning experiments.

Table 4.1 Details of planning experiments for untextured discs.

Tribological Testing Parameters (Control tests)	
Materials	Hardened (60 HRC) mirror finished (S_q ~ 0.04 µm) 52100 steel disc and ball
Load	20 N
Speed	1 cm/s
Stop condition (time duration of the test)	10000 laps (time - approx. 8.5 hours)
Lubricant	3 drops (approx. 0.1 ml) of nano-engineered lubricant (NL) formulation

The load and speed were chosen to simulate a boundary-to-mixed lubrication regime while the stopping point was chosen to ensure that the COF values reached a steady-state value. The test was repeated three times to measure consistency in the observed COF trend and its repeatability. It is important to note that since the interaction between the asperities and lubricant is a stochastic event, emphasis was placed on identifying the representative trends observed during tribotesting experiments and for interpreting the results.

Before the test, both the disc and the ball were sonicated in acetone for 10 minutes. The lubricant formulation was also sonicated to ensure the uniform mixing of additives in the base oil. The load arm of the equipment was balanced to 'zero load' condition using the balance weights before placing the 20 N load. The radius of the wear track was kept at 5 mm. The testing parameters and the stop condition were input into the software interface as highlighted by red boxes in Figure 4.2. Before starting the test, the disc and the ball were cleaned with isopropyl alcohol to remove any contaminants from the surface and three drops of lubricant were carefully applied on the disc surface using disposable transfer pipets. After the test, the sample disc and ball were removed and dipped in hexane to remove excess oil. The same testing and cleaning protocol was used for all further tribological testing experiments.

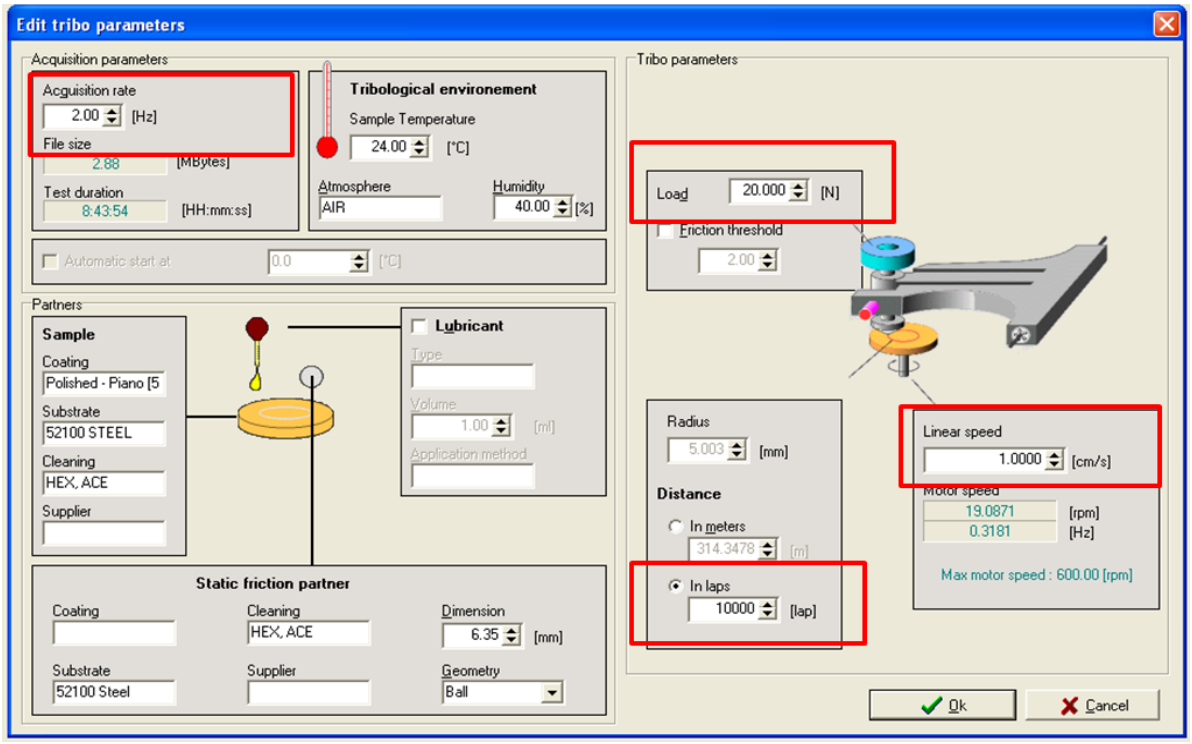

Figure 4.2 Screenshot of tribological testing software interface.

Figure 4.3 shows the results of the tribological control experiments on the untextured discs showing the plot of COF vs. time (indicated by number of rotational laps). The friction

plots show three distinct regions: a region characterized by an initial rise in friction (R1), a region characterized by a steady drop in friction (R2), and a region characterized by a stable steady-state friction (R3). Also, as seen from the figure, the trend in COF behavior was consistent and repeatable across three tests. Hence, these experimental parameters were finalized for detailed experiments to study the evolution of texture as a function of time (number of laps). Time intervals were chosen to understand the evolution of texture and tribofilm in these three regions. The experiments were conducted using nano-engineered lubricants (NL) and with base oil for comparison and the results are discussed in Chapter 5.

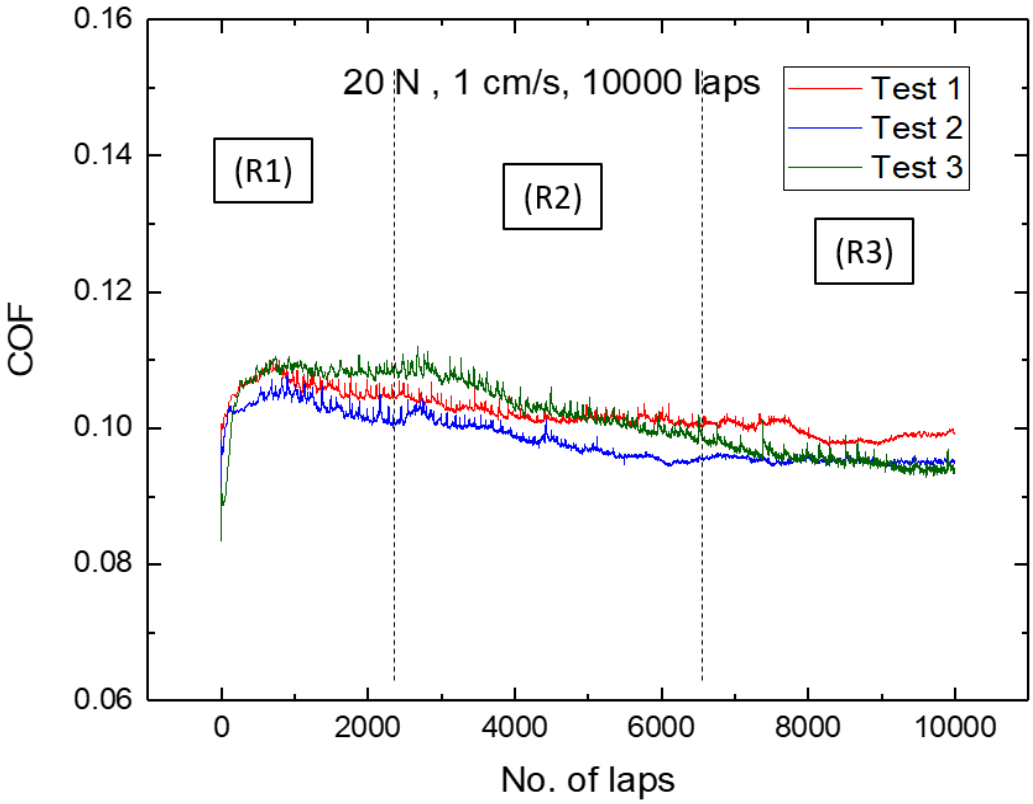

Figure 4.3 Control tests with untextured discs for identifying parameter matrix.

Table 4.2 shows the parameter matrix used for experiments using untextured discs to study the evolution of isotropic surface texture and tribofilm. The time intervals were chosen to understand the behavior of texture and tribofilm in the three regions identified above.

Table 4.2 Parameter matrix for studying evolution of texture using untextured discs (Research objective 1).

		Region 1 (R1)		Region 2 (R2)		Region 3 (R3)	
	Time intervals / Analytical tools	1000 laps	2000 laps	4000 laps	5000 laps	7000 laps	Control 10000 laps
FUNCTIONAL	COF						
	Wear Scar Diameter (WSD)						
	Trend						
PHYSICAL / STRUCTURAL	Laser Microscope (Texture)						
	SEM						
	TEM Tribofilm						
CHEMICAL							
	Raman						
	EDS						

The experimental analysis and measurements were divided into three types of analysis: 1) functional, 2) physical, and 3) chemical. The functional characterization of samples was performed to understand the friction and wear behavior of lubricants and was carried out by analyzing the tribotesting data (COF plots and observed trends) and by analyzing the wear scar diameter (WSD). Surface texture measurements were performed using a Keyence VK-X 250 microscope on the samples to understand the evolution of surface texture (distribution of surface features in terms of height, spatial arrangement, and functional attributes such as peak curvatures) at microscopic and sub-microscopic level length scales as a function of time. The

surface morphology of the wear scars was analyzed using SEM and optical micrographs. Tribofilm chemistry was studied using a Raman microscope and EDS mapping to understand the chemical composition of the tribofilm compounds and to evaluate tribofilm coverage. The sub-microscopic interactions between the tribofilm and the surface were studied using cross-sectional TEM. The results of these experiments are discussed in detail in Chapter 5.

B. Texturing Techniques and Selection

From the results of the experiments on untextured discs, the directionality of texture in alignment with the motion in a pin-on-disc setup was identified as a key design parameter. Since the pin-on-disc setup was used in a rotational mode, directional texture was applied on discs in the form of concentric circular grooves. The two methods were explored to fabricate directional texture on the steel discs are described below.

I. Laser surface texturing (LST)

Laser surface texturing (LST) has been widely used for fabricating different texture patterns on surfaces for tribological applications. [112]–[114] LST allows control over surface features and can be used with a wide variety of materials including metals, ceramics, and polymers. [47], [113] In a typical laser texturing system, a pulsed laser with nanosecond, picosecond, or femtosecond pulse duration is utilized to selectively etch the material surface. The laser beam is focused on the material surface and a high amount of energy is deposited into the material in short pulses leading to local material ablation. It was also noted that shorter pulse duration (pico to femto) are beneficial to reduce the heat affected zone and the formation of undesirable burrs/defects around the etched area. [115], [116] The solid works/CAD design file containing the desired surface patterns (including size, shape and distribution of features) is used to drive the laser movement. The process is optimized by controlling processing variables such

as laser power, laser spot size, and the speed of laser movement. This control ensures the desired pattern is replicated on the material of choice.

For this research, LST was performed on 52100 steel discs with the help of a commercial laser job shop (Providence Texture, http://providencetexture.com/) using a femtosecond laser system. Figure 4.4 shows the circular groove design that was finalized for the experiments. Only part of the disc was textured to make the process timely and cost effective. The groove width was chosen based on instrument capability, resulting in a 2:1 aspect ratio (depth ~ 10 µm). Pitch was kept at 30 µm to ensure at least five grooves were in contact with the ball at the start of the test (initial contact area diameter was estimated to be 150 µm assuming Hertzian point contact).

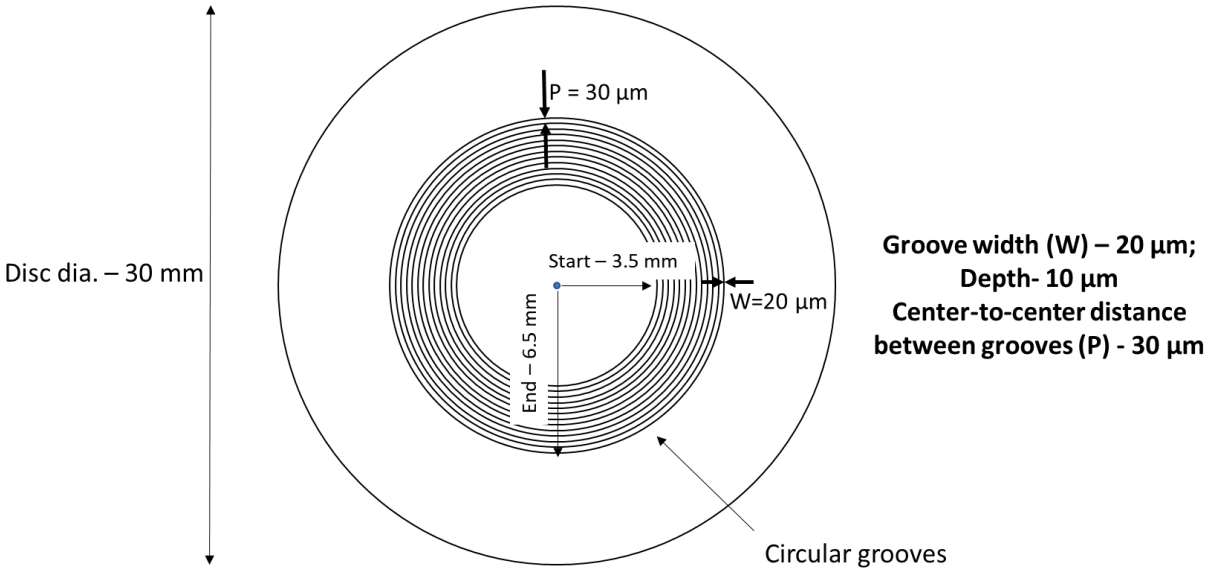

Figure 4.4 Circular groove design for LST of 52100 steel discs.

The processed samples were characterized using a laser microscope to ensure that the design specifications were met. The images confirmed (Figure 4.5 - left) that the specified pitch (30 µm) and depth (10 µm) was fabricated on the steel discs. However, some material re-deposition along the groove edges was also observed. Additional polishing was performed (Figure 4.5- right) using diamond paste (2 µm particle size) to remove the material re-deposition

on the edges and surface of the grooves. Polished disc samples were then used for feasibility and planning experiments discussed below in Section 4-C.

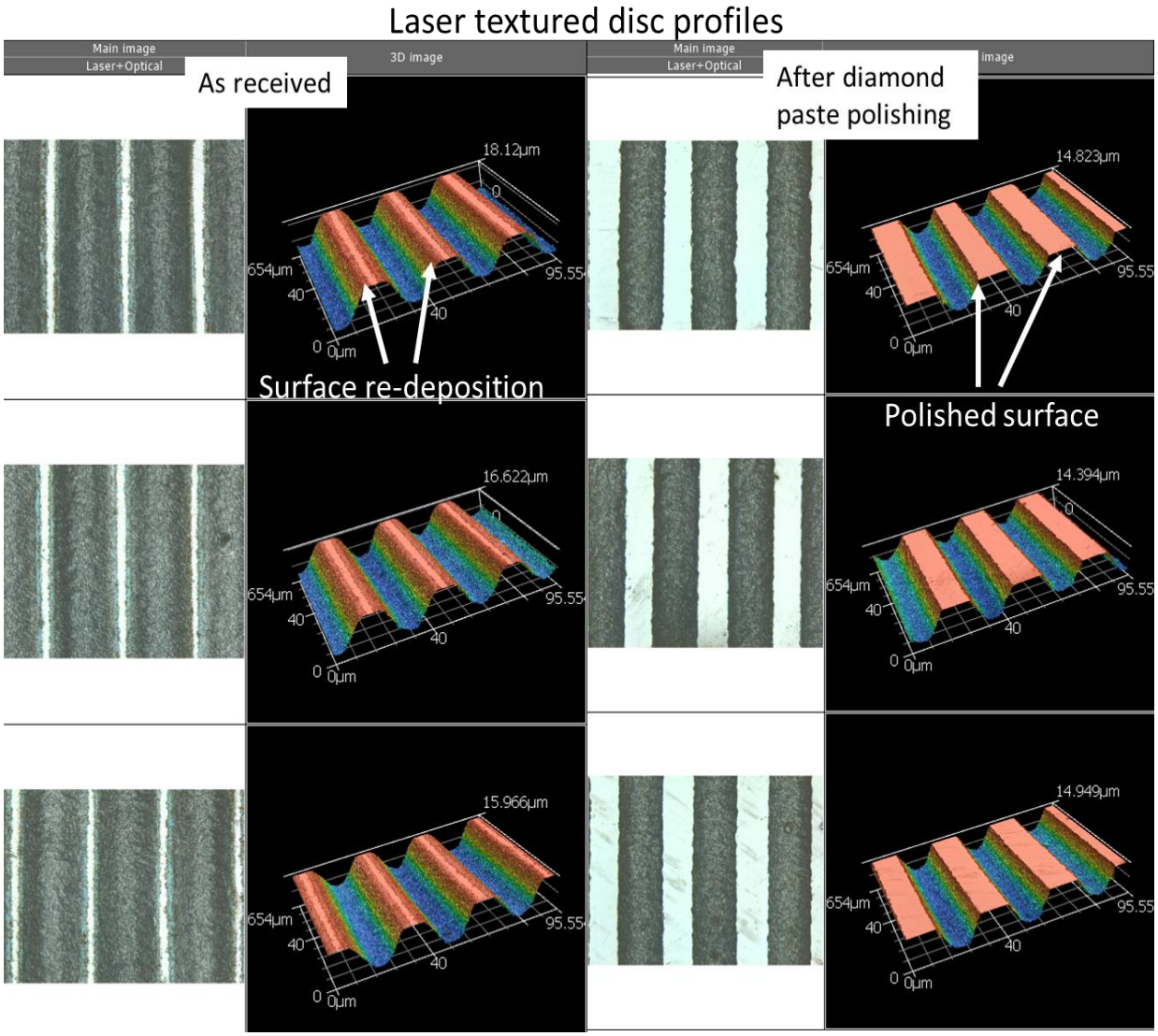

Figure 4.5 Comparison of as received and polished LST disc profiles.

II. Mechanical Polishing

In addition to LST, directional concentric texture was also applied on to the steel discs by using SiC abrasive papers. The feasibility experiments were carried out by texturing steel discs using manual polishing setup on a Buehler Ecomet 300 grinder/polisher [117] with different grit sizes of SiC abrasive papers (Buehler CarbiMet). [118] After the feasibility experiments

confirmed the effectiveness of mechanical polishing (Figure 4.8), a vertical milling machine setup as shown in Figure 4.6 was used to fabricate textured discs for further experiments. Milling machine setup was chosen over manual polishing as it offers better process control in terms of concentric alignment of asperities and because it is scalable to process a large volume of discs. Adhesive-backed SiC paper was put on a flat circular chuck mounted on the milling machine head as shown. The disc was centered (to ensure a concentric texture was applied) with respect to center of milling machine head and held flat with the help of steel plates and a jaw assembly. The rotating chuck with abrasive paper was lowered and held in contact with the disc at fixed load for 2 minutes resulting in concentric scratches on the steel disc. It should be noted that milling machine setup was used to perform abrasive polishing on steel discs and no actual milling operation was performed.

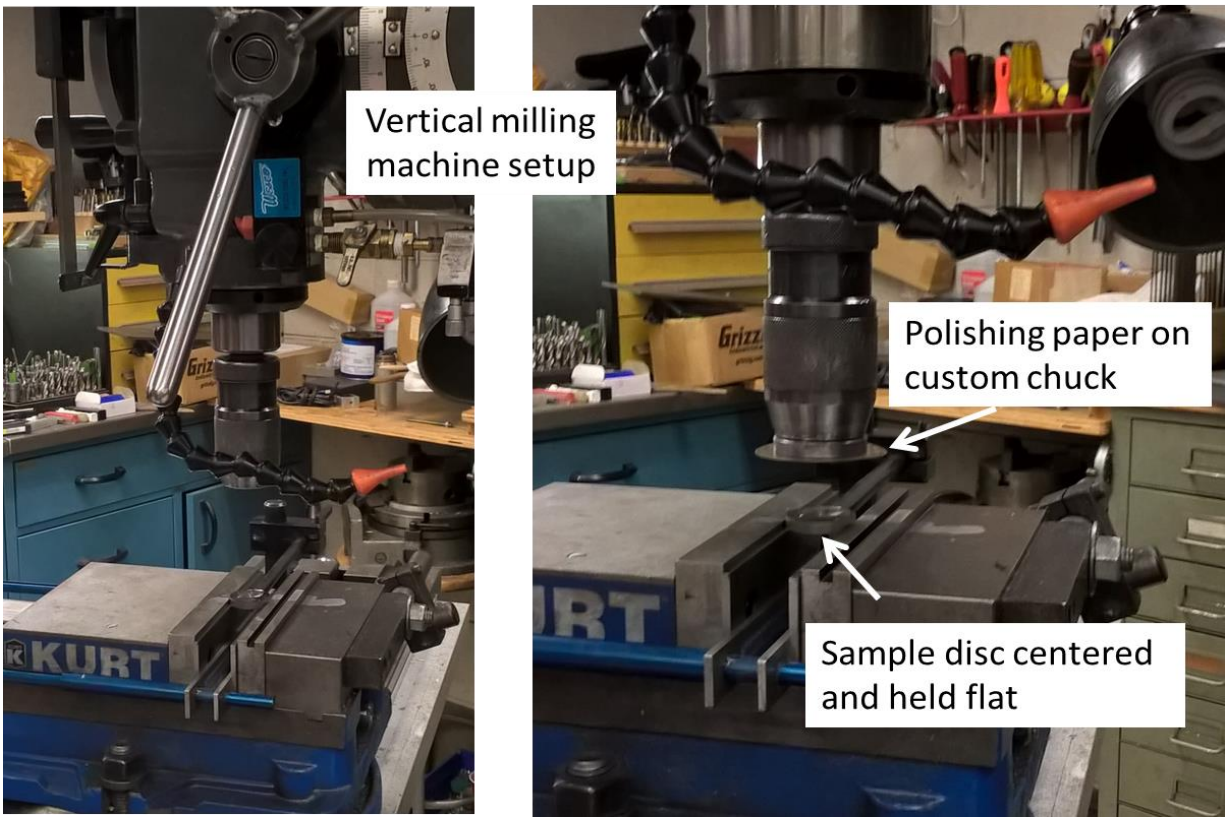

Figure 4.6 Vertical milling machine setup used for mechanical polishing (photo by author).

A comparison of surface profiles on two textured discs (textured using LST and P1200 grit size SiC paper) is shown in Figure 4.7. The surface profiles shown in the figure were taken perpendicular to the texture direction. As seen from the figure, the LST disc had a precise pattern where the distance between the adjacent grooves and their height was fixed as per the desired design specifications. On the other hand, the mechanically textured discs had a locally random distribution of surface asperities (in height and width, Figure 4.7) and yet showed directional texture on a large scale where the concentric abrasion marks could be seen on the disc surface.

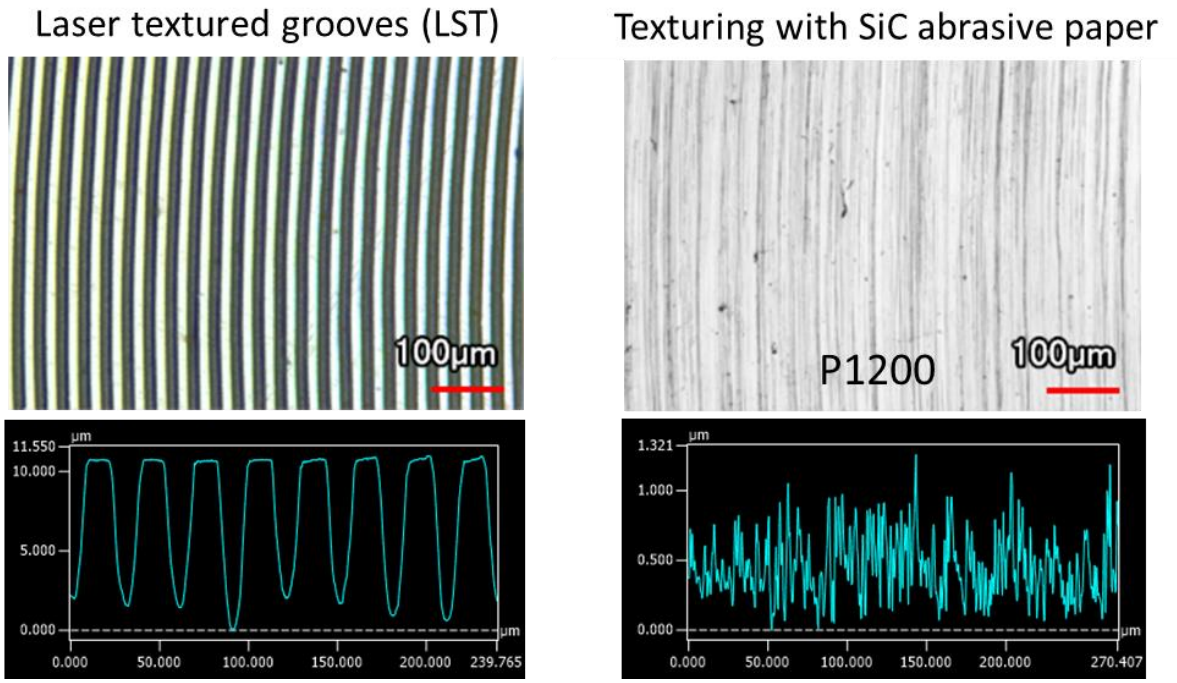

Figure 4.7 Comparison of LST and P1200 grit size textures; surface profiles measured perpendicular to the orientation of texture.

C. Research Objective 2 – Feasibility and Planning Experiments with Textured Discs

I. Choice of texturing method

The textured discs fabricated by LST and mechanical polishing were evaluated using tribological tests during the feasibility stage. The tests were performed using the same parameters (load, speed, lubricant, and time duration) used for the control tests on the untextured

discs listed in Table 4.1. Figure 4.8 shows COF plots for feasibility tests on textured discs. The results show a comparison between the LST disc and the mechanically polished discs using three different grit size polishing papers (P400, P800, P1200). It should be noted that a lower grit size number corresponds to coarser abrasive grain size and thus P1200 polishing paper would result in a finer texture than P400 paper.

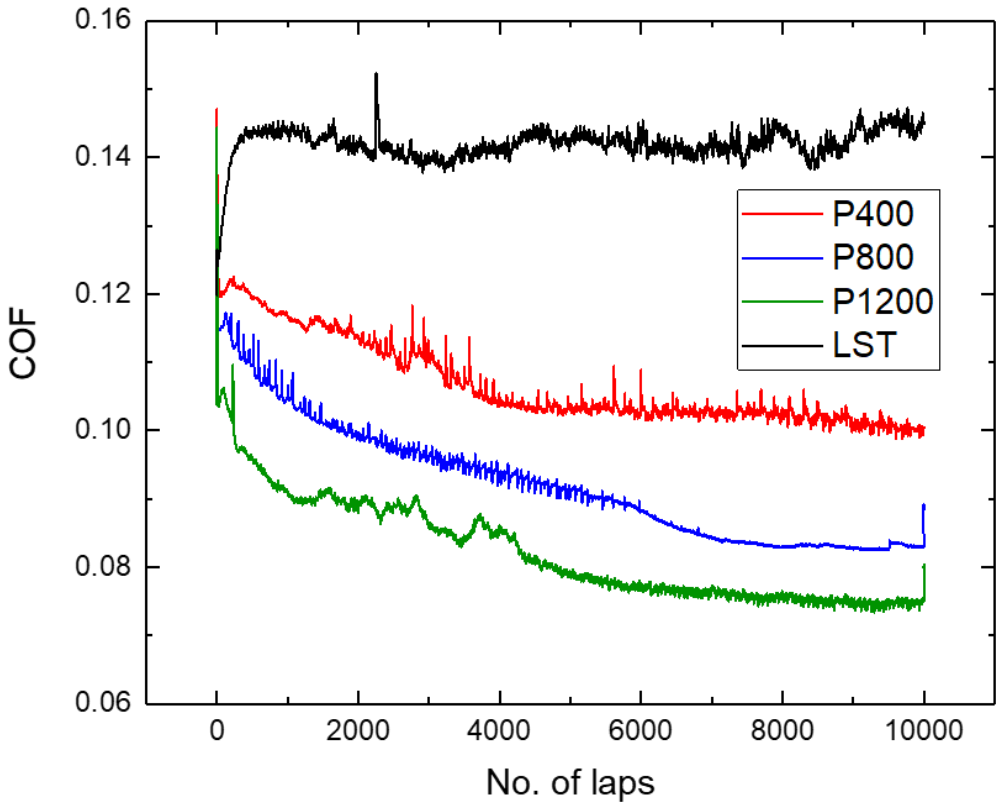

Figure 4.8 Frictional response of textured discs.

From the results, it was found that laser textured grooves were not suitable (see Appendix C for more details) under the tribo-testing parameters used and showed a very high COF value (Figure 4.8) and severe wear on the disc and the ball. Among the mechanically polished discs, the P1200 polished disc showed the lowest COF values (possibly due to finer texture) which was the desired result. Hence, mechanical texturing with P1200 grit size SiC paper was chosen as the preferred texturing method for studying the evolution of textured surfaces.

In addition to the above tests performed with NL, another tribological test was carried out to compare effect of direction texture (applied using P1200 grit size SiC paper) on frictional response using base oil as lubricant. The comparison of frictional response between PAO and NL is shown in Figure 4.9. The frictional response trend observed for PAO with textured discs showed very high COF values. This was similar to the frictional response of PAO for untextured discs where very high friction and wear was observed. Since, the directional surface texture did not modulate the performance of the base oil, the time interval tests for studying the role of surface texture (research objective 2) were conducted by using a nano-engineered lubricant (NL).

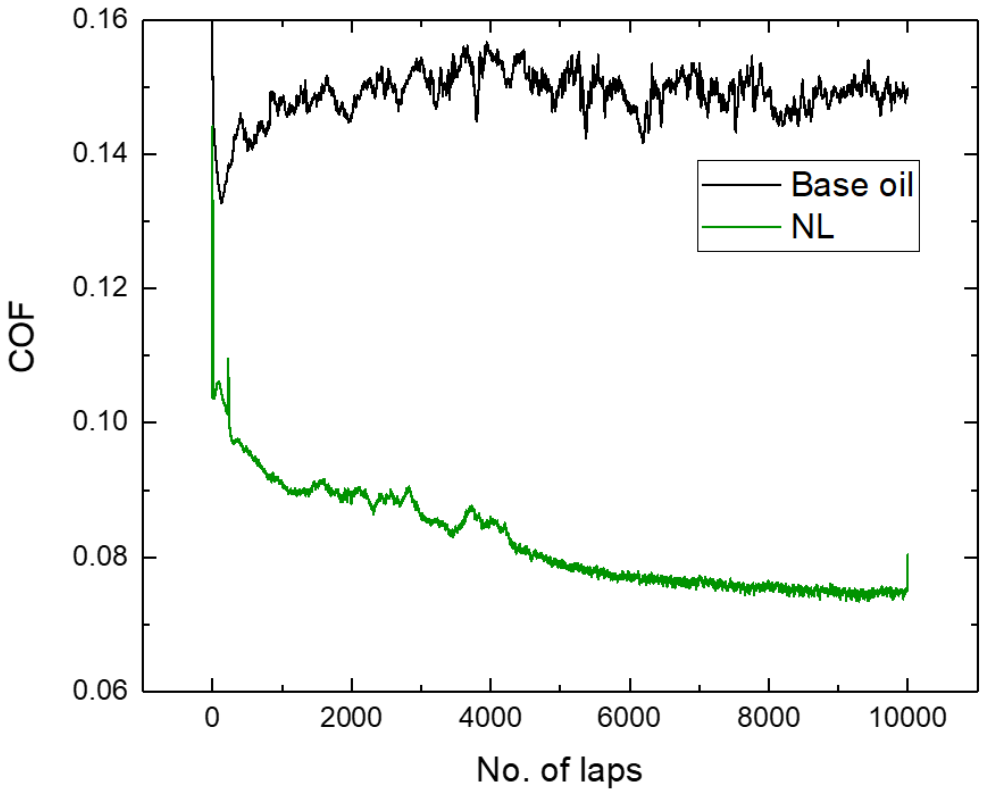

Figure 4.9 Comparison of frictional response of base oil and NL for textured disc.

II. Planning experiments and parameter matrix

After the texturing method and lubricant were chosen as described above, planning experiments were conducted with textured discs (P1200 grit size) in order to measure the

consistency in COF trends and to identify time intervals of interest. The experimental procedure and tribological testing parameters were not changed from methods described in Section 4-A. The results of control experiments on textured discs using NL are shown in Figure 4.10. Three regions of COF evolution can be identified from the figure. Initially, in region 1 (R1), COF started very high (at 0.16 as compared to 0.09 observed in case of untextured discs) before dropping sharply to lower values within first 50 laps, followed by a slight increase. In region 2 (R2), around 1000 laps, the COF started to drop down steadily till reaching the steady-state COF values in region 3 (R3) around 6000 laps. The COF behavior and trend showed consistent and repeatable behavior, so the experimental technique was chosen for further experiments.

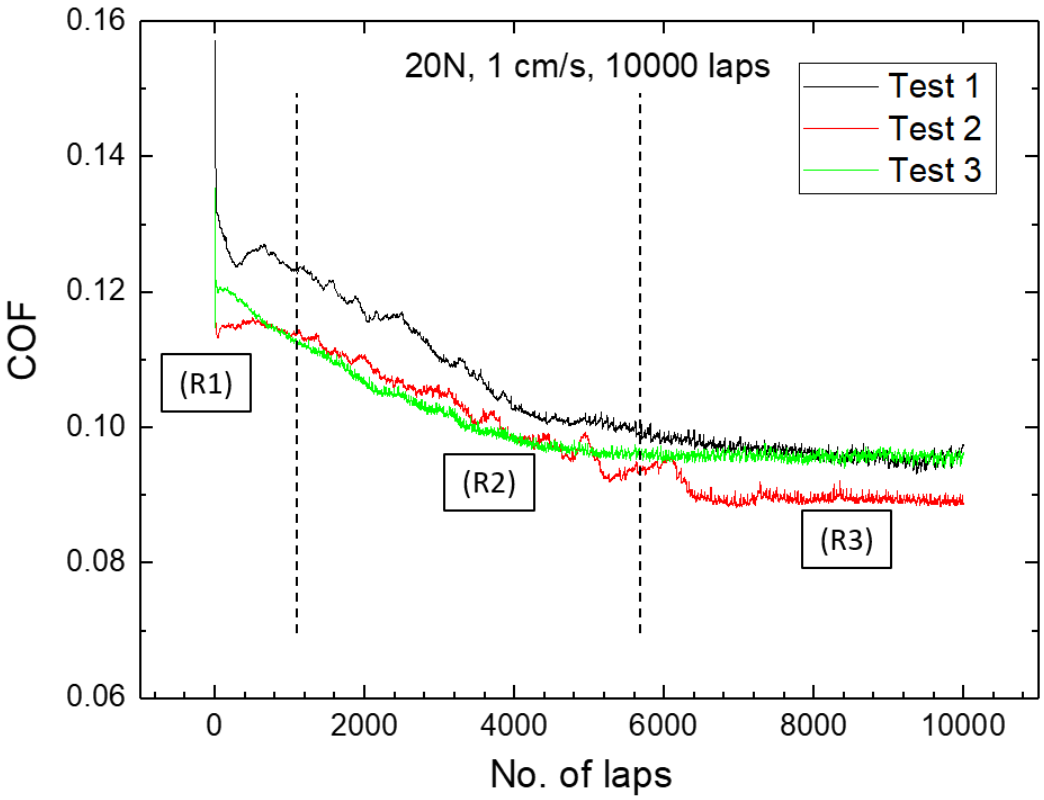

Figure 4.10 Control tests with textured discs for identifying the parameter matrix.

Table 4.3 shows the parameter matrix used for experiments to study evolution of the fabricated texture and its role in manipulating the tribofilm properties. Time intervals

(experimental variable) were chosen to investigate the behavior of texture and tribofilm in each region identified above and are listed in the top row of the table.

Table 4.3 Parameter matrix for experiments on the evolution of texture on anisotropic textured discs (Research objective 2).

		Region 1 (R1)			Region 2 (R2)			Region 3 (R3)		
	Time intervals / Analytical technique	200 laps	500 laps	800 laps	2000 laps	3500 laps	5000 laps	7000 laps	8500 laps	Control 10000 laps
FUNCTIONAL	COF									
	Wear Scar Diameter (WSD)									
	Trend									
PHYSICAL / STRUCTURAL	Laser Microscope (Texture)									
	SEM									
	TEM Tribofilm									
CHEMICAL	TEM Tribofilm									
	Raman									
	EDS									

Similar to the parameter matrix presented for untextured discs (Table 4.2), the analysis and measurements were divided in three parts: 1) functional, 2) structural/physical, and 3) chemical. The same characterization tools and techniques (listed in the table column) and

measurement methodology described above in Section 4-A were used to understand the role of surface texture in the manipulation of tribofilm formation and evolution. The TEM analysis was focused on understanding sub-microscopic events at the individual asperity level. Based on the results of functional (COF plots and wear data) and physical analysis (SEM and surface texture measurements), one sample was picked from each stage (R1, R2 and R3) for TEM analysis.

The experimental results for the textured discs in the presence of NL were compared to the results for untextured discs for comparative analysis and interpretation. Chapter 5 presents the results of the experiments on untextured discs and discussion of the process mechanism (research objective 1). Chapter 6 is focused on experimental results and discussion on textured discs along with process mechanism (research objective 2). Chapter 7 provides the concluding remarks as well as future directions for this research.

5. RESULTS AND DISCUSSION - RESEARCH TASK 1

This chapter discusses the results of the experiments performed according to the parameter matrix developed in Table 4.2. Figure 5.1 shows the results of control tests along with the three identified lubrication regions defined as break-in, development, and steady-state. Additionally, the time intervals (no. of rotational laps in a tribotest) chosen for the experiments are marked on the plot by solid black lines.

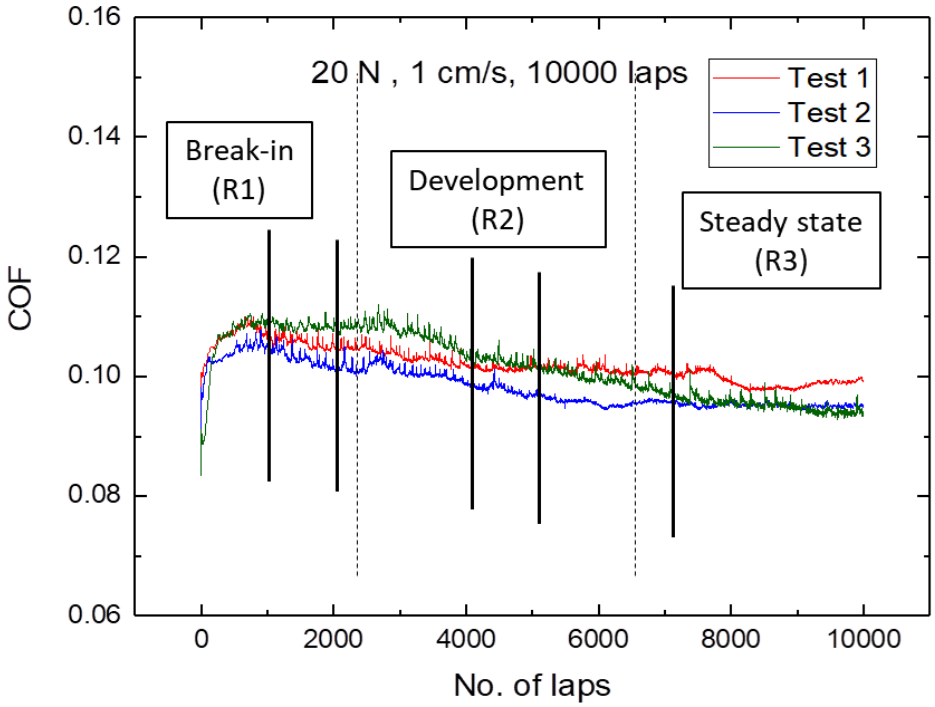

Figure 5.1 Identification of the three stages of lubrication and tested time intervals.

The proposed lubrication mechanism during the three stages of lubrication defined in Figure 5.1 is discussed below:

1. Break-in stage (R1): At the start of the tribological tests, there is direct asperity-to-asperity contact while operating under boundary lubrication. As a result, the COF increases while the surface asperities re-organize and re-align in the direction of relative motion. This self-adjustment of surface asperities under the applied load in the initial

stages of motion is termed as ‘break-in’ and has been widely recognized in automotive applications. [119], [120] The energy dissipated due to increase in COF as well as the creation of broken-in (fresh surface exposed) reactive asperities is believed to result in the activation of tribo-chemical reactions between the lubricant and surface (as studied by Raman measurements described later).

2. Development (R2): As the tribo-chemical reactions progress with time, COF steadily drops down due to tribofilm formation. At the same time, the surface features (peaks and valleys) also stabilize and evolve along with the tribofilm towards a stable steady-state.
3. Steady-state stage (R3): Over time, the rates of tribofilm formation, shearing, and replenishment balance with rates of creation of fresh asperities and wear debris (together contributing to texture evolution). In this balanced state, stable COF values are observed.

Table 5.1 lists the details of experiments performed to study the evolution of texture and tribofilm using the isotropic starting texture (untextured discs) for the selected time intervals. Load and speed were chosen to simulate boundary/mixed lubrication conditions. The above discussed lubrication mechanisms were evaluated by the physical, chemical, and functional characterization of the tribofilm and surface texture as per the parameter matrix developed before (Table 4.2). As discussed previously, experimental parameters such as load, speed, and lubricant chemistry were not changed, and time was the only parameter that was varied. Tests were also conducted using pure base oil (PAO) as a lubricant for comparative reference and analysis. The time intervals listed in Table 5.1 were chosen to represent three stages of lubrication proposed above. Each test was repeated three times to measure the consistency of the coefficient of friction (COF) trends. Functional, physical, and chemical characterization and analysis of samples tested at different time intervals is presented below along with the interpretation of results.

Table 5.1 Experimental details for studying evolution of texture using untextured discs.

Tribological Testing Parameters (Research Objective 1)	
Materials	Hardened (60 HRC) mirror finished (S_q ~ 0.04 µm) 52100 steel disc and ball
Load	20 N
Speed	1 cm/s
Stop condition (duration)	Break-in (R1) - 1000 laps, 2000 laps Development (R2) - 4000 laps, 5000 laps Steady-state (R3) - 7000 laps
Lubricant	3 drops (approx. 0.1 ml) nano-engineered lubricant (NL) and pure base oil (PAO)

A. Functional Analysis: COF, Wear Scar Diameter (WSD) and Trends

The COF plots (COF vs. time) obtained from the tribological tests for all tested time intervals are presented below. WSD on the steel balls as well as optical images of wear track measured with a Keyence VK-X 250 microscope at 20X lens magnification are also presented.

I. 1000 laps and 2000 laps time interval samples - Break-in stage (R1)

Figure 5.2 shows the COF plots and wear scars from the break-in stage (R1) for base oil (PAO) and nano-engineered lubricant (NL). The results from 1000 laps test are shown in the left box while results from 2000 laps test are shown in the box on right side of Figure 5.2.

<u>COF plots comparison (top of Figure 5.2):</u>

COF comparison between NL and PAO is shown at the top of Figure 5.2 for 1000 and 2000 laps testing time. As seen in both the plots, the COF for PAO started increasing at around 200 laps (after about 10 mins of testing time) and eventually reached as high as 0.15 within first 500 laps (about 30 mins) of testing. Since PAO was unable to form a surface protective tribofilm, direct asperity-to-asperity contact was unavoidable under harsh BL conditions. This results in work hardening of the asperities and led to material wear. The presence of hardened wear particles along with direct asperity-to-asperity contact between the contacting surfaces resulted

in high COF values observed in the case of PAO. This process of the creation of wear debris particles and work hardening continued over time as indicated by high COF values presented in this section for all time intervals.

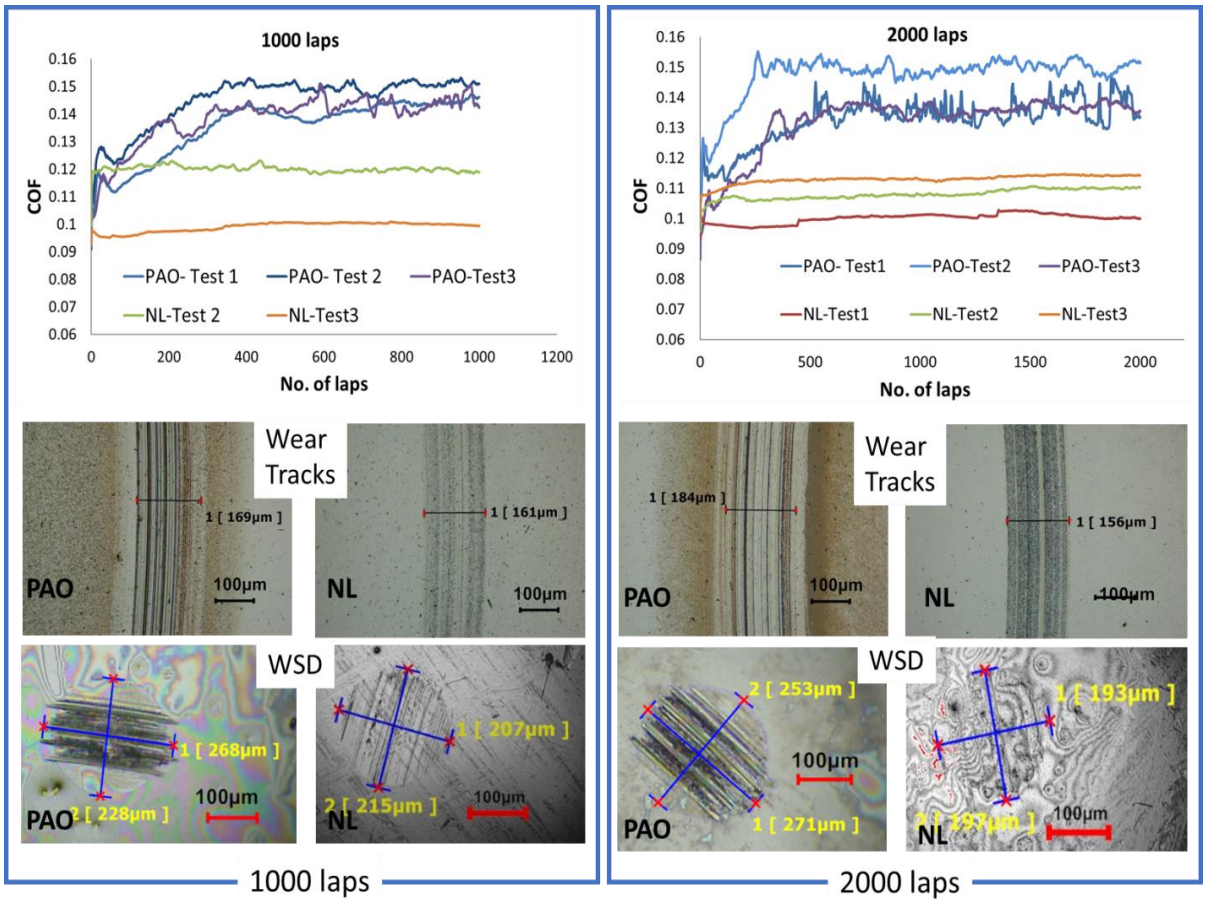

Figure 5.2 COF plots and wear scar images for the break-in stage (R1).

On the other hand, the COF trend observed for NL was consistent with (R1) trend in control tests (Figure 5.1) where the friction rose at the beginning of the test and then remained stable around 0.11-0.12 value (lower than PAO). This slight increase in COF was attributed to the interaction and re-organization/re-alignment of isotropic surface asperities before the start of tribo-chemical reactions. Variation in COF between repeat tests could also be seen and was attributed to the stochastic nature of asperity-to-asperity engagement expected during the break-in period under BL. However, it should be noted that even though the COF values varied from

test-to-test, the overall trend in COF remained consistent. A more detailed and holistic comparison between PAO and NL from a functional response point of view (COF plots and WSD trends) is presented in Section 5-A.III after results for steady-state at 7000 laps are shown.

Optical micrographs comparison (bottom of Figure 5.2) – 20X lens magnification:

Optical images of the wear tracks with PAO as lubricant showed evidence of surface wear as indicated by the presence of grooves (dark colored scratches on the wear track). Similar grooves were also observed on the wear scar diameter on the ball. This observation was consistent with the high values of COF noted above and was evaluated further by the surface roughness analysis and SEM images discussed later in this chapter. The optical images of the wear track in the case of NL showed a cluster of black spots that indicated the presence of lubricant agglomerates (confirmed by SEM/EDS mapping as described later) on the wear track. As compared to PAO, the degree of wear was small, as indicated by the lesser number of grooves observed on wear track and on the WSD. The cumulative variation in WSD as a function of time is included later at the end of this subsection.

Overall, the COF plots and wear scar comparison showed that NL protected the surface better than PAO under BL conditions as evidenced by lower COF value and lower WSD values.

II. 4000 laps and 5000 laps time interval samples - Development stage (R2)

Figure 5.3 shows the COF plots (top of the figure) and wear scar images (bottom) for base oil (PAO) and nano-engineered lubricant (NL) at time intervals of 4000 and 5000 laps.

COF plots comparison (top of Figure 5.3):

During the development stage (R2), the COF for NL dropped steadily to 0.09-0.1 after an initial increase was observed during R1. This trend at 4000 and 5000 laps was consistent with the observed trend for control tests (Figure 5.1). In addition, the variation in COF between tests was

relatively small (COF plots are clustered closer together) as compared to R1. This suggests once the tribofilm formed and developed during R2, the COF response showed more controlled behavior in the case of NL. PAO, on other hand, showed higher COF values than NL for both time intervals (around 0.14). The frictional response for PAO was also more erratic as indicated by the presence of random spikes and noise in the COF plots. These spikes in the COF could be attributed to presence of hardened wear debris in the contact region generated because of poor lubrication, as noted previously. The severity of wear and the presence of wear debris was confirmed by SEM imaging discussed later in this chapter.

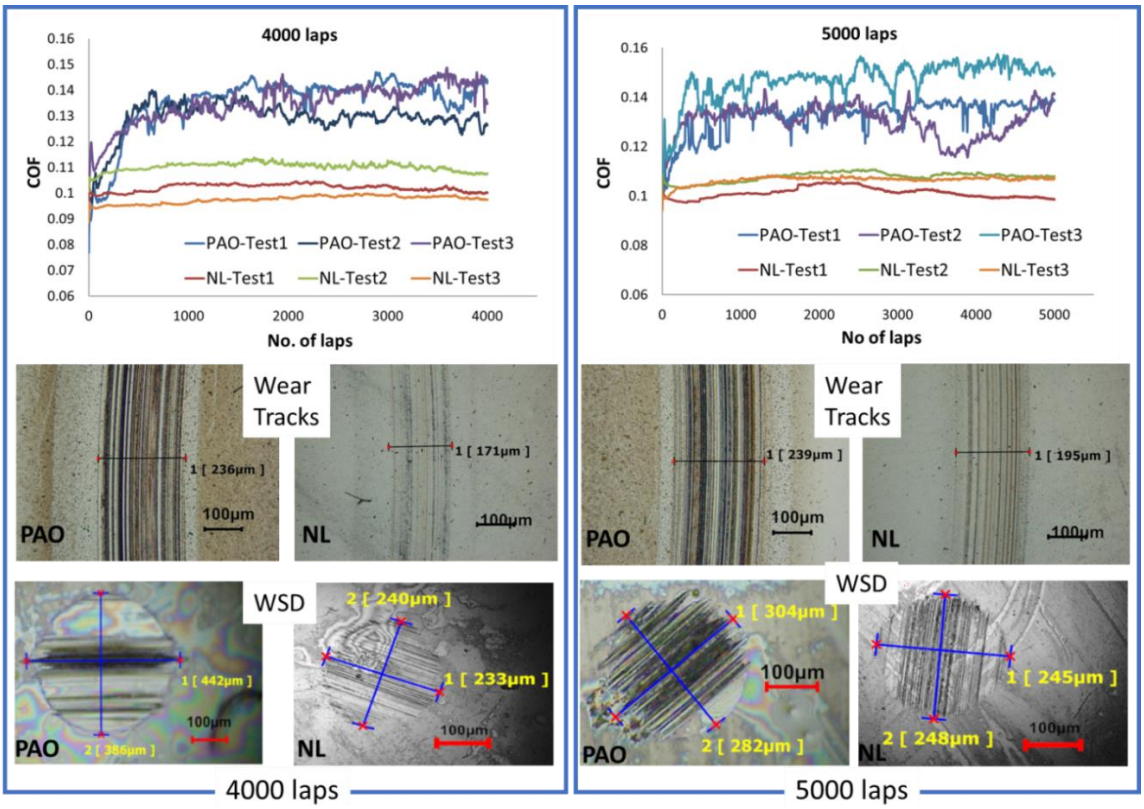

Figure 5.3 COF plots and wear scar images for the development stage (R2).

Optical micrographs comparison (bottom of Figure 5.3) - 20X lens magnification:

Optical micrographs (and SEM images discussed later) showed the presence of grooves in the wear track for PAO confirming the above interpretation of severe wear. Similar deep

grooves were also observed on the WSD indicating severe wear in case of PAO. Additionally, lower WSD values for NL as compared to PAO also confirmed that NL offered better boundary lubrication by protecting the surface better and reducing wear. Optical micrographs of the NL in R2 showed a lesser number of lubricant agglomerates (more reacted lubricant) on the wear track as compared to R1 as evidenced by the reduced number of black spots. This observation was consistent with the hypothesis that during R2, the progression of tribo-chemical reactions led to the formation and stabilization of the tribofilm (lubricant particles react with the surface asperities) which controlled the lubrication. These observations were further studied and confirmed using SEM imaging and Raman microscopy as discussed later in this chapter.

III. 7000 laps time interval samples - Steady-state stage (R3)

Figure 5.4 shows the COF plots (left) and wear scars (right) from the steady-state stage (R3) for base oil (PAO) and nano-engineered lubricant (NL) at 7000 laps time interval.

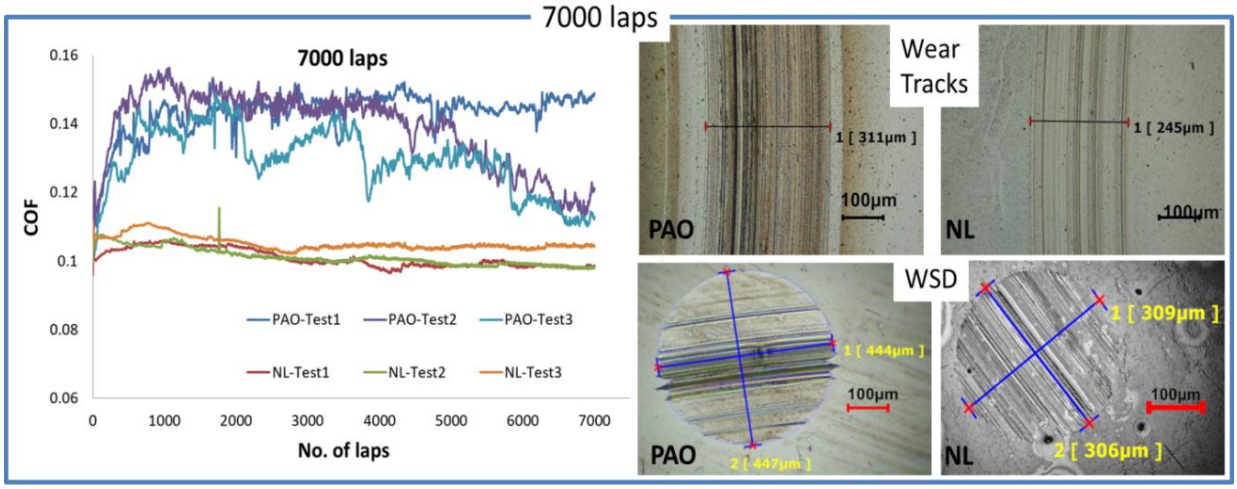

Figure 5.4 COF plots and wear scar images for the steady-state stage (R3).

COF plots comparison (left of Figure 5.4):

For PAO, similar to observations made in R1 and R2, the COF increased rapidly to about 0.15 within first 500 laps of testing. In general, the COF values for PAO showed more noise and

fluctuation, which was attributed to stochastic interaction between mating surfaces and wear debris under harsh BL conditions. The COF values dropped down at the end for Test 2 and Test 3 possibly because of the creation of complementary surface features on the disc and ball that could be seen in the optical micrographs. However, it should also be noted that the COF plots for PAO showed repetitive periods of local rise and drop (for example, from 2000 to 4000 laps for PAO-test 3). This suggested that under BL, and without surface protecting tribofilm, the surface asperities continuously deformed and wore off to form complementary surface features on disc and the ball. These events were highly stochastic (as highlighted by variation between repeat tests) and resulted in a local drop in COF; this process continued to repeat itself periodically.

In contrast, the COF for NL showed a more controlled frictional response that was attributed to formation of a stable surface protective tribofilm. The trend in COF was consistent with the observed trend for control tests where a stable steady-state COF was observed at the end of the test. Even though NL showed stable and lower steady-state friction values, the stochastic nature of tribological events was highlighted by variation in the trend between repeat tests in R1 and R2. The difference between the local trends for different tests was more noticeable up to the first 5000-6000 laps in Figure 5.4 (which corresponded to progression of events in R1, R2) where the surface texture and tribofilm evolved and stabilized as noted previously. A small spike was observed for NL-test 3 (green plot) around 1800 laps time duration which possibly was due to presence of a debris particle getting trapped in the contact region. Once the lubrication moved into steady-state, the COF plot trend was much more consistent between tests confirming the validity of steady-state behavior and the previously discussed lubrication mechanism.

Mean COF values calculated for the three tests in steady-state for NL were 0.102 ± 0.002 and 0.137 ± 0.007 for PAO. Overall, low COF values, less noise and variation were noted for NL

into the steady-state as compared to PAO, confirming the effectiveness of NL in harsh boundary lubrication conditions.

Optical micrographs comparison (right of Figure 5.4) - 20X lens magnification:

Wear scar images also confirmed the effectiveness of NL over PAO similar to previous observations in R1 and R2. As depicted in Figure 5.4, wear track images for PAO showed signs of progressive wear and poor lubrication as indicated by increased wear track width and presence of grooves. The grooves in the case of PAO appeared deeper and sharper as compared to NL from the presented optical micrographs. This observation was further confirmed by the SEM micrographs and surface texture characterization presented later in this chapter. A similar presence of deep grooves was also seen on the WSD image of the ball. WSD values for PAO were higher than NL, consistent with the fact that NL provides better boundary lubrication.

For NL, the wear track image showed the presence of fewer grooves and a reduced number of lubricant agglomerates (black spots in the wear track). This could be attributed to the synergistic evolution of texture and tribofilm which resulted in stable steady-state low COF values. This interpretation was further studied by physical and chemical characterization of texture and tribofilm on the wear track. Grooves on the WSD for NL were also more uniform as compared to PAO, consistent with the controlled frictional response observed for NL.

The progression of WSD for the tested time intervals is shown in Figure 5.5. The error bar (25 μm) corresponds to manual error in measurement with the help of imaging software. The sharp increase in WSD value at 4000 laps for PAO was possibly due to the presence of a high number of deep grooves observed on one of the tested samples. This sudden variation in surface roughness and the presence of deep grooves on the 4000 laps sample was also observed in the surface texture measurements presented later in this chapter.

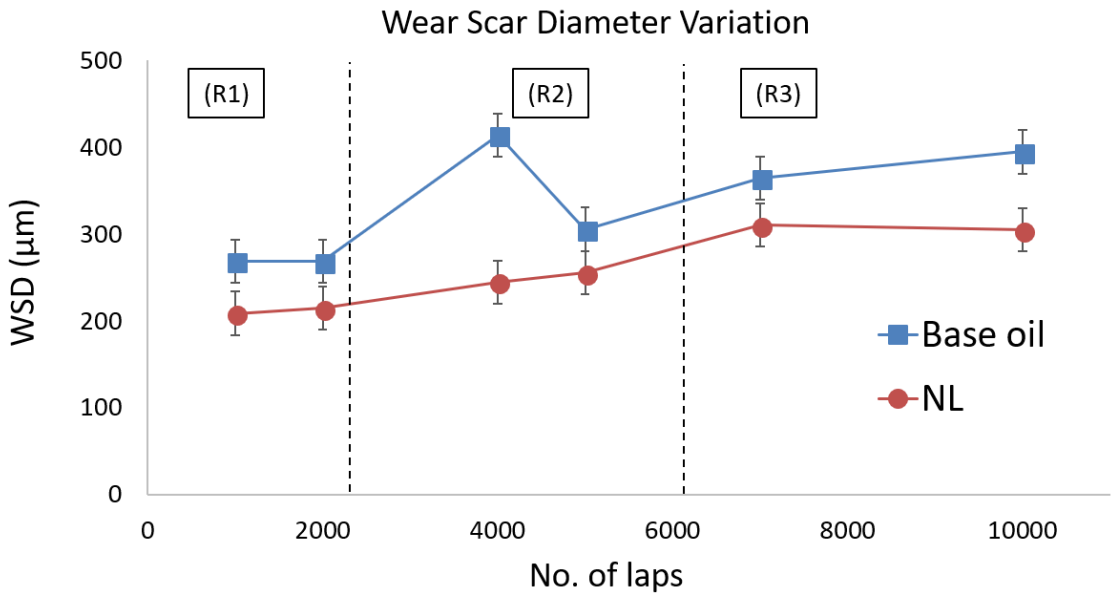

Figure 5.5 Comparison of WSD progression for NL and PAO.

Excluding the sudden increase at 4000 laps, the WSD values for PAO showed continuous increase with time. The WSD for NL showed small increments in R1 and a steady increase in R2 before stabilizing in R3. The small increments in R1 are attributed to the fact that lubrication is dominated by unreacted lubricant agglomerates (discussed below in Section 5-B) before the onset of tribo-chemical reactions. In R2, as surface texture and tribofilm evolved and stabilized with the progression of tribo-chemical reactions, the WSD increased steadily before reaching a stable steady-state in R3.

Overall, WSD values for PAO were higher than NL at all time intervals confirming the effectiveness of NL in providing better surface protection and reducing wear.

B. Physical and Chemical Analysis: SEM/EDS Measurements

I. Break-in stage (R1) – 1000 laps and 2000 laps samples

Figure 5.6 shows the SEM micrograph comparison of representative NL and PAO samples from the break-in stage at the 1000 laps and 2000 laps time intervals. SEM images are shown at 350X (showing whole wear track) and at 5000X for magnified view of the weat track.

The EDS map and signature obtained at 5000X magnification for NL is shown on the right side of the figure. EDS maps for PAO are not shown as no additional chemical information was to be gained for PAO samples with no tribofilm formation.

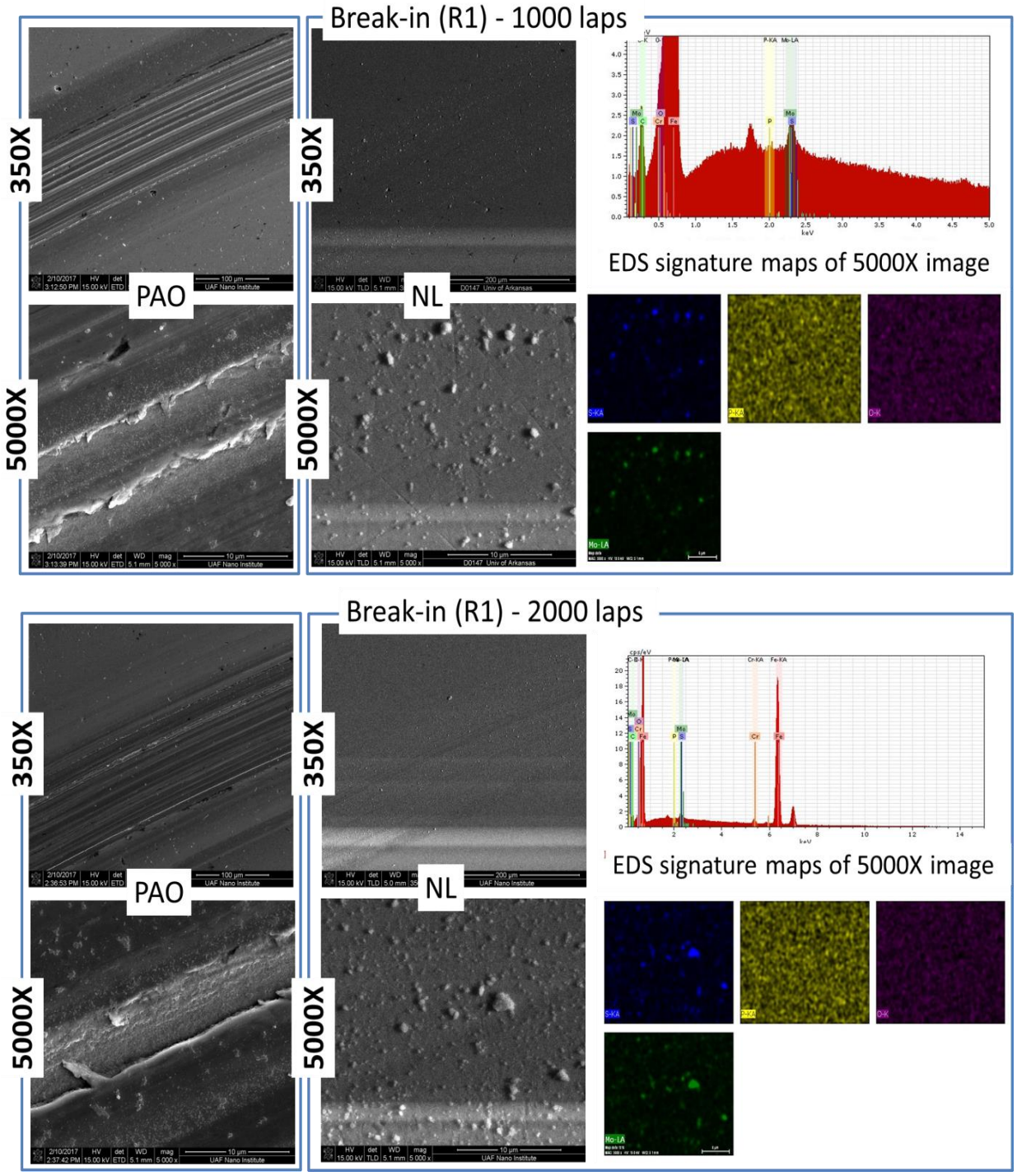

Figure 5.6 SEM/EDS analysis of wear track for NL and PAO during the break-in stage (R1).

For both samples (1000 and 2000 laps), the SEM micrographs for PAO showed the increase in surface roughness compared to virgin raw disc surface (verified by surface texture measurements) and the presence of grooves indicating material wear. This confirmed the previous hypothesis made in Section A, that pure base oil (PAO) is not an effective lubricant under the boundary lubrication regime as it fails to form a protective layer to prevent asperity-to-asperity contact. As seen previously, the COF rose rapidly to 0.15 in case of PAO within the first 500 laps (30 mins) of testing. Thus, at 1000 and 2000 laps, the presence of grooves, deformed and welded asperities, along with wear debris on the wear tracks was an expected result consistent with previous interpretations.

NL, on the other hand, did not show significant wear or appreciable change in surface morphology. The low magnification images did not show a significant presence of grooves in the wear track (in comparison with PAO). High magnification images showed wear tracks populated with lubricant agglomerates consistent with previous optical microscopy observations. EDS maps confirmed the presence of tribo-active elements with Mo and S signatures matching the corresponding agglomerates from the SEM image. These observations were interpreted as follows. During the break-in stage, physisorbed lubricant agglomerates on the sample surface control the lubrication before the onset and stabilization of tribo-chemical reactions. This interpretation was evaluated further by Raman spectroscopy and cross-sectional TEM imaging discussed later in this chapter.

II. Development stage (R2) - 4000 laps and 5000 laps samples

Figure 5.7 shows the SEM micrographs (at 350 and 5000X magnifications) comparison of representative NL and PAO samples in the R2 (4000 and 5000 laps). The EDS map and signature obtained at 5000X magnification for NL is shown on the right side of the figure.

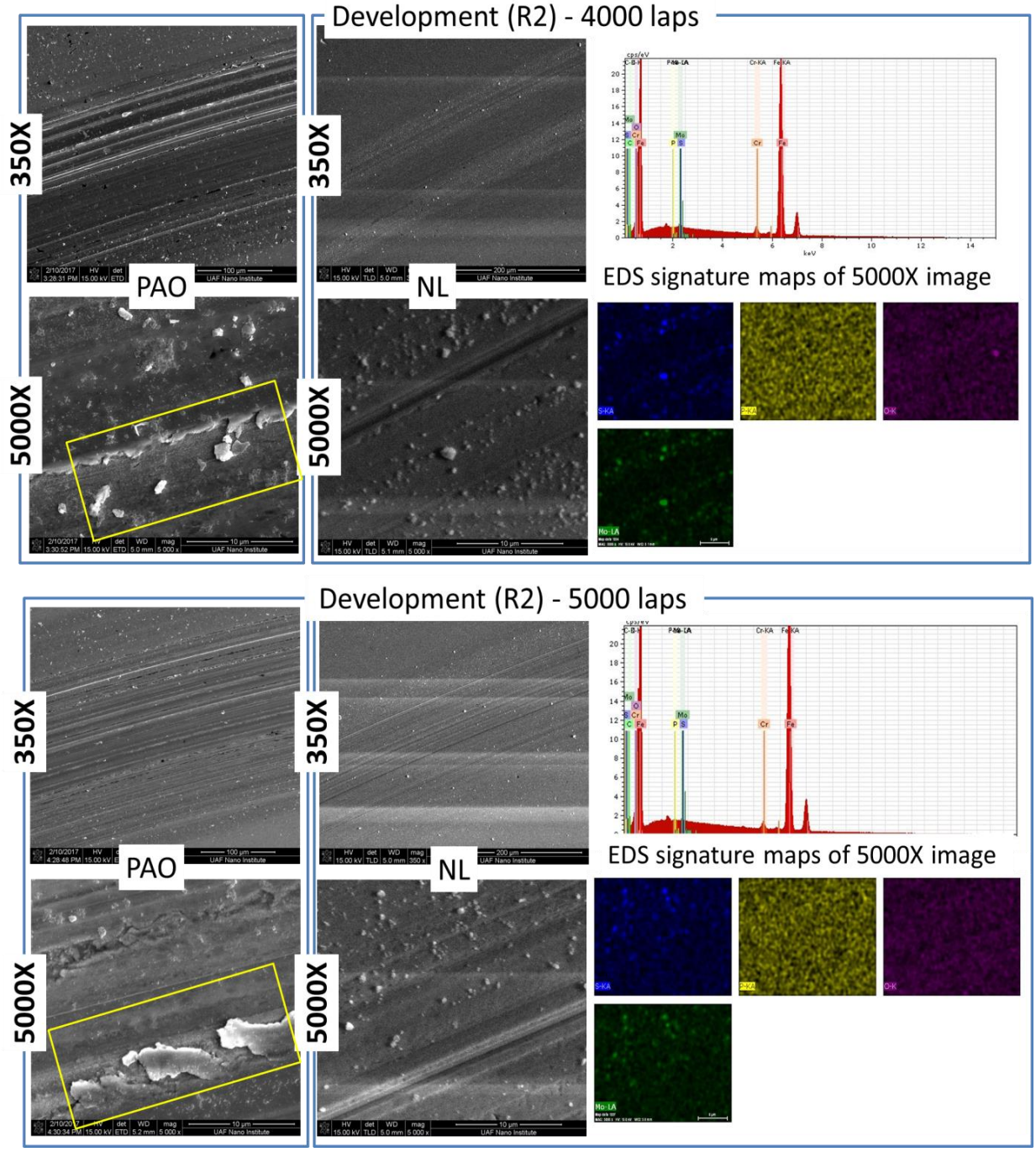

Figure 5.7 SEM/EDS images of the wear track for NL and PAO during the development stage (R2).

The SEM micrographs for PAO (left side of the figure) at 350X magnification for both samples showed the clear presence of grooves, which was consistent with the high COF values and the optical micrographs presented in previous section. 5000X magnification images

confirmed the degree of severe wear where debris particles were observed on the wear track. Additionally, broken and deformed asperities (highlighted by the yellow box) were observed which might explain the noise observed in the COF plots. Under the applied load, some of the broken asperities and wear debris got welded and sheared as seen from the above images. This indicated that under harsh boundary lubrication condition, the direct metal-to-metal contact led to severe wear in the case of PAO.

SEM images and the corresponding EDS maps for NL showed that the number of physisorbed agglomerates decreased in comparison to R1 indicating that lubricant particles tribo-chemically reacted with the surface. However, the EDS maps primarily showed the signal coming from lubricant agglomerates. This indicated that the physisorbed layer masked the signal coming from chemically reacted tribofilm. Additionally, change in the surface morphology and presence of directional grooves was also seen in the SEM images (both at 350 and 5000X magnification). This confirmed the re-organization and re-alignment of surface asperities along the direction of motion and formation of directional texture. Overall, it can be concluded that lubrication in this region was governed both by the presence of lubricant agglomerates as well as tribo-chemically reacted layers. In other words, both the physisorbed lubricant and chemically reacted surface contributed to the synergistic evolution of texture and tribofilm.

III. Steady-state stage (R3) - 7000 laps samples

Figure 5.8 shows the SEM micrographs (350X and 5000X magnification) of representative NL and PAO samples in R3 (7000 laps) and EDS map and signal for the NL sample collected at 5000X magnification.

Similar to previous observations made for behavior in R1 and R2, the SEM image for PAO (left side of the figure) shows the presence of grooves at 350X magnification. The presence

of welded asperities was seen near the edge of the groove at 5000X. Additionally, the surface morphology within the groove (highlighted by the yellow box) appeared to be deformed and smoothened under the applied load in the direction of motion. This observation supported the previous interpretation (Section 5-A.III) of the formation of complementary surface features at 7000 laps which lowered the COF values observed in the case of PAO.

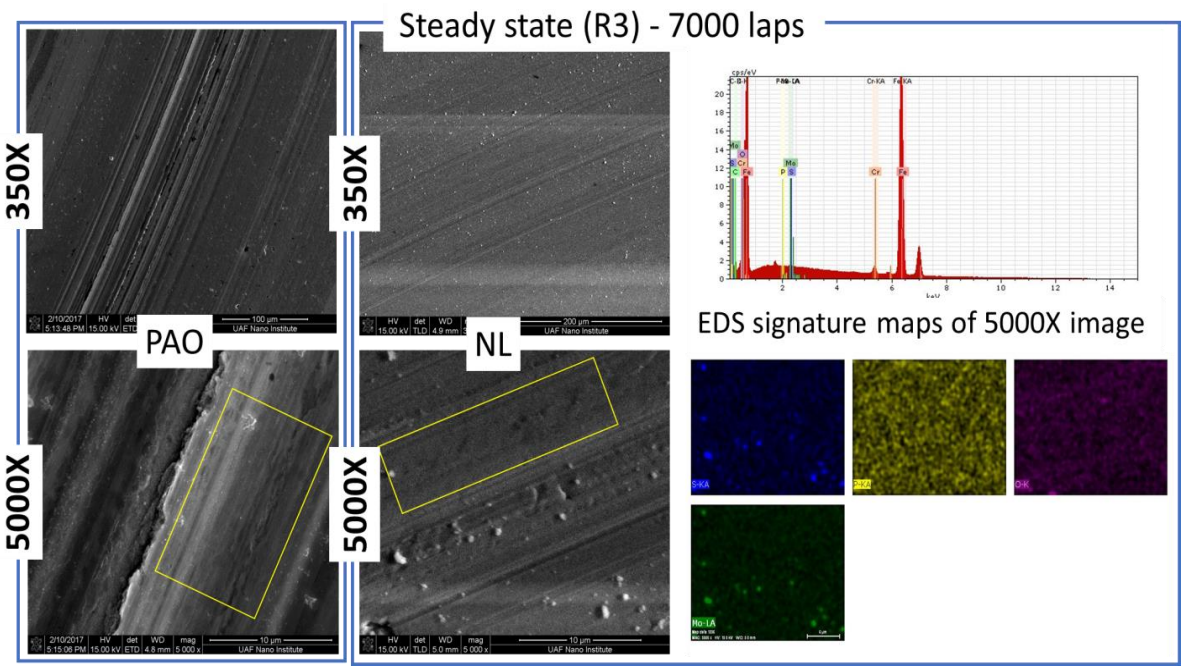

Figure 5.8 SEM/EDS analysis of the wear track for NL and PAO during the steady-state (R3).

The SEM image at 350X for the NL showed the distinctive presence of directional grooves on the wear track. The presence of grooves was further confirmed at 5000X magnification along with changes in the surface morphology highlighted by the yellow box. The wear track still showed the presence of lubricant agglomerates suggesting that physisorbed lubricant was still part of the tribological interface, however, the density of lubricant agglomerates had gone down as compared to R1 and R2 indicating a progression of the tribo-chemical reactions and the formation of tribofilm. The change in surface morphology and tribofilm chemistry was further evaluated by surface texture measurements and Raman/TEM

analysis as discussed later in this chapter. EDS map confirmed the presence of tribo-active elements on the wear track although it was noted that the physisorbed lubricant shadowed the signal from chemically reacted film (similar to R2). Physisorbed lubricant was, hence, physically removed from the wear track before chemical analysis was performed by using Raman spectroscopy and TEM as discussed later in this chapter.

Figure 5.9 shows a compilation of SEM/EDS images and a comprehensive comparative comparison of PAO and NL texture/tribofilm evolution used to understand the tribological events from a holistic point of view.

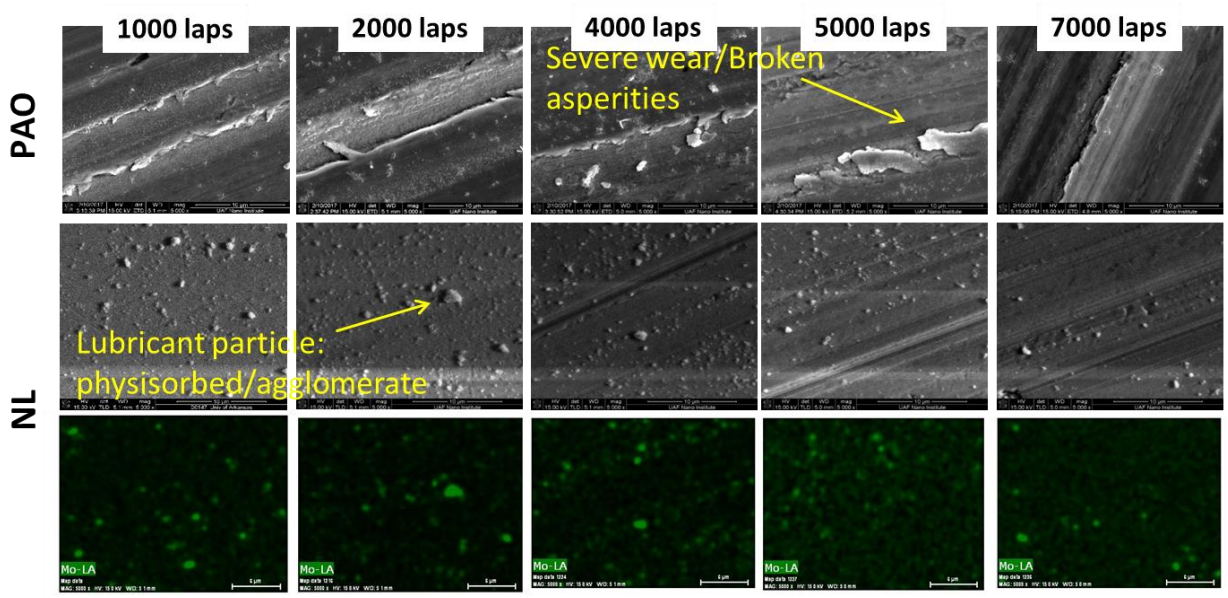

Figure 5.9 SEM/EDS comparison of texture/tribofilm evolution.

As seen from the figure, for PAO, significant wear on the surface is visible even at 1000 laps (shortest time interval tested) and the wear progressively increased with time until 7000 laps where COF dropped down and smoother surface features were observed within the groove.

Overall, for NL, the density of lubricant agglomerates progressively went down from R1 to R3. Additionally, the SEM micrographs also showed distinct surface features (such as grooves and directionally smeared deposits) on the wear track in the direction of relative motion. This

indicated the progression of tribo-chemical reactions involving lubricant particles and directional surface features, which resulted in a steady-state physical and chemical topography on the surface observed in R3. The physical and chemical characterization of tribofilm performed using laser microscope and Raman/TEM analysis is presented below.

C. Surface Texture Characterization (Laser Microscope)

The wear tracks on discs were measured using a Keyence VK-X 250 laser microscope as described in Chapter 3. The surface texture parameters of interest were then calculated by using multifile analyzer software as described in Section 3-B. Four locations on the wear track were imaged at 20X lens magnification on representative discs and their average values and standard deviation are reported below.

I. Areal texture parameters

The results and interpretation of evolution of areal texture parameters described in Table 3.2 is presented below. The L-filter value of 0.08 mm was chosen from the ISO recommended values and consistent with the cut-off filter chosen for profile measurements. [86], [87] Filtering was performed to remove the long wavelength components (waviness) from the measurement data and calculate roughness parameters. The surface texture parameters were also calculated on a virgin sample (raw disc data point) and are shown as a reference at zero position on X-axis.

Areal surface roughness (S_q)

Surface roughness (S_q) is one of the most basic parameters used to describe the deviation of surface features with respect to the mean plane.[104], [106] Areal surface roughness (S_q) was chosen over profile roughness (R_q) because areal roughness parameters are more meaningful in describing functional properties of texture as discussed in Section 2-B. S_q is commonly used to specify surface finish as it describes the overall deviation of heights within the sample

measurement area. Hence, S_q was chosen to evaluate the overall change in surface roughness over time. Figure 5.10 shows the variation of S_q for NL and PAO for the tested time intervals. The plot is divided into three regions (for all texture measurements presented from this point onwards) to understand the progression of texture and to correlate with previous observations. The raw disc data point corresponds to measurements on a virgin untextured disc samples.

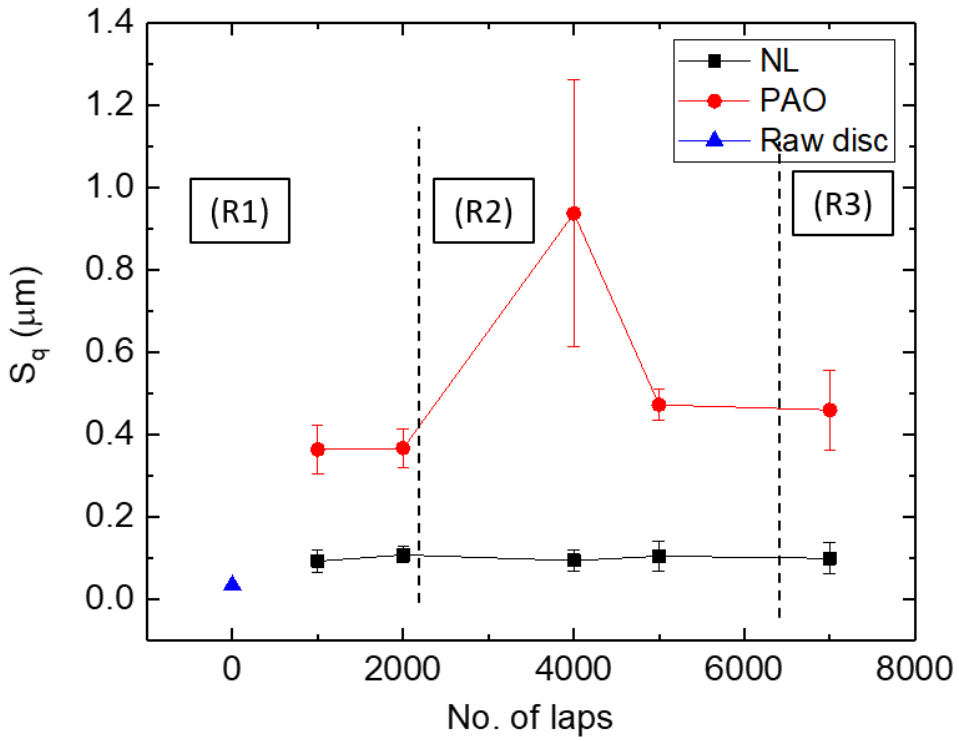

Figure 5.10 Evolution of areal surface roughness (S_q).

As seen from Figure 5.10, in the case of NL, surface roughness increased from a low starting value (S_q ~ 0.04 µm for raw disc) during the formation stage (R1) due to asperity-to-asperity contact before the activation of tribo-chemical reactions. During the development stage (R2), S_q dropped down slightly and then stabilized as the surface texture developed further (as seen from formation of directional features in SEM images) along with tribo-chemical reactions toward steady-state conditions. In the steady-state (R3), where surface asperities are protected by tribofilm, surface roughness remained stable.

For base oil, where no stable tribofilm formed, surface roughness values were higher indicating presence of deeper grooves and taller peaks. This observation was consistent with the optical/SEM micrographs and was further evidenced by other texture parameters described below. The sharp increase and variation seen in the 4000 laps sample for PAO was similar to the outlier noted on WSD evolution (Figure 5.5) and could be attributed to the presence of a large number of deep grooves on one of the tested samples. Additionally, it can be seen that sample-to-sample variation (error bars for standard deviation in measured values) in the case of PAO was larger than those of NL. This observation was consistent with the fact that NL showed more controlled frictional response than PAO as discussed earlier from COF plots comparison.

Arithmetic mean peak curvature (S_{pc})

Mean peak curvature values (S_{pc}) indicate the sharpness of peaks averaged over the measurement area. This feature parameter was chosen to understand the curvature of surface asperities (points of contact in a tribological system) in the measurement area. The larger S_{pc} value (inverse of peak curvature) will indicate the presence of sharp peaks as illustrated in Table 3.2 while smaller S_{pc} values would indicate more rounded (or protected) peaks. Figure 5.11 shows the evolution of peak sharpness values calculated over the wear track as a function of time for NL and PAO.

Consistent with the previous observation of surface roughness evolution, the asperity-to-asperity contact in R1 led to an increase in the sharpness of peaks for both cases. In the case of NL, S_{pc} value dropped in R2 and R3. This indicated that the progression and stabilization of the tribo-chemical reactions through R2 and R3 resulted in the formation of a stable tribofilm that protected the surface asperities. In addition, consistent with the previous observations made from COF plots, the variation in S_{pc} values was higher in the break-in period (R1) and then decreased

in R2 and R3. This further highlighted the fact that the initial engagement of asperities during R1 was a stochastic event and, thus, showed larger variation between the tests. Standard deviation values showed a slight increase at 7000 laps. This was possibly due to presence of wider features on one of the discs as noted by the R_{sm} parameter discussed below. The sample-to-sample variation for untextured discs is discussed further in comparison with textured discs in Chapter 6.

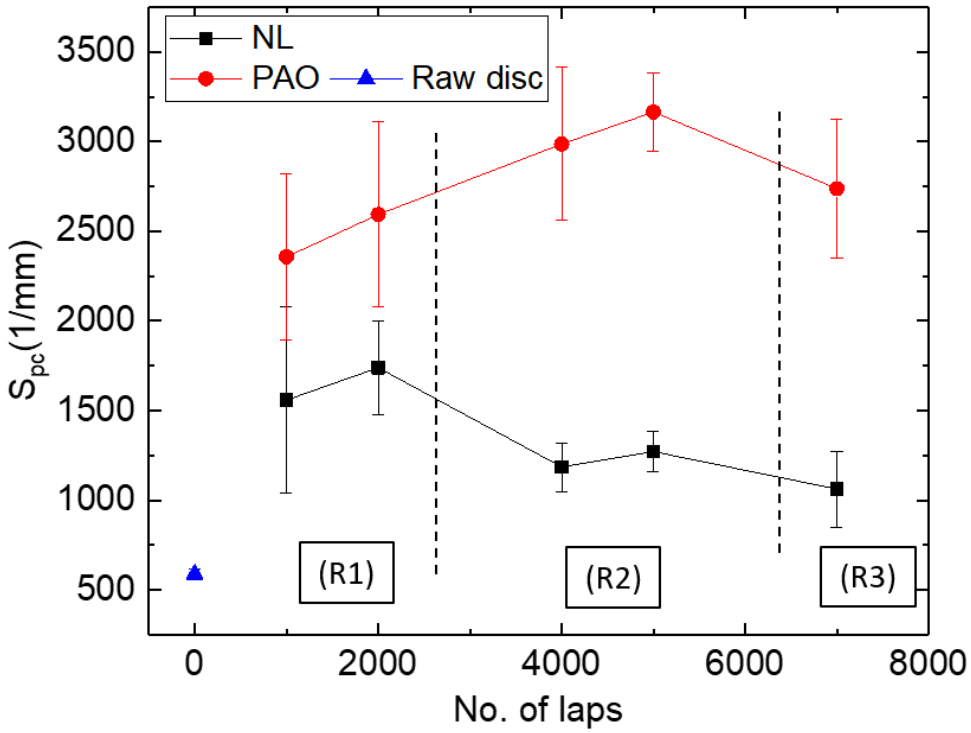

Figure 5.11 Evolution of mean peak curvature for NL and PAO.

Whereas, in the case of PAO where surface asperities were not protected, the S_{pc} values increased over time. Interestingly, the S_{pc} value for PAO dropped at the 7000 laps time interval. This was consistent with the previous interpretation of the SEM images (Figure 5.8) which showed smoother features within the grooves and a drop in the COF for 7000 laps condition. Also, the S_{pc} values for PAO were approximately two-to-three times larger than NL in the R2 and R3 stages indicating that surface asperities were well protected with tribofilm by NL; this reduced their sharpness in comparison to PAO which failed under harsh operating conditions.

Density of Peaks (S_{pd})

Figure 5.12 shows the variation of density of peaks as a function of time. As described earlier, this parameter describes the number of peaks per unit measurement area. The peak density for raw discs was high, suggesting the presence of a large number of isotropic surface asperities. During the break-in period, the asperities underwent re-organization and re-alignment, thus lowering the density of peaks within the wear track for both NL and PAO. This sharp initial drop from 0 to 1000 laps was about 10000 peaks/mm^2 for NL and about 27000 peaks/mm^2 for PAO. This observation was consistent with the fact that PAO failed after the first 200 laps of testing (indicated by rise in COF) and thus led to a larger number of surface asperities being worn off during the break-in (R1) period. NL, on the other hand, protected the surface asperities better via lubricant agglomerates observed on the surface during R1.

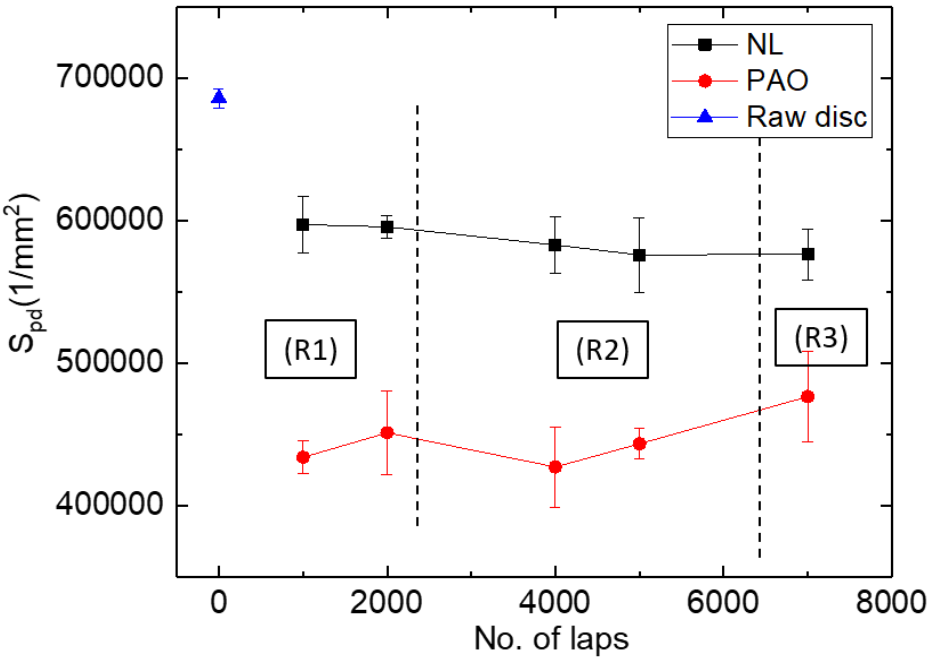

Figure 5.12 Evolution of density of peaks (S_{pd}) for NL and PAO.

For NL, the number of peaks dropped down steadily in R2 as surface texture was further stabilized (as seen from formation of directional grooves on the wear track in SEM images)

along with tribofilm before reaching a steady-state value. The S_{pd} values for NL were about 25-30% higher than PAO in R2 and R3, suggesting that the surface asperities were better protected by NL both through physisorbed agglomerates and tribo-chemical layers; this was consistent with previous observations and analyses.

For PAO, no consistent trend was observed as S_{pd} values increased initially, then decreased, and then increased again. This indicated the repetitive creation and dissolution of peaks under harsh BL conditions was due to direct metal-to-metal contact. This observation was consistent with the repetitive rise and drop in COF noted for 7000 laps in Section 5-A.III.

II. Profile texture parameters

The results and interpretation of evolution of profile texture parameters described in Table 3.1 are presented below. As illustrated in Figure 3.7, the cross-sectional profile slice was taken perpendicular to the wear track orientation to calculate the profile parameters of interest. The cut-off wavelength to filter waviness component was set at 0.08 mm as per ISO guidelines and consistent with L-filter cut-off used for areal measurements.

Mean height of profile elements (R_c)

As the name and description of the parameter suggests, R_c was used to describe overall height and depth of features (or peak-to-valley heights) averaged over a given profile (Table 3.1). Figure 5.13 shows the evolution of R_c for the tested time durations for NL and PAO.

For NL, mean peak-to-valley height in the wear track increased in R1 (consistent with the surface roughness evolution noted before) as initial surface asperities were re-aligned and re-organized. As surface texture developed further in R2 and R3 (creation of directional grooves seen in SEM images), R_c values increased from 4000 laps to 7000 laps. This slight increase was attributed to the creation and subsequent evolution of directional peaks/valleys oriented in the

direction of motion. This observation was further supported by the trend in R_{sm} (mean width of profile elements) discussed next. Overall, it was concluded that over time, surface texture evolved synergistically by forming directional features that aided tribofilm formation and stabilization. These observations are further investigated using cross-sectional TEM imaging discussed later.

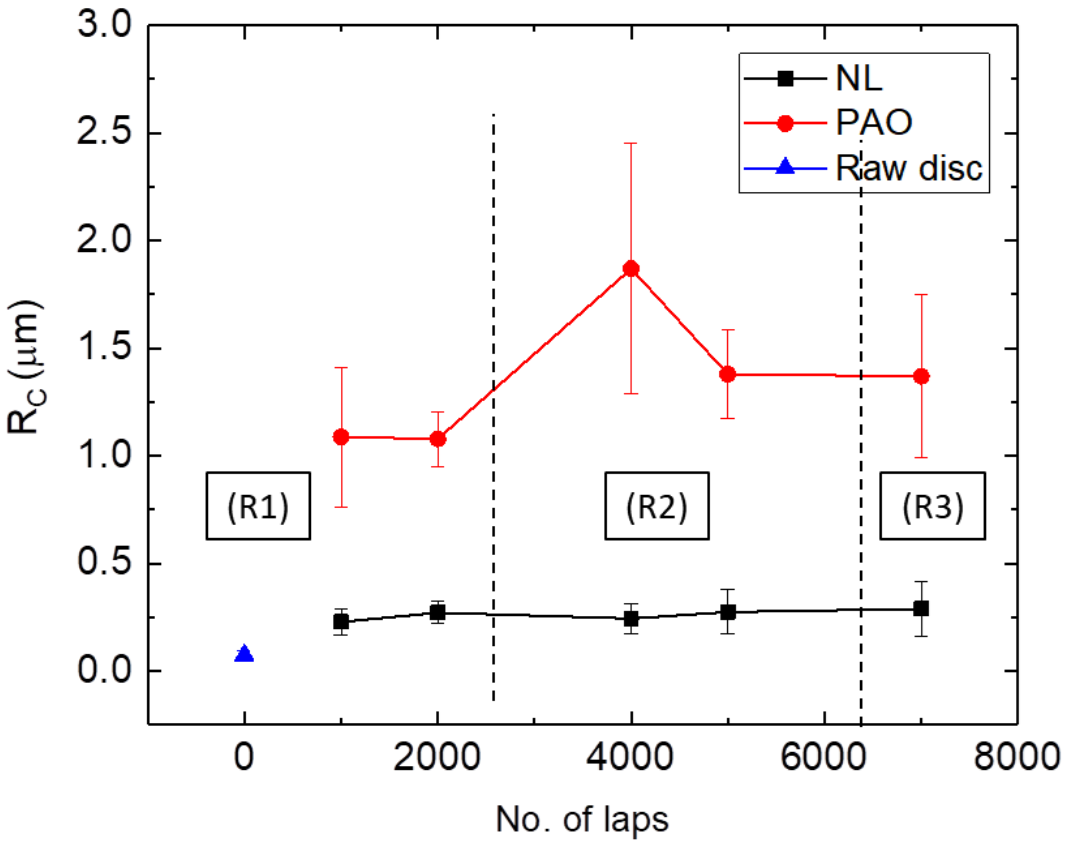

Figure 5.13 Evolution of mean heights (R_c) as function of time.

R_c values for PAO are four to five times higher than NL, indicating severe wear due to unprotected surface asperities under boundary lubrication conditions and in agreement with the SEM and optical images. The increasing height of surface features indicated the formation of deeper grooves for PAO as noted from optical and SEM micrographs. Also, the standard deviation values for PAO were higher than NL confirming the stochastic nature of asperity

engagement and evolution of surface texture. Similar to previous observations, the 4000 laps data point showed very high R_c and was a possible outlier to the overall trend.

Mean width of profile elements (R_{sm})

R_{sm} is used to characterize the spatial distribution or average periodicity of surface features in a profile measurement. Closely spaced features will have lower R_{sm} value while wider features will have higher R_{sm} value. The evolution of R_{sm} values for NL and PAO for tested time intervals is shown in Figure 5.14. It is important to note that the raw disc data point is not shown in Figure 5.14. Since R_{sm} values are indicative of the directionality of texture, for a raw disc (which has isotropic, non-directional texture) it does not carry any meaningful information. [121]

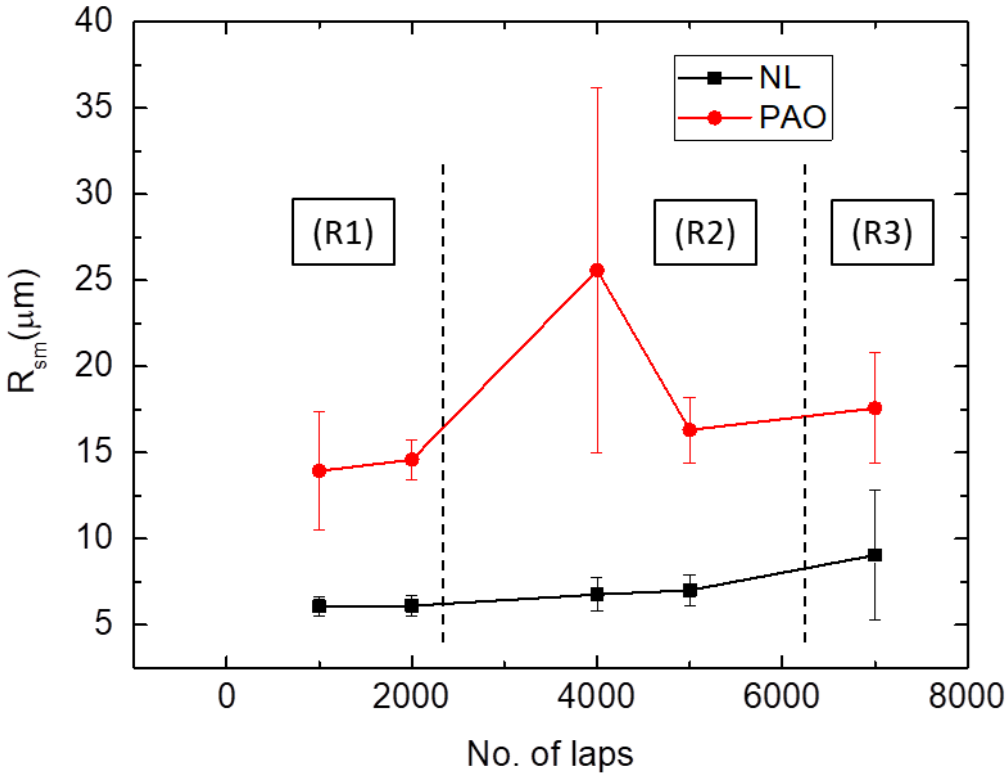

Figure 5.14 Comparison of R_{sm} values for NL and PAO at different testing times.

The initial re-organization and re-alignment of asperities led to the formation of periodic surface features within the wear track and thus directional surface features were created as seen

from SEM images. Higher R_{sm} values for PAO indicated that poor surface protection led to not only deeper but also wider spatial features (grooves) unlike NL which showed a steady increase in the periodic spatial features across the wear track in R2 and R3. This increase in average periodicity was attributed to the creation and evolution of directional texture features concurrent with the stabilization and evolution of tribofilm as also seen in SEM images.

The 7000 laps data point for NL shows a large standard deviation value (as noted before) that was attributed to the presence of wider groove on one of the samples. Similarly, consistent with previous discussion, the 4000 laps data point for PAO showed a very high standard deviation and was a possible outlier to the overall trend. Overall, the standard deviation values for PAO were higher than NL consistent with previous observations. More detailed discussion of the evolution of R_{sm} for untextured discs is included in next chapter where comparison to textured discs is made.

The observations and interpretations of the evolution of surface texture presented in this section are evaluated further by chemical analysis to gain more insights into the evolution of chemical texture and tribofilm as described in next section.

D. Chemical Analysis: Raman Spectroscopy and FIB/TEM

As noted during the chemical analysis performed by EDS (Section 5-B), physisorbed lubricant shadowed the signal coming from chemically reacted tribofilm. Hence, to perform a chemical characterization using Raman and cross-sectional TEM, physisorbed lubricant was removed during the sample preparation stage. This was achieved by physically cleaning part of the wear track using a cotton tip applicator and hexane as solvent. It was assumed that the application of gentle mechanical pressure with the applicator would only remove the weakly bonded physisorbed lubricant agglomerates without affecting stronger chemically reacted layers.

The representative samples from each stage were chosen for cross-sectional TEM analysis based on the previous results. Results of Raman and FIB/TEM measurements on samples from 1000 laps (R1), 4000 laps (R2) and 7000 laps (R3) are presented below.

I. Raman measurements

Raman measurements were taken at three spots across the wear track on each sample disc as shown in Figure 5.15. As shown in the figure, the measurement spot (marked by laser beam in the images) was moved across the wear track width in order to collect a Raman signal from three different locations. This was done in order to get a Raman signal from a more representative portion of the wear track. The top edge, center, and bottom edge denote the relative position of the measurement area with respect to the wear track. Measurements were taken on two representative discs for each time interval and the collected data was averaged.

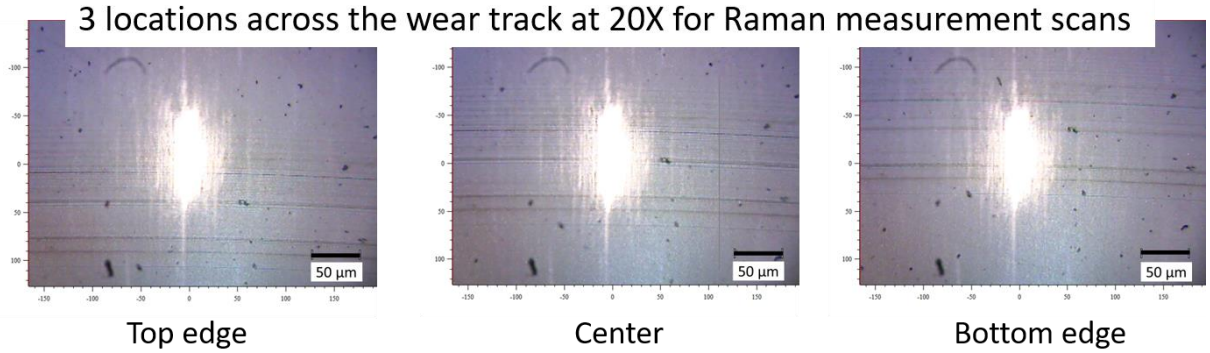

Figure 5.15 Illustration of locations for Raman measurement across the wear track.

In order to correct for the steel substrate background, separate scans were performed on a bare steel disc using the same scan settings; this scan data was then subtracted from the raw data to generate the corrected averaged Raman spectrum. Figure 5.16 shows the corrected Raman spectra obtained for the three stages of lubrication: the 1000 laps time interval from break-in stage (R1), the 4000 laps time interval from development stage (R2), and the 7000 laps time interval from the steady-state (R3).

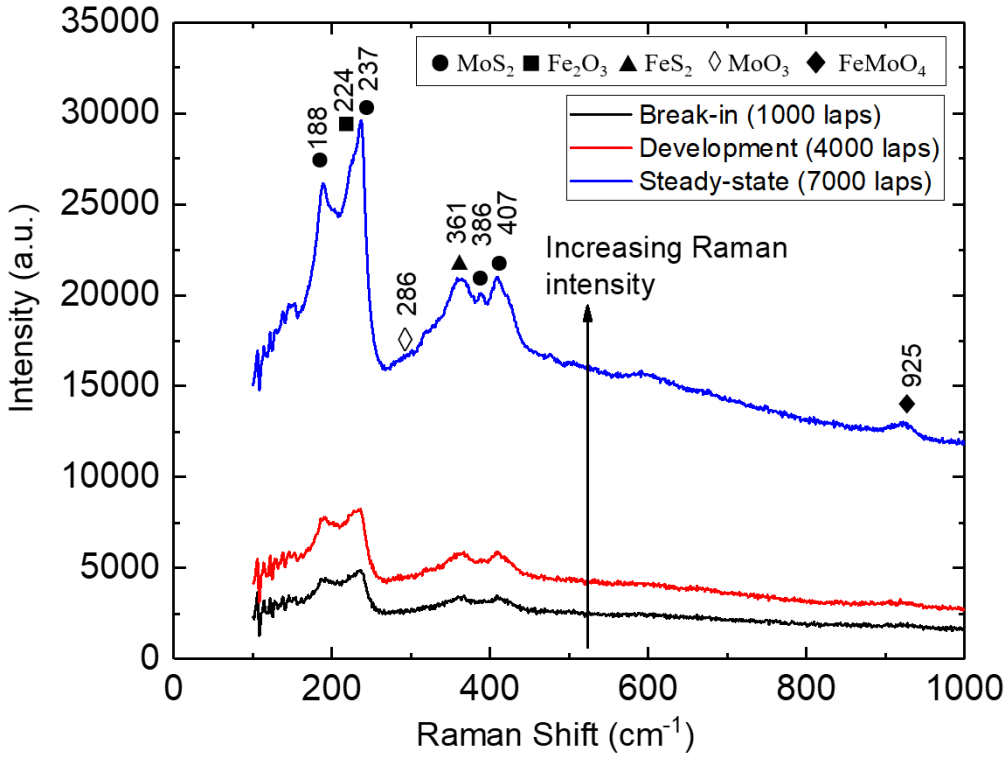

Figure 5.16 Averaged Raman spectrum for the three stages of lubrication.

Raman spectra obtained for samples tested at different time intervals were helpful for analyzing the evolution and progression of tribofilm in the three stages of lubricant. As shown in Figure 5.16, the intensity of the Raman peaks increased over time and at the same time the peaks became well-defined as tribofilm moved from formation and development (in R1 and R2) to the steady-state (R3). This suggests that the coverage of tribofilm (chemically reacted) increased over time. This observation was consistent with the observations from EDS maps as noted in Figure 5.9. In the break-in period (R1), the lubrication was dominated by unreacted lubricant (hence, less Raman signal intensity after the removal of unreacted lubricant) whereas in the steady-state (R3), the stable tribo-chemical film primarily governed the lubrication. The Raman spectra confirmed the presence of MoS_2 in the tribofilm. The two primary modes of S-Mo-S vibrations in MoS_2, E^1_{2g} (386 cm^{-1}) and A_{1g} (407 cm^{-1}) were identified. E^1_{2g} mode corresponds to in-plane vibration of S-Mo-S while A_{1g} is assigned to out of plane vibrations. [122] Additionally,

other peaks corresponding to MoS_2 (188 and 237 cm^{-1}) tribofilm were also observed and are consistent with the literature reports. [3], [30], [80] Apart from MoS_2, several other new peaks emerged corresponding to different compounds formed because of the tribo-chemical reactions. These peaks were identified and assigned as Fe_2O_3 (224 cm^{-1}), FeS_2 (361 cm^{-1}) [123] and molybdate $FeMoO_4$ (925 cm^{-1}). [124] These observations and tribofilm chemistry is consistent with previous reports on MoS_2 NL tribofilms. [3] A weak signature of MoO_3 was also observed at 286 cm^{-1}. Furthermore, it is noted that the $FeMoO_4$ peak at 925 cm^{-1} becomes prominent in the steady-state. This suggests that the tribofilm was composed of various chemistries other than MoS_2 and their increasing intensity over time was indicative of the progression of tribo-chemical reactions on the wear track. Under the application of applied load, the reactions between ferrous substrate and MoS_2 nanoparticles capped with polar long chains fatty acids led to formation of several lubricious compounds identified above. Polar hydrocarbon chains help the adsorption of nano-engineered additives on the substrate by acting as anchoring points. The adsorbed lubricant additives then tribo-chemically react with the surface under harsh operating conditions. [28], [125] The reaction between sulphur from the exfoliated nanoparticles (confirmed by TEM observations) and the steel substrate resulted in formation of iron sulfide species observed in the tribofilm and was consistent with previously reported lubrication mechanisms. [126], [127] The oxygen from the fatty acids and the phospholipid functional groups reacted with the ferrous substrate and lubricant particles to form iron oxide and iron molybdate compounds which were observed in the Raman spectra.

To summarize, results of Raman measurements confirmed the presence of MoS_2 based tribofilm and several other lubricious compounds formed because of tribo-chemical reactions between the steel substrate and nano-engineered lubricant additives. The intensity and sharpness

of peaks increased over time, indicative of denser tribofilm, and was further evaluated by using cross-sectional TEM measurements discussed below.

II. FIB/TEM measurements

Representative sample discs at 1000 laps, 4000 laps, and 7000 laps were picked for FIB/TEM study based on previous results. As previously discussed, TEM measurements were performed to probe the interaction between the lubricant and surface asperities at sub-microscopic scale and to identify the morphology and structure of the tribofilm.

To prepare samples for TEM study, the area of interest was first identified on each sample with the help of an EDS map and point scan as illustrated in Figure 5.17. Protective platinum layer was first deposited on the tribofilm surface to prevent damage to the tribofilm layer during FIB operation. TEM samples were then prepared by following the method described in Section 3-A.III and the results are presented below.

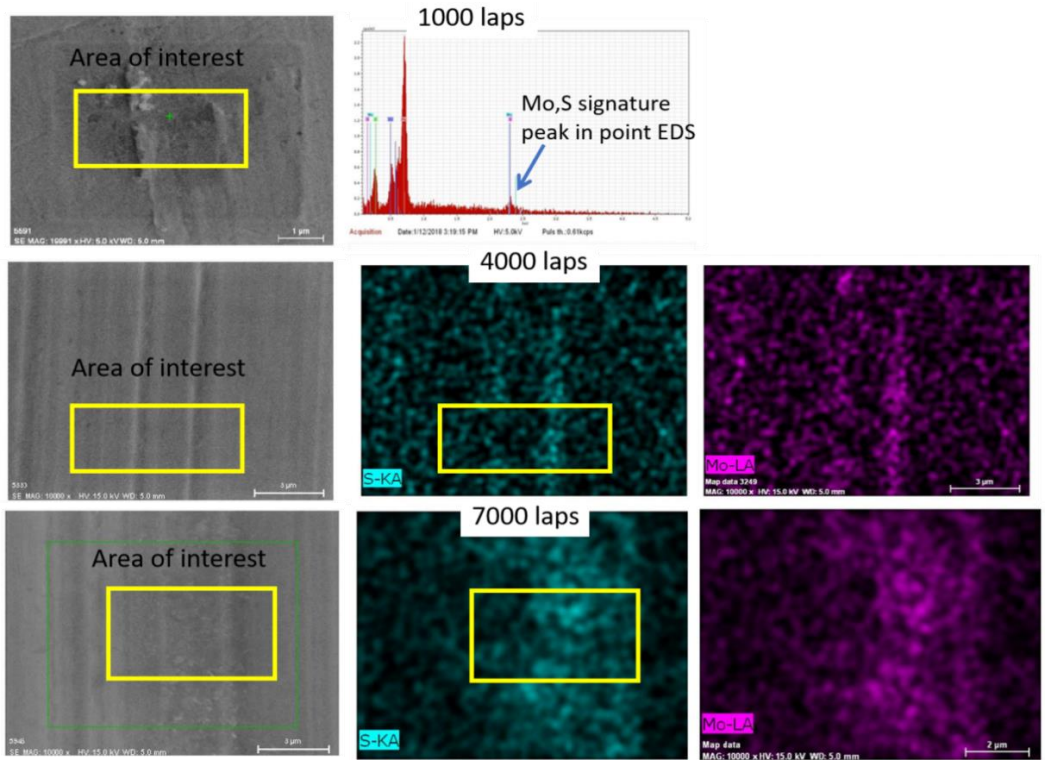

Figure 5.17 Identification of the regions of interest used for TEM sample preparation.

Figure 5.18 shows the compilation of high resolution TEM images for the three samples, namely 1000 laps (top row), 4000 laps (middle row), and 7000 laps (bottom row).

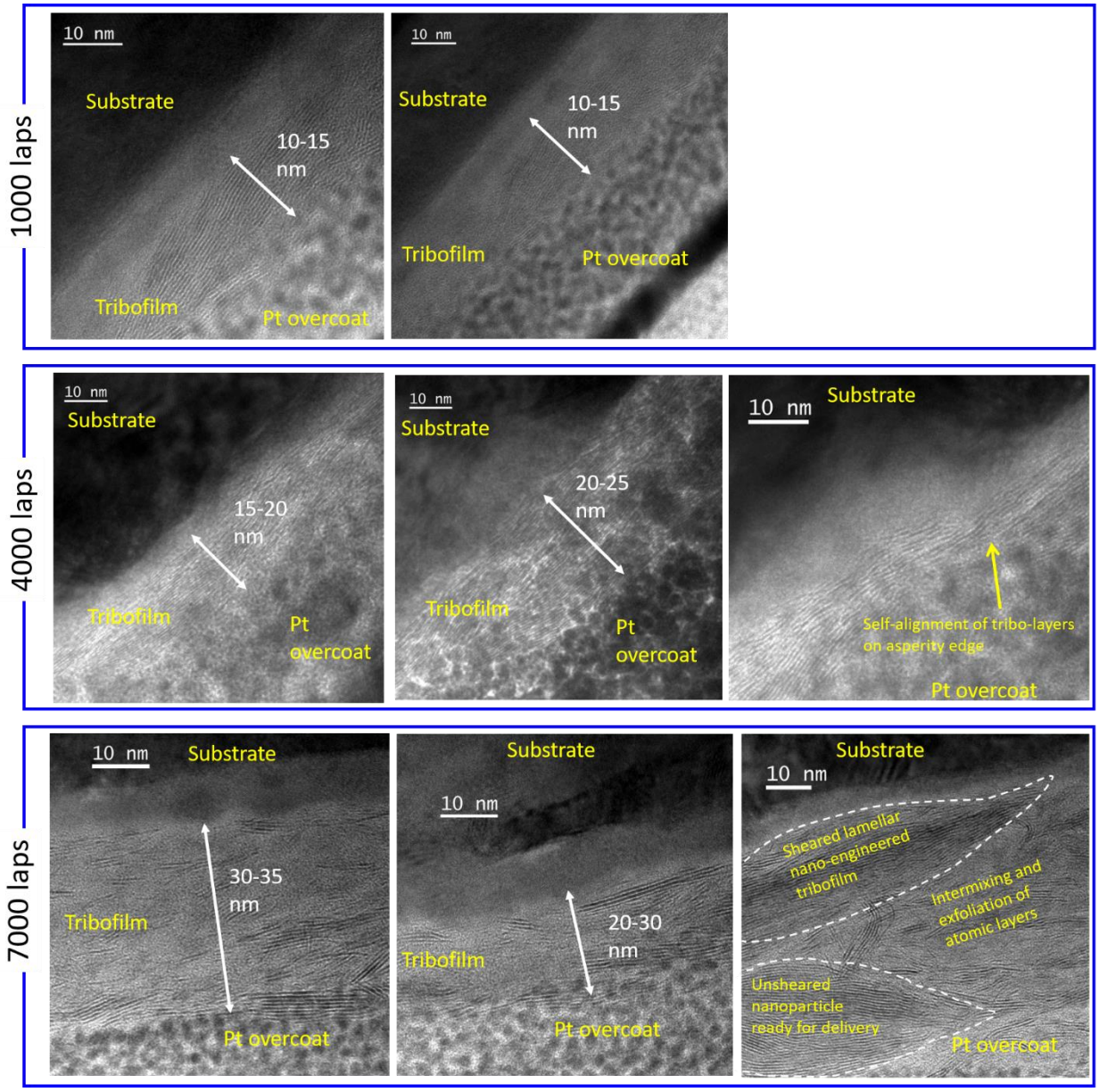

Figure 5.18 Cross-sectional TEM images for the 1000 laps, 4000 laps, and 7000 laps samples.

The corresponding EDS scans are shown in Figure 5.19 where the EDS signal was taken at a point marked by a red cross in the adjacent TEM image. The results from Figure 5.18 and Figure 5.19 together are discussed in this subsection. This discussion is followed by a discussion

of proposed lubrication mechanisms through the three regions based on the collective observations of all the results presented in this chapter.

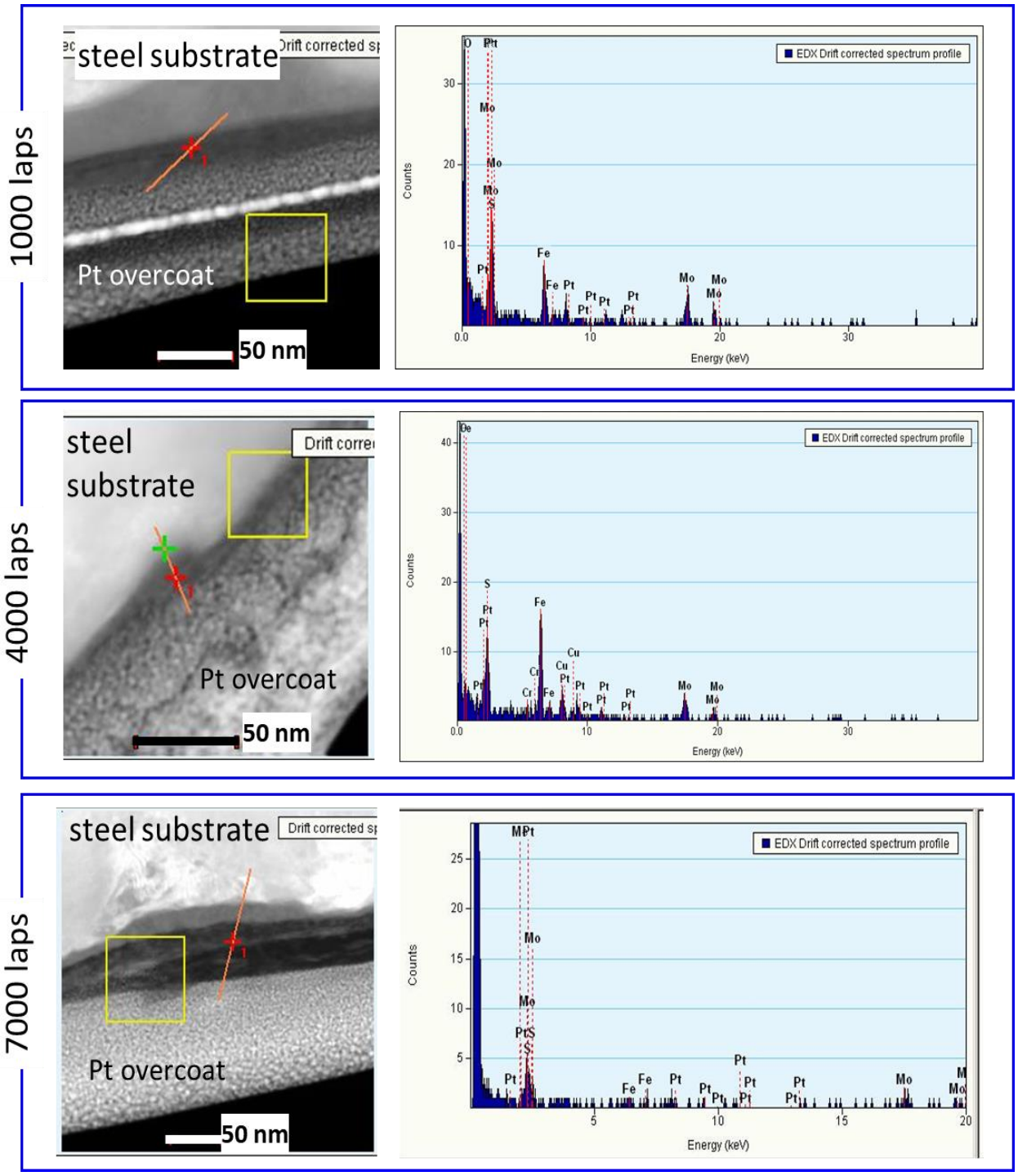

Figure 5.19 Compilation of EDS scan for the 1000 laps, 4000 laps, and 7000 laps samples.

For the 1000 laps sample(R1), lamellar MoS_2 tribo-layers of 10-15 nm thickness (Figure 5.18, top row) were observed. MoS_2 chemistry was confirmed by EDS scan. The tribo-layers were aligned with respect to the substrate and no exfoliated lubricant layers were observed. As seen from Figure 5.17, the cross-section was taken where no surface grooves were present (unlike the 4000 and 7000 laps samples) and, thus, the TEM images were indicative of a surface laminated with an adhered lubricant particle. This was consistent with the previous discussion of the SEM images and Raman data, which suggests that lubrication was mainly governed by unreacted lubricant particles and no surface features, such as directional grooves, were present.

For the 4000 laps (R2) sample, the high-resolution images (Figure 5.18, middle row) showed the presence of a lamellar structure of (15-25 nm thick) MoS_2 layers commensurate with a substrate surface. The EDS scan (Figure 5.19) confirmed the presence of MoS_2 tribo-layers in the tribofilm. The increase in thickness was consistent with the increase in Raman signal intensity observed in the last section. Additionally, the self-alignment of tribofilm over an individual asperity edge was also observed. The thickness of tribofilm near the asperity edge was about 5-6 MoS_2 layers (<10 nm) and increased back to about 20 nm on either side (stored lubricant) of the asperity edge. This indicates that as time increased, directional surface features (grooves observed in the SEM images and characterized by texture parameters R_c and R_{sm}) were created on the wear track. At the same time, the lubricant particles were sheared, exfoliated, and reacted with the substrate as the tribo-chemical reactions progressed. This process of the creation of directional features and tribofilm formation continued over time during the development stage before balancing into a stable steady-state in R3.

In the 7000 laps sample (R3), the thickness of the tribofilm increased (Figure 5.18, bottom row) compared to previous two samples which was in accordance with the high intensity

and sharp peaks observed in Raman spectrum for 7000 laps. The EDS scan (Figure 5.19) confirmed the presence of tribo-active elements in the tribofilm. Additionally, intermixing and exfoliation of individual layers was clearly observed, unlike previous samples (R1 and R2). The exfoliation of nanoparticles was attributed to the interaction between the lubricant and the mating surface asperities under the applied load where the individual lubricant particles could get sheared in the contact region. The TEM image on bottom right shows the sheared nanoparticle laminated the surface confirming the tribo-activity under application of load. In the same image, an unsheared nanoparticle was also observed which suggests that the exfoliation and shearing of nanoparticles was a continuous process. Interestingly, the few monolayers closer to the substrate were well aligned with the substrate contour while the orientation of lamellar layers away from the substrate was nonspecific. This suggests that the exfoliated lamellar layers reacted and laminated the substrate surface under the applied load. At the same time, the above observation also highlights the continuous and dynamic process involving a multi-body system consisting of mating surfaces and lubricant particles at the sub-microscopic scale. Locally, at the asperity level, the combination of chemical reactions, compression, and exfoliation of nanoparticles under extreme conditions led to lamination of surface features while at the same time leading to the exfoliation, intermixing, and shearing of lubricant particles and storage in nearby valleys.

In summary, TEM images along with Raman spectra show the progression of tribofilm as well as the interaction of nanoparticle lubricant with substrate surface. The dynamic interaction results in lamination of surface contours along with exfoliation and intermixing of lubricant particles and storage concurrent with changes in surface texture. The overall lubrication mechanism based on collective observations from functional, physical, and chemical characterization is presented below.

E. Discussion of Results and Lubrication Model

The above observations of the evolution of texture and tribofilm along with the structural and chemical analysis are collectively interpreted to formulate the lubrication mechanism/model described below:

i. During the break-in stage (R1), the lubrication is governed by the unreacted MoS_2 lubricant. The asperity-to-asperity contact leads to an increase in surface roughness where the features are re-aligned and re-organized with respect to direction or motion. The increase in surface roughness is manifested by the creation of directional peaks and valleys within the wear track that allow for the storage of lubricant. Energy dissipated during the break-in period as well as the creation of freshly exposed peaks together lead to the onset of tribo-chemical reactions and the lamination of the surface with lubricant layers.

ii. In the development stage (R2), the surface texture and tribofilm dynamically evolve via continuous interaction and tribo-chemical reactions between the lubricant and surface asperities. This manifests in the formation of grooves and the reduction in density of the unreacted lubricant agglomerates (as seen in Figure 5.9). The asperity edges are coated with lamellar lubricant and additional lubricant gets stored in the valleys as confirmed by TEM images and a reduction in peak curvature values. The increase in tribofilm thickness and coverage was confirmed by Raman spectroscopy.

iii. In the steady-state (R3), stable friction is achieved due to the balance of surface texture (seen from surface texture data) and tribofilm. Particularly, the dynamic nature of tribofilm is captured in the TEM images. The substrate surface is protected by well-aligned, laminated and reacted lubricant layers. The continuous dragging and shearing of

individual nanoparticles leads to the exfoliation and storage of lubricant layers. This observation is consistent with the previously proposed micro and nano-reservoir mechanism. [28], [128], [129] It was noted that such stored lubricant layers not only help in supply of lubricant to nearby surface asperities but also increase the overall contact area and support the load. [128] The friction reduction is also attributed to the chemical reactions leading to the formation of lubricious FeS_2, molybdate ($FeMoO_4$) and Fe_2O_3 compounds as identified by Raman measurements.

F. Conclusion

In conclusion, NL protects the surface better owing to the formation of stable tribofilm in comparison with base oil (PAO) which shows severe wear on the sample surface. Isotropic surface asperities on the polished steel discs are re-organized with respect to the directional relative motion between the two mating surfaces during the break-in and development stage concurrent with the onset and stabilization of the tribo-chemical reactions. The creation of valleys helps the storage of lubricant particles as well as the storage of exfoliated and sheared layers. Overall, the density and coverage of tribofilm increases from R1 to R3 consistent with the COF behavior and evolution of texture and was verified by Raman and TEM measurements.

The effect of directional surface texture on the manipulation of tribofilm properties for friction management is discussed in the next chapter. The results of tribological testing and characterization on the textured discs are presented and discussed. Building further on the mechanism discussed above, the role of intentionally created peaks and valleys (textured disc) on tribofilm dynamics is explored further in the next chapter.

6. RESULTS AND DISCUSSION - RESEARCH TASK 2

This chapter discusses the results for the experiments performed on textured discs according to the parameter matrix described in Table 4.3. The details of the experimental variables and test conditions are listed in Table 6.1 for studying the evolution of texture and tribofilm using textured discs with a directional starting texture. As noted in Chapter 4, the tests were performed only using nano-engineering lubricant (NL) as no information was to be gained by testing base oil (PAO). Results of the experiments with untextured discs discussed in Chapter 5 were used as a comparative reference for the interpretation of the results. The time intervals listed in Table 6.1 were chosen to represent the three stages of lubrication as proposed in Figure 4.10. The discussion of lubrication mechanism during the three stages is presented earlier on page 54 (Chapter 5). Each test was repeated three times to evaluate consistency in the COF trend.

Table 6.1 Experimental details for studying evolution of texture using textured discs.

Tribological Testing Parameters (Research Objective 2)	
Materials	Hardened (60 HRC) mirror finished 52100 steel balls (S_q ~ 0.04 µm), textured 52100 steel discs (60 HRC, concentric directional texture, S_q ~ 0.16 µm)
Load	20 N
Speed	1 cm/s
Stop condition (time duration in number of rotational laps)	Break-in (R1) - 200 laps, 500 laps, 800 laps Development (R2) - 2000 laps, 3500 laps, 5000 laps Steady-state (R3) - 7000 laps, 8500 laps
Lubricant	3 drops (approx. 0.1 ml) nano-engineered lubricant (NL)

Before discussing the experimental results for textured discs, an overall comparison between COF trends for untextured discs and textured discs is depicted in Figure 6.1 and summarized in Table 6.2. As noted in Table 6.2 and seen in Figure 6.1, textured discs showed a smaller duration of break-in period (about 1000 laps) as well as an earlier onset of steady-state (at around 6000 laps) when compared to untextured discs. This can be attributed to the fact that

the surface asperities were already partially broken-in and aligned with respect to the direction of motion in the rotational setup. Additionally, the increase in surface roughness and sharper peaks might lead to higher energy dissipation during the break-in period and early onset of tribo-chemical reactions in the case of textured discs. These observations are evaluated during the measurement and interpretation of the data presented in this chapter.

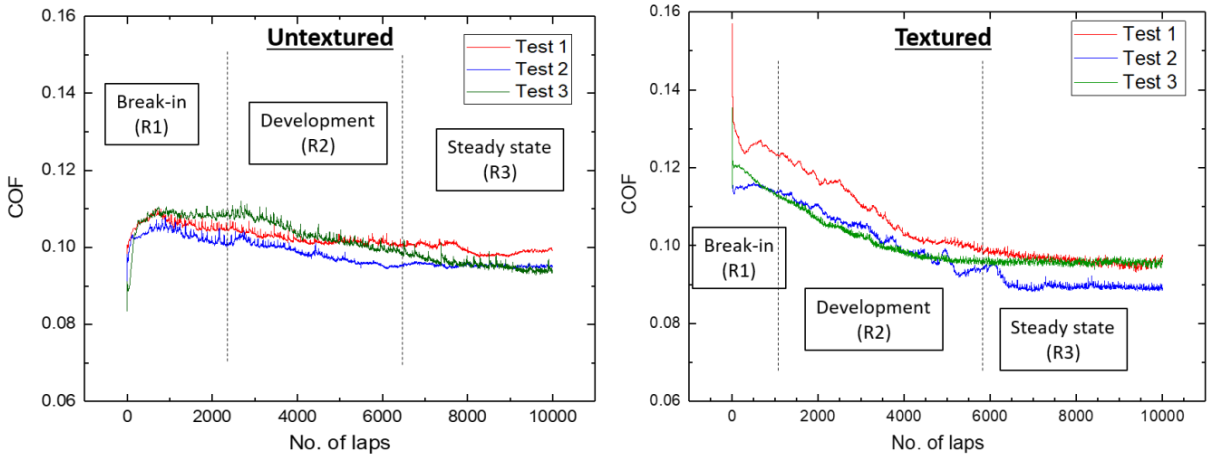

Figure 6.1 COF trend comparison between untextured and textured discs.

Table 6.2 Comparitive summary of COF behavior for untextured and textured discs.

Surface condition / Phases of propagation	**Untextured** (Mirror finish, S_q ~ 0.04 µm, isotropic surface features)	**Textured** (S_q ~ 0.16 µm, directional concentric texture)
Break-in stage (R1)	• COF started low (~0.07) and rises up to~0.11 • Duration~2000 laps	• COF started very high (~0.14-0.15), followed by sharp drop and small increment • Duration~1000 laps
Development stage (R2)	• COF value dropped down steadily with small slope as compared to textured disc (0.105 to 0.095) • Duration –~4000-4500 laps	• COF steadily dropped down with slope higher than untextured disc (overall variation from~0.125 to~0.095) • Duration –~4500-5000 laps
Steady-state stage (R3)	• COF stabilizes at steady-state value of 0.1 • Steady-state COF from t=6500 laps onwards	• COF dropped down to a steady-state value of 0.095 • Steady-state COF from t=6000 laps onwards

A. Functional Analysis: COF, Wear Scar Diameter (WSD) and Trends

This section presents the results of tribological testing (COF plots) and optical microscope measurements of the wear tracks and WSD on the steel ball counter-surface. The representative optical micrographs of the wear track and WSD are presented.

I. Break-in stage (R1) - Samples from 200 laps, 500 laps and 800 laps time intervals

Figure 6.2 shows the COF friction plots and representative images for the wear track and wear scar diameter during the break-in stage for 200, 500, and 800 laps time durations. The trend in COF was consistent with the control tests for textured discs (Figure 4.10 and Table 6.2), where the COF started at a higher value (0.16-0.2) and showed a rapid drop followed by small increment. This trend was more prominently seen in case of 200 laps sample shown in the figure and could be explained as follows. At the beginning of test, the COF value rose due to a high starting surface roughness and the presence of high peaks (characterized by S_{pk} texture parameter described in Table 3.3 and shown in Figure 6.9 below). Once these initial high peaks were worn off, the COF started to drop down as the surface asperities from the core material surface engaged in mating contact and started to re-align and re-organize in the direction of motion.

In addition to verifying consistency with reference to the control tests, the trends in the COF plots were also used to identify the representative samples for further analysis. Since the interaction of surface asperities during the break-in stage is a probabilistic event, the focus was given more to identifying the right trends in the COF rather than absolute values of the COF. For example, the Test 2 and Test 3 samples were chosen as representative examples for 200 laps, while the Test 1 and Test 3 samples were chosen as representative samples for 500 laps. The test-to-test variation in trends was more prominent during early stage (for 200 and 500 laps time intervals) due to the stochastic interaction between the asperities and because of disc-to-disc

variation in microscopic and sub-microscopic textures fabricated by mechanical polishing. As the texture and tribofilm stabilized in R2 and moved toward a steady-state in R3, the trend in the COF plots was expected to be more consistent from test-to-test as confirmed in next subsections.

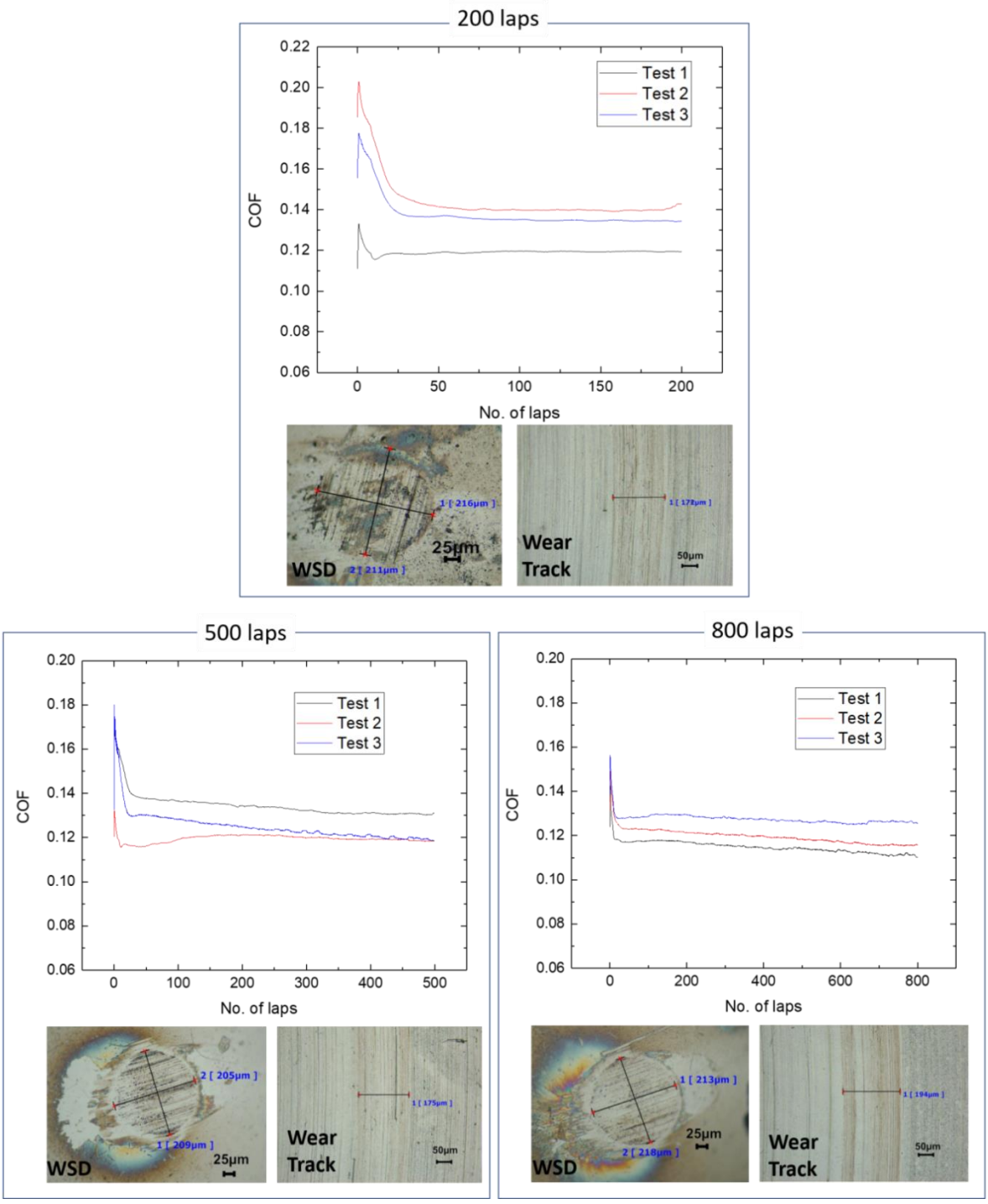

Figure 6.2 COF plots and optical wear scar images for break-in stage (R1).

Also, the WSD and the wear track width values shown in the optical micrographs (Figure 6.2) for textured discs were higher than untextured discs (Figure 5.2). This was attributed to the fact that textured discs had higher surface roughness than untextured discs causing more wear during the break-in stage before the onset of tribo-chemical reactions and tribofilm formation.

II. Development stage (R2) - Samples from 2000 laps and 3500 laps time intervals

Figure 6.3 shows the COF plots and representative images for the wear track and WSD for the 2000 and 3500 laps time durations. Plots and images for the 5000 laps duration are not shown for better clarity and to avoid repetition (there is no additional information to be gained beyond information presented below with help of the 2000 and 3500 laps samples).

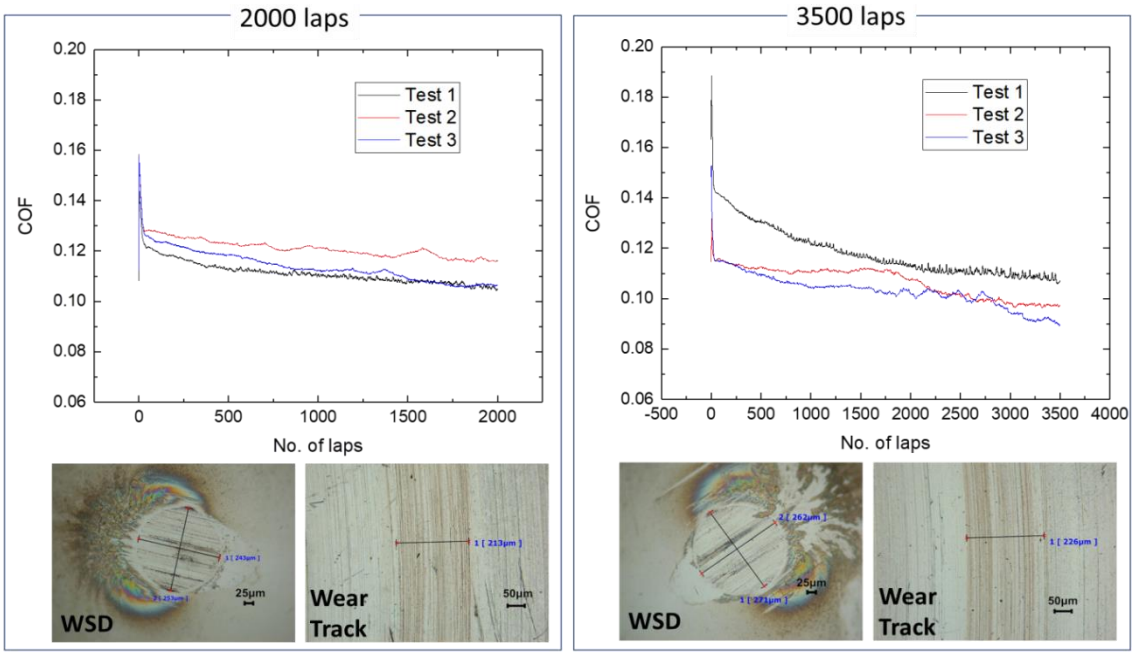

Figure 6.3 COF plots and optical wear scar images for the development stage (R2).

As shown, the COF plots follow the overall trend observed during the control tests. Test-to-test variation can still be seen due to the stochastic nature of the interaction between surface asperities. Additionally, Test 1 (black curve) in both these cases showed the presence of small spikes and noise. This could be attributed to the possible presence of wear debris in the contact

region. The WSD for the 2000 laps-Test 1 (as shown in Figure 6.4) was also larger than Test 2 and Test 3, confirming the above hypothesis.

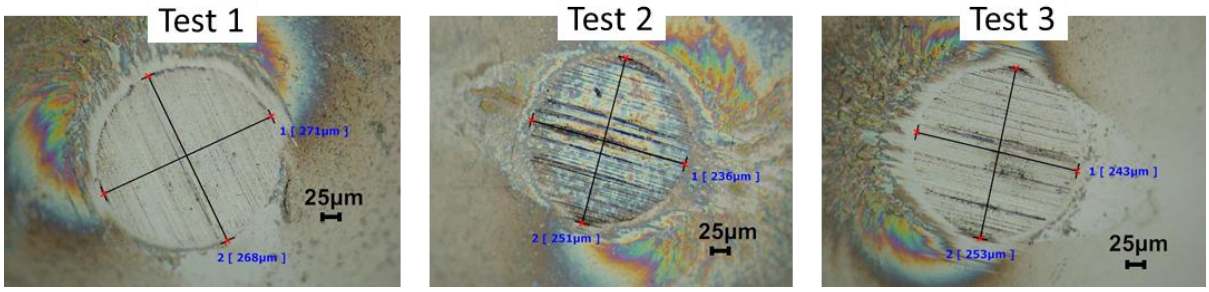

Figure 6.4 WSD comparison of three tests for 2000 laps time interval.

It can also be seen that the COF plots also showed local periods of small increase and decrease in friction (for example, in the 2000 laps-Test 2, between 700 and 1400 laps and again from 1500 to 1700 laps). These can be attributed to the dynamic changes in tribofilm and surface texture during development and stabilization in R2. This possibly happened via a reaction of fresh surface asperity followed by tribofilm formation and delivery of the protective layer on a local asperity scale. This observation was partially evaluated by sub-microscopic cross-sectional TEM imaging of an individual asperity and is described later in this chapter.

The WSD and wear track width increased in this period (R2) as the texture re-organized further along with formation and stabilization of tribofilm. The WSD values in this stage were higher than the observed values for the untextured discs in R2, suggesting that the overall cumulative wear for textured discs was higher because of their higher starting surface roughness.

III. Steady-state stage (R3) - Samples from the 7000 laps and 8500 laps time intervals

Figure 6.5 shows the COF plots and representative images for the wear track and WSD for the 7000 and 8500 laps time durations. Overall, the COF plots followed the expected trend consistent with the control test and showed steady-state COF values where steady-state friction values were observed from 6000 laps onwards. The 8500 laps tests showed a slight increase in

COF at the end of the test, which was slightly unexpected as compared to all other data points. It is possible that this slight increase in COF was because of the increased presence of lubricant agglomerates observed on the wear track in optical images (black band in bottom right of Figure 6.5) and also in SEM/EDS observations (Figure 6.8, 8500 laps). This might also explain the mechanism of local cycles of increasing and decreasing COF noted in the previous section. The presence of lubricant agglomerates on the wear track led to a local rise in COF and then friction dropper off as these agglomerates were consumed via shearing, exfoliation, and delivery on the surface asperities under the applied load in a continuous, dynamic process.

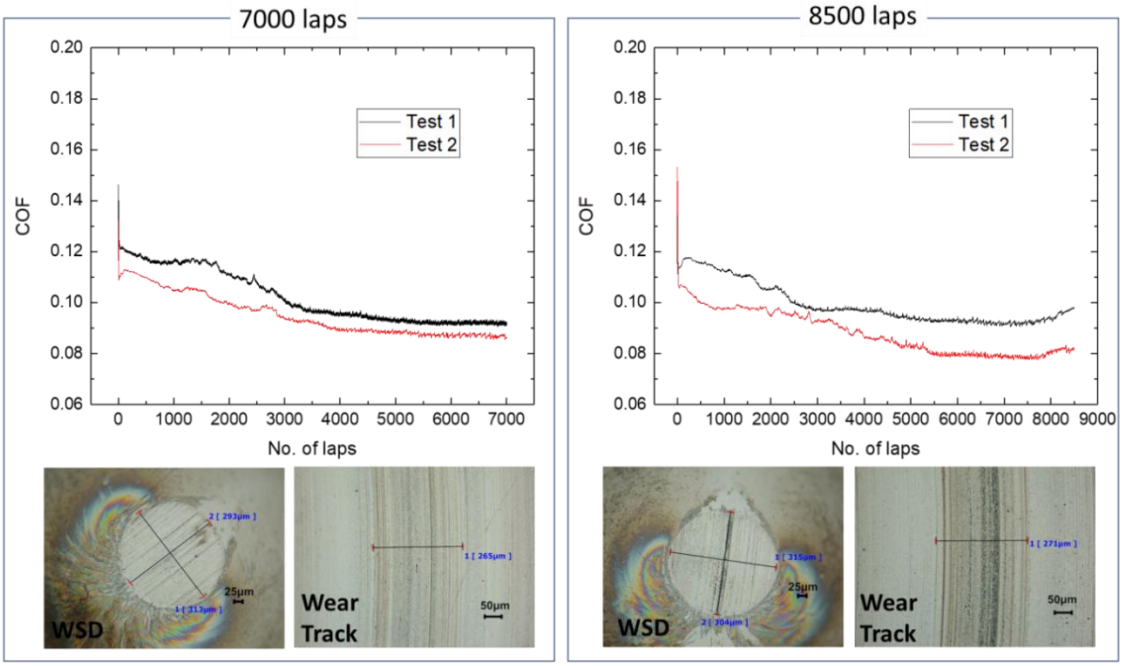

Figure 6.5 COF plots and optical wear scar images for steady-state stage (R3).

The wear track widths and WSD values were comparable to the values for untextured discs in a steady-state stage. This indicated that even though the textured discs showed higher initial wear owing to a higher starting surface roughness, the early activation of tribo-chemical reactions and steady-state conditions reduced the wear rate with increasing time, allowing the textured discs to reach steady-state values that were comparable to the untextured discs.

The comparative evolution of average WSD values for untextured and textured discs is presented in Figure 6.6. It should be noted that the regions (R1, R2 and R3) marked in Figure 6.6 are with respect to the three regions defined for textured discs, which are different from three regions defined for untextured discs (as seen before in Figure 6.1). In addition, the error bars represent the manual error in measurement of WSD (similar to Figure 5.5). As discussed above, the WSD for textured discs was higher during the break-in (R1) and development (R2) stage due to higher starting surface roughness and stabilized to comparable steady-state values. Additionally, consistent with the COF plots, textured discs showed early onset of steady-state as further explored using surface texture characterization.

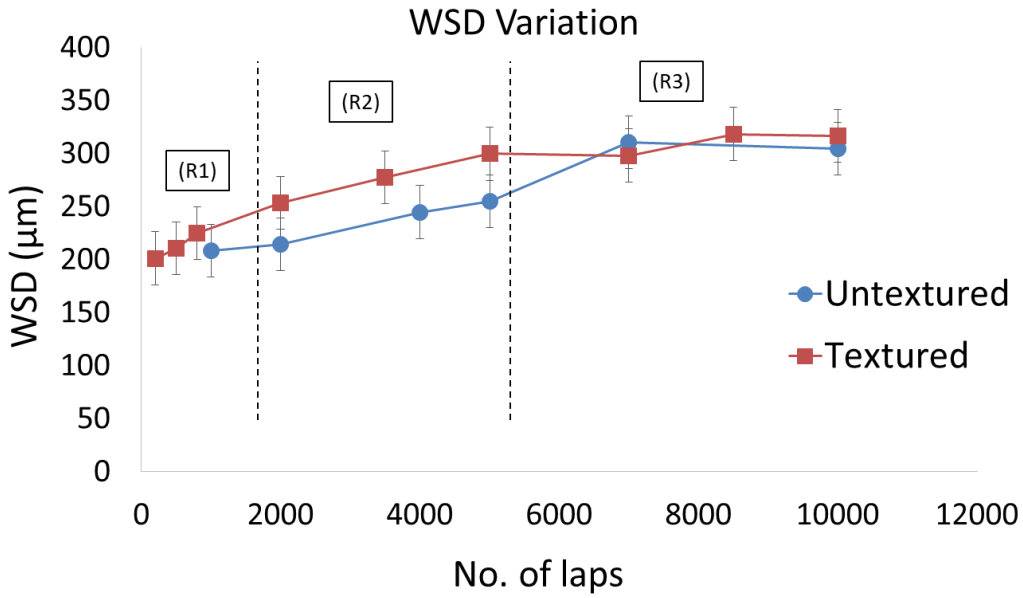

Figure 6.6 WSD evolution comparison between textured and untextured discs.

B. Physical and Chemical Analysis: SEM/EDS Measurements

This section presents the results and analysis of SEM/EDS measurements on textured discs. The SEM micrographs of representative samples are shown at 350 and 5000X magnifications along with the EDS signal map at 5000X magnification for all presented samples (consistent with SEM/EDS images presented in Chapter 5).

I. Break-in stage (R1) samples

Figure 6.7 shows the SEM micrographs and EDS maps for the break-in stage for 200 laps (top), 500 laps (bottom left), and 800 laps (bottom right).

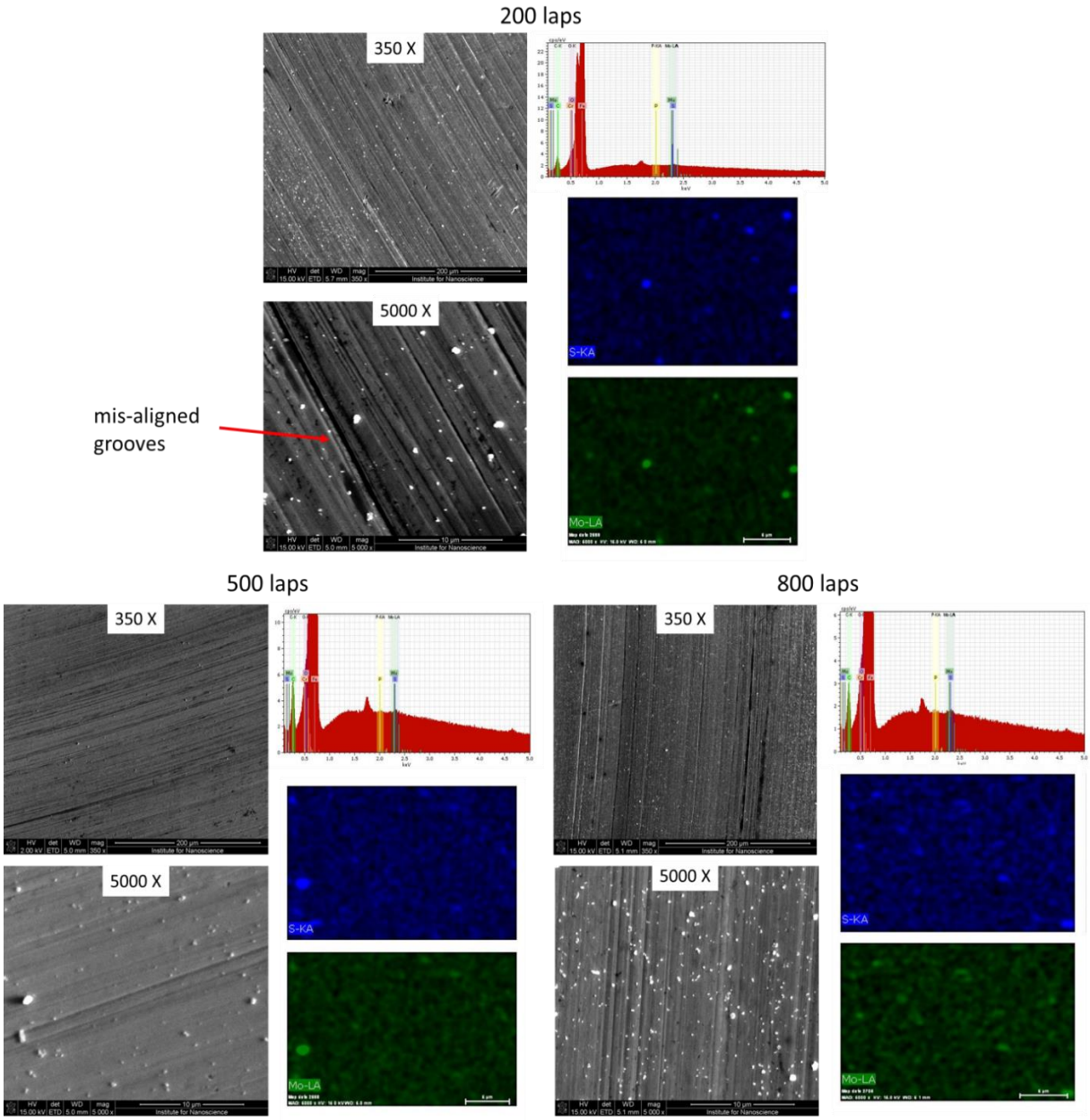

Figure 6.7 SEM micrographs and EDS maps for the break-in stage (R1).

As previously discussed, even though the textured discs showed directionality on a large scale, the features at micron and submicron scales were still locally random because of the

mechanical polishing operation. This difference resulted in disc-to-disc variation in COF response during the break-in stage where surface asperities interacted and underwent realignment and re-organization (as shown in Figure 6.2). The SEM micrographs in Figure 6.7 confirm the re-alignment of directional features during the break-in stage. As shown, a mis-aligned groove was observed on the wear track at 200 laps, whereas the overall directionality of features became more aligned in the direction of motion as time increased as seen from SEM images of the 500 and 800 laps samples at the bottom of Figure 6.7. These observations indicate that the frictional response during the early part of break-in stage was dominated by the re-alignment of surface asperities and was consistent with the remarks made in Section 6-A.I from the COF trends.

Lubricant agglomerates were also observed on the wear track; however, their overall density was small compared to the untextured discs during the break-in stage as seen from EDS signal and maps in Figure 5.6. The EDS maps show the presence of tribo-active elements on the wear track; however, lubricant agglomerates dominated the mapping EDS signal. This observation is similar to previous observations made on untextured discs and holds true for all the EDS maps presented in this chapter. The physisorbed lubricant was, thus, physically removed before Raman and TEM analysis as described in previous chapter.

II. Development stage (R2) and steady-state (R3) samples

Figure 6.8 shows the SEM micrographs and EDS maps for the development stage (2000 and 3500 laps - top) and steady-state stage (7000 and 8500 laps - bottom) samples. As depicted in Figure 6.8, the overall alignment of surface features was consistent and uniform with the direction of motion in all SEM images. This indicates that during the development and steady-state stage, the surface texture and tribofilm evolved and stabilized resulting in a stable frictional response while preserving the original directional texture template.

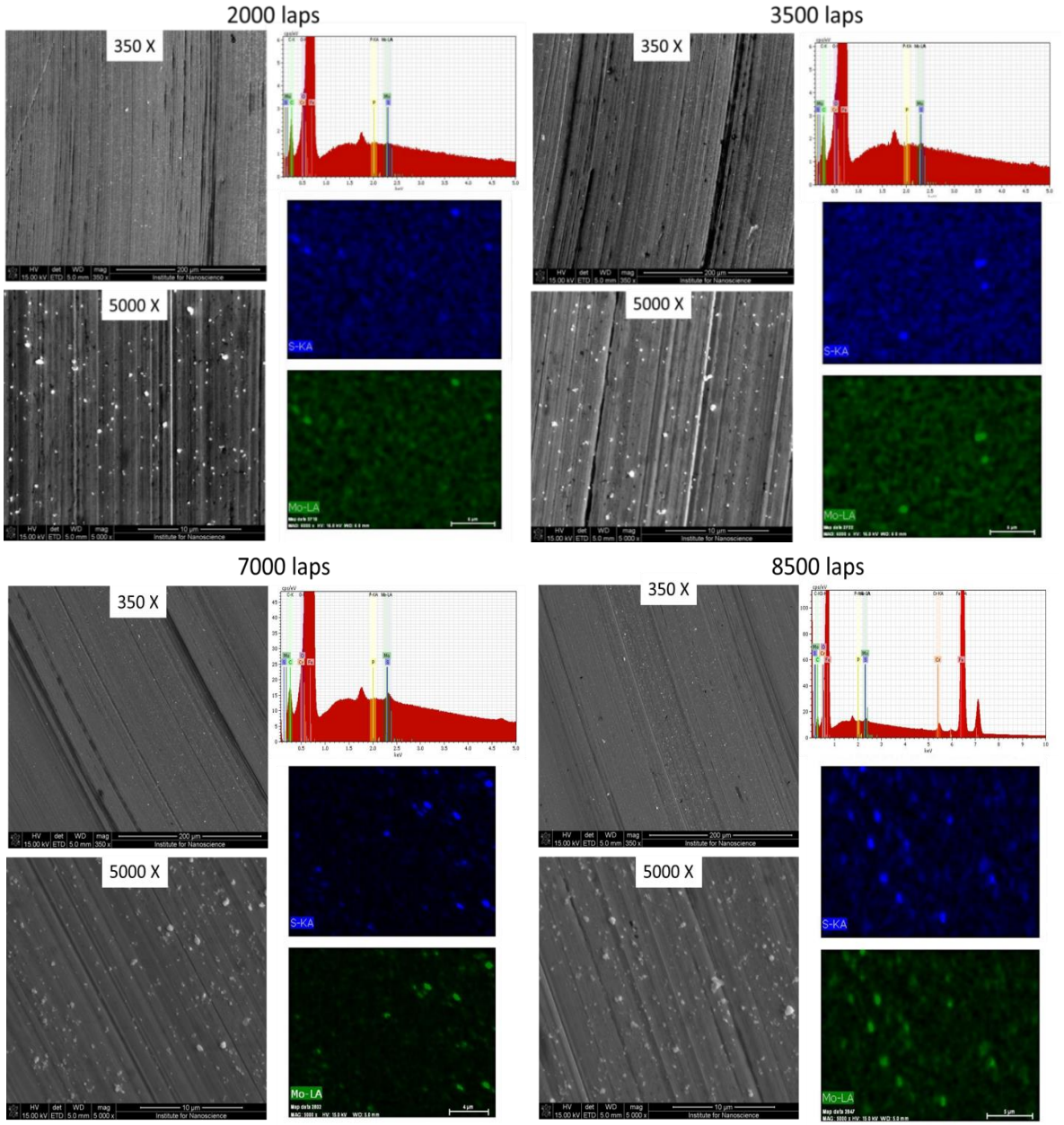

Figure 6.8 SEM micrographs and EDS maps for the development stage (R2) and steady-state stage (R3) samples.

Additionally, the clear presence of periodic grooves on the surface (suggesting spatial distribution of peaks and valleys on the wear track) was seen in the SEM images. This indicates that even though the surface features were re-aligned and re-organized during the break-in period, the directional texture consisting of distribution of peaks and valleys was still maintained. Furthermore, the density of lubricant agglomerates on the wear track remained mostly steady

(except for slight increase at 8500 laps as previously discussed) at all tested time intervals. This was possibly because of the presence of valleys available as reservoirs for lubricant. In contrast, the untextured discs did not have directional presence of valleys at the beginning of the test where lubricant particles could be stored and, thus, showed wear tracks populated with lubricant agglomerates during the break-in period. The comparison of valley volumes between textured and untextured discs is presented in the next section, which supports the above interpretation.

As per the lubrication mechanism discussed at the end of Chapter 5, the valleys acted as a storing space for lubricant particles while peaks acted as anchoring and reaction points for shearing and exfoliation of the lamellar solid lubricant. The behavior of peaks and valleys in presence of lubricant nanoparticles was further studied using cross-sectional TEM imaging and is discussed later in this chapter.

C. Surface Texture Characterization (Laser Microscope)

The results of surface texture measurement and analysis performed using a Keyence VK-X 250 laser microscope and Keyence multifile analyzer software are discussed in this section. Comparison of textured and untextured virgin disc surfaces is presented first to understand the difference in starting surface textures used during the experiments. This is followed by results and analysis of evolution of the surface texture on textured discs. Texture evolution data obtained for untextured discs as discussed in Chapter 5 was used as a comparative reference.

As noted in Section 3-B, selected functional and volumetric parameters calculated from materials ratio curve were used to compare starting surface texture for textured and untextured discs. Figure 6.9 shows the comparison between the textured and untextured discs using four selected texture parameters. These parameters were chosen for comparison as they are related to the average amplitude and volume of peaks and valleys in the measurement area.

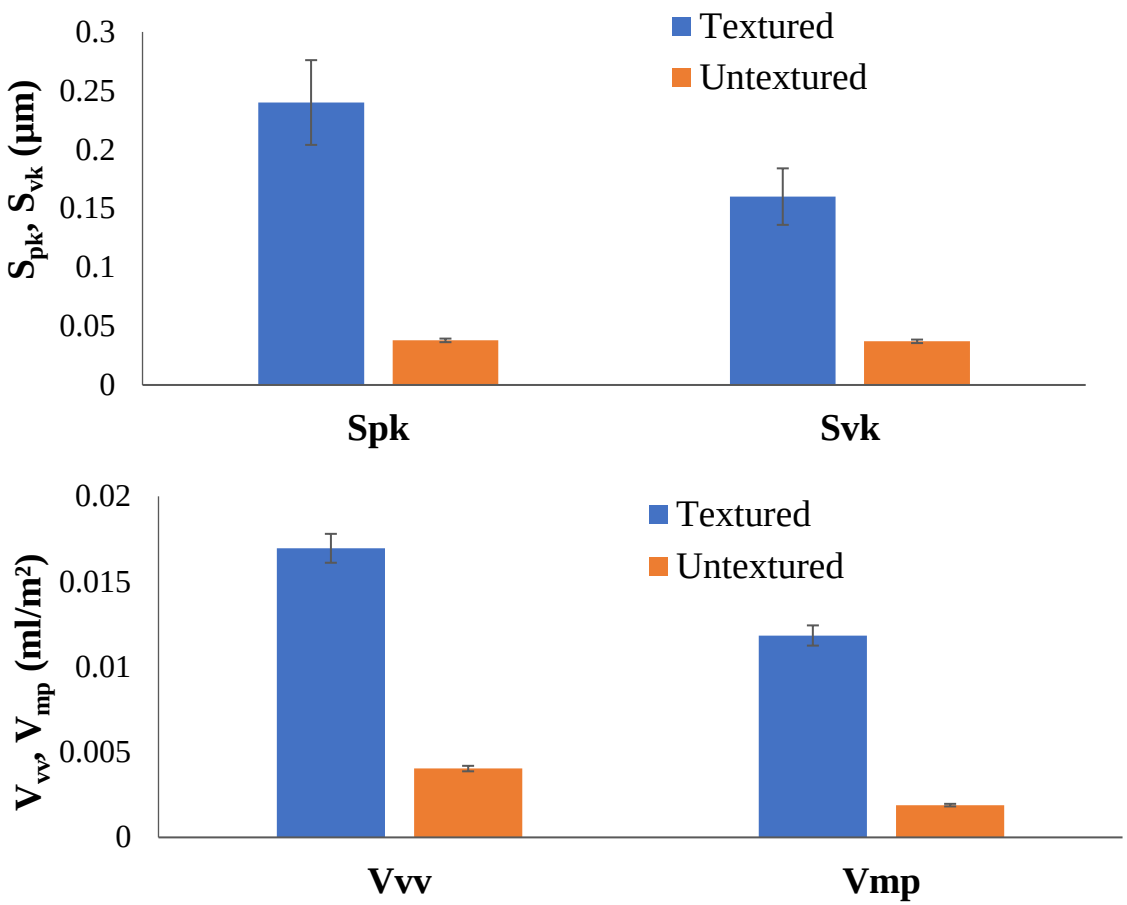

Figure 6.9: Comparison of selected volume parameters between raw textured and untextured discs.

As shown, the textured discs had both higher (about 4-5 times) S_{pk} (reduced peak height) and S_{vk} (reduced valley depth) values than untextured discs. Larger S_{pk} values explain the higher COF (Figure 6.2) in the break-in region where high peaks were worn off and larger WSD values were observed. Additionally, higher S_{vk} values imply deeper valleys helpful for lubricant retention and storage. Thus, initially, the valleys were not deep enough to store the lubricant particles in case of untextured discs. This could be the reason behind the high density of lubricant agglomerates observed on the wear track during the break-in period in the case of untextured discs. The standard deviation for textured discs was also higher when compared to untextured discs for all four of the parameters discussed above. This variability was attributed to

the mechanical polishing method that resulted in locally random textures at microscopic and sub-microscopic scales as previously noted. Similarly, the textured discs also showed 4-5 times higher peak and valley volumes (V_{mp} and V_{vv}) than untextured discs, indicating that more lubricant could be stored and delivered in the case of textured discs. Higher V_{mp} in the case of textured discs suggests more energy dissipation during the break-in stage and explains the early onset of tribo-chemical reactions for textured discs.

The evolution of areal and profile surface texture parameters is discussed below. The wear tracks on representative discs were measured and analyzed with same procedure described in Section 5-C.

I. Areal texture parameters

The results and interpretation of the evolution of areal texture parameters described in Table 3.2 is presented below. The L-filter and cut-off value (for areal and profile measurements, respectively) was chosen to be 0.08 mm, consistent with the ISO guidelines [86] and previous measurements. The raw disc data points shown at zero number of laps on X-axis denotes the texture parameters calculated on virgin disc samples using the same measurement settings.

Areal rms surface roughness (S_q)

Variation of areal surface roughness as a function of time is shown in Figure 6.10. It should be noted that the three regions (R1, R2 and R3) marked in the plot are with respect to the three regions defined for textured discs and are different for untextured discs as previously noted.

For textured discs, in the break-in period (R1), the surface roughness values initially increased and then dropped down. This was attributed to initial re-alignment of surface asperities (consistent with SEM micrographs observations) followed by the breaking in of core surface asperities that reduced the surface roughness. The observed trend in the variation of S_q in the

break-in stage (R1) followed a similar trend as that of the COF in R1 (Figure 6.2), indicating that the lubrication was surface roughness dominated at the beginning of tribotest. In the development stage (R2) and the steady-state stage (R3), the surface texture and tribofilm stabilized resulting in stable, steady-state friction. The S_q values for the textured discs stayed higher than the untextured discs at all time durations, suggesting that after the initial breaking-in of the asperities and onset of tribo-chemical reactions, the surface asperities were protected with tribofilm, preventing any further reduction in surface roughness.

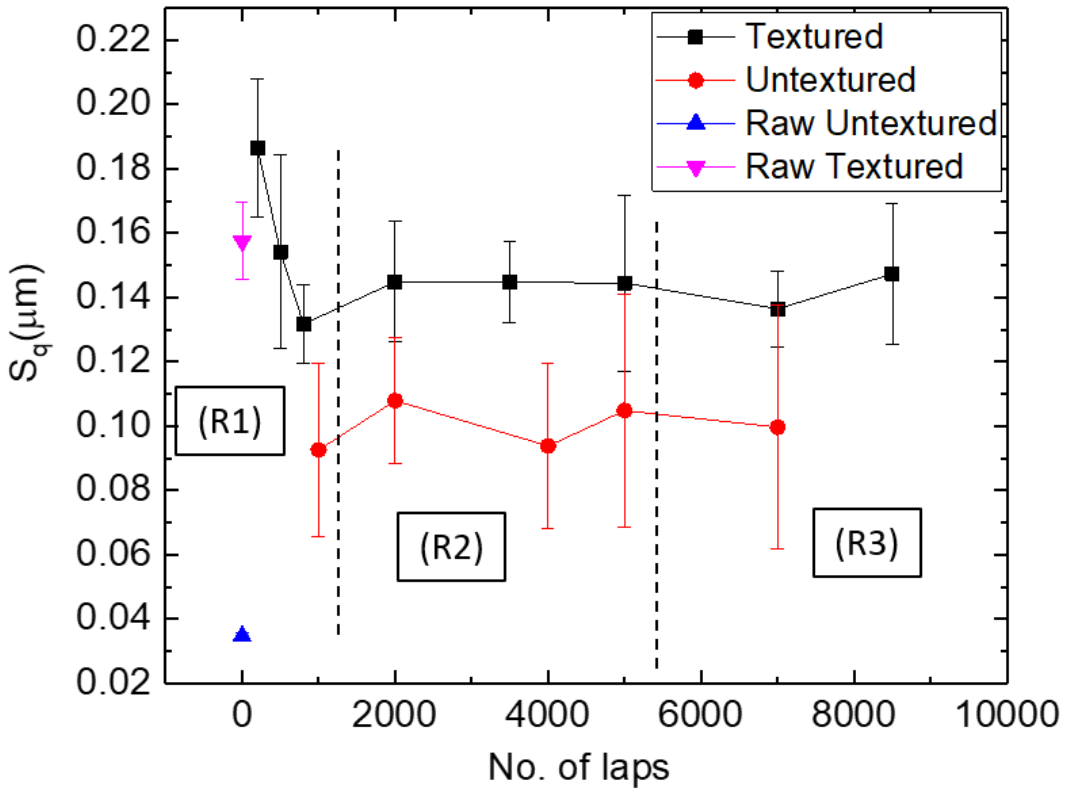

Figure 6.10 Evolution of the areal surface roughness (S_q) for textured and untextured discs.

In contrast, surface roughness for untextured discs increased during the break-in stage (up to 2000 laps) before dropping down and then stabilizing. This was because of the fact that initially isotropic surface features first had to re-organize and evolve into a directionally aligned texture before stabilizing and reaching a steady-state. In addition, as seen in Chapter 5 for

untextured discs, this interaction between the mating surface, creation of directional features, and eventual stabilization was a dynamic and stochastic process. This explains the larger standard deviation values for untextured discs in R2 and R3 in comparison with textured discs where the surface texture already had directional aligned surface asperities. As seen from the SEM images for textured discs (Figure 6.8), the microscopic presence of directional grooves was maintained into the steady-state. This suggests that the fabricated texture template controlled and manipulated the lubrication events during the test. Whereas, in case of untextured discs, surface texture self-adjusts (process-controlled evolution) in the presence of tribofilm under an applied load to deliver effective boundary lubrication.

Arithmetic mean peak curvature (S_{pc})

As seen in previous chapter, S_{pc} parameter was used to characterize average sharpness of peaks within the measurement area. Figure 6.11 shows the variation of mean peak curvature over time for textured and untextured discs.

For textured discs, the trend in evolution of S_{pc} followed a similar trend in the surface roughness (S_q) shown in Figure 6.10. At the beginning, S_{pc} increased due to the re-alignment of surface asperities as noted previously. However, direct asperity-to-asperity contact in case of textured discs led to rapid drop in the sharpness of peaks within first 1000 laps and triggered the onset of tribo-chemical reactions. The rapid activation, along with the ready presence of reservoirs (as opposed to untextured discs where these reservoirs are created during the tribotest) for lubricant storage, led to early stabilization and onset of steady-state in case of textured discs in comparison with untextured discs. As seen from Figure 6.11, the S_{pc} values for textured discs stabilized at lower time duration, confirming the observation that adding directional texture resulted in an early onset of tribo-chemical reactions and stabilization.

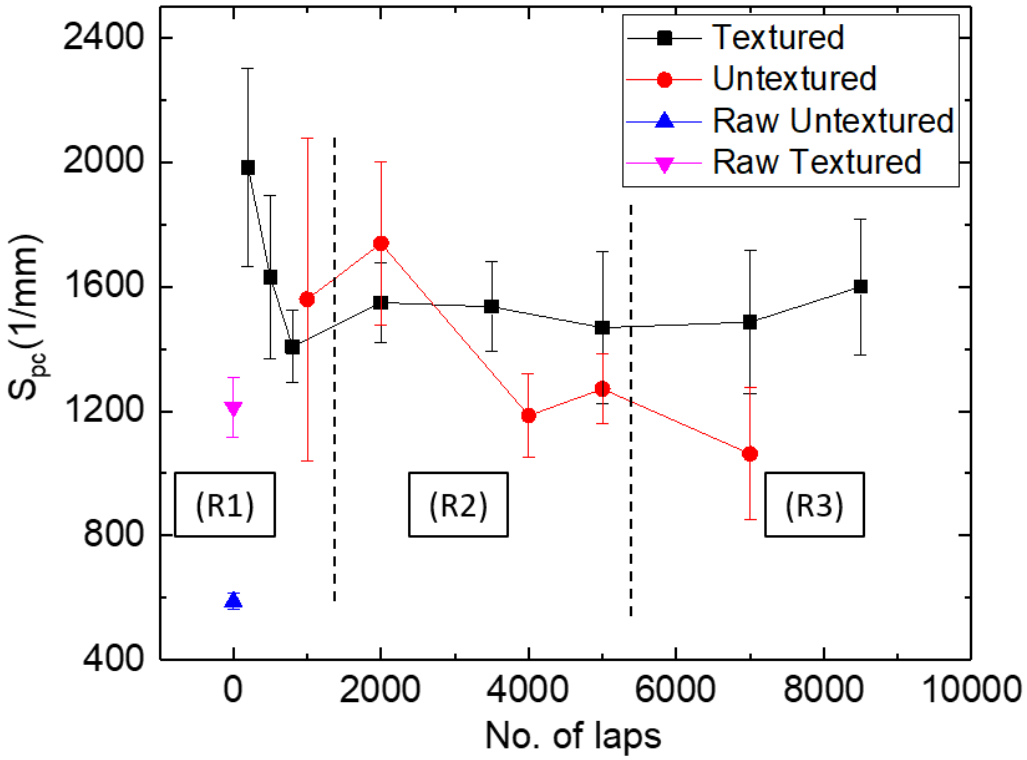

Figure 6.11 Variation of the mean peak curvature (S_{pc}) for textured and untextured discs.

Other differences between the textured and untextured discs are also worth noting. For untextured discs, S_{pc} values increased until 2000 laps due to initial re-alignment as well as re-organization of surface asperities (creation of directional features), then dropped during R2 before stabilizing to steady-state (possibly after formation of deep enough micro-reservoirs). The drop in S_{pc} values after 2000 laps was attributed to the further stabilization and development (also confirmed by drop in density of peaks after 2000 laps seen in Figure 6.12 below) of directional asperities formed during the R1 stage and was synergistic with tribo-chemical reactions. A similar drop in S_{pc} values was observed within the first 1000 laps for textured discs. This suggests that the addition of directional texture shifts the onset of tribo-chemical reactions and development to shorter times. In other words, not having an initial directional arrangement of asperities for untextured discs delays the onset of tribo-chemical reactions. These observations are consistent with the previous interpretations and COF data.

Density of peaks (S_{pd})

Comparison of the change in density of peaks as a function of time is shown in Figure 6.12 for textured and untextured discs. At the beginning, the S_{pd} value decreased sharply for both textured and untextured discs due to direct asperity-to-asperity contact. However, for textured discs the re-organization of asperities after initial re-alignment led to a slight increase in peak density before stabilization. It can also be seen that textured discs showed early onset of stabilization and steady-state possibly due to the presence of partially broken-in and partially aligned asperities compared to untextured discs, which is consistent with previous observations.

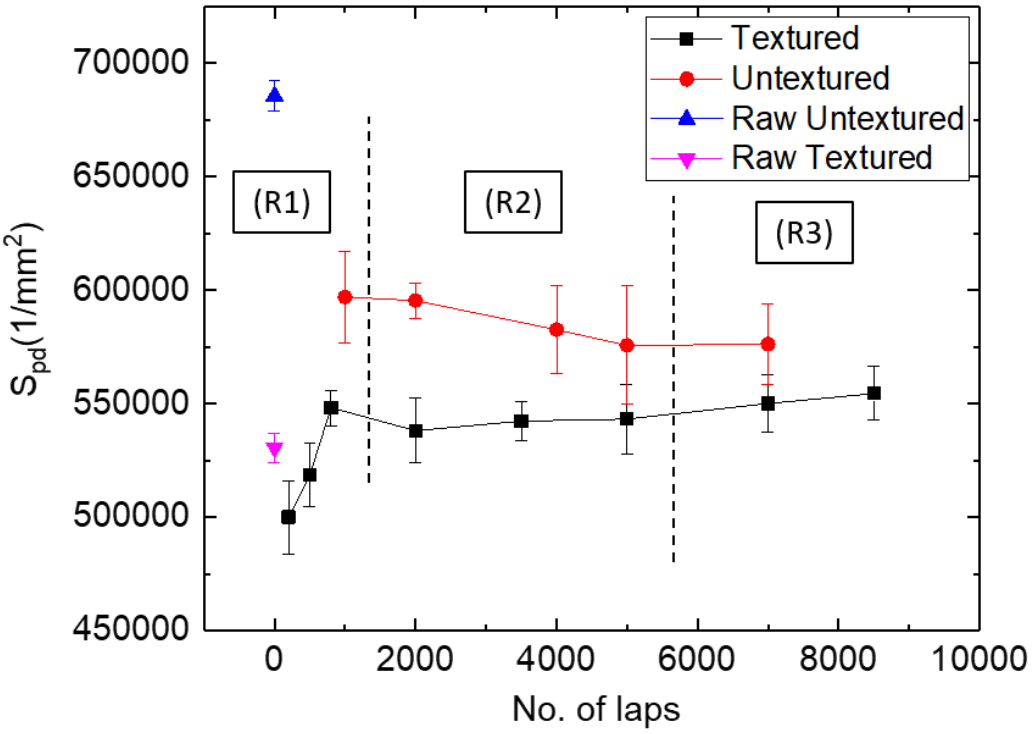

Figure 6.12 Variation of the density of peaks (S_{pd}) for textured and untextured discs.

Interestingly, for untextured discs, the overall change in S_{pd} values from raw disc (68000/mm^2) to the break-in period (60000/mm^2) to the steady-state values (58000/mm^2) was larger than that of textured discs (variation between 50000/mm^2 and 55000/mm^2). The difference between S_{pd} values for raw discs could be attributed to the fact that textured discs had a higher

valley volume (as discussed before) along with the presence of partially aligned peak/valley features. Whereas, untextured discs initially had a large number of closely spaced isotropic surface asperities, the asperities re-aligned and re-organized during the break-in period as a part of the process-controlled texture evolution. This stabilization of surface texture involved the creation of directional grooves (reservoirs) as noted in Chapter 5. Together, those factors led to a higher standard deviation and longer times to reach the steady-state in the case of untextured discs (as discussed previously for variation of S_{pc}) compared to textured discs which already had partially aligned asperities in the form of directional peaks and valleys by design.

II. Profile texture parameters

The results of profile measurements on the wear track on textured discs at different time intervals are presented below. The profile measurements were carried out using the process described in Section 3-B and illustrated in Figure 3.7. Two profile sections were taken on the raw data perpendicular the wear track direction as shown in Figure 3.7 and average values from all measurements are reported. The cut-off filter settings of 0.08 mm were used in accordance to ISO guidelines to filter out waviness component from the profile. [87]

Mean height of profile elements (R_c)

Figure 6.13 shows the evolution of mean heights across the wear track for textured and untextured discs for tested time intervals. Overall, the variation in R_c followed a similar trend to areal surface roughness (S_q). For textured discs, the initial increase in R_c could be attributed to the re-alignment of the asperities as seen in the SEM images. This was followed by a steady decline attributed to the wearing off core asperity peaks and was consistent with the trend observed above in the sharpness of peaks (S_{pc}) in Figure 6.11. After the initial re-organization of surface features during the break-in stage (R1), R_c values did not change appreciably in the

development stage (R2) and the steady-state (R3) stage, indicating the effectiveness of lubrication in maintaining the initial texture template.

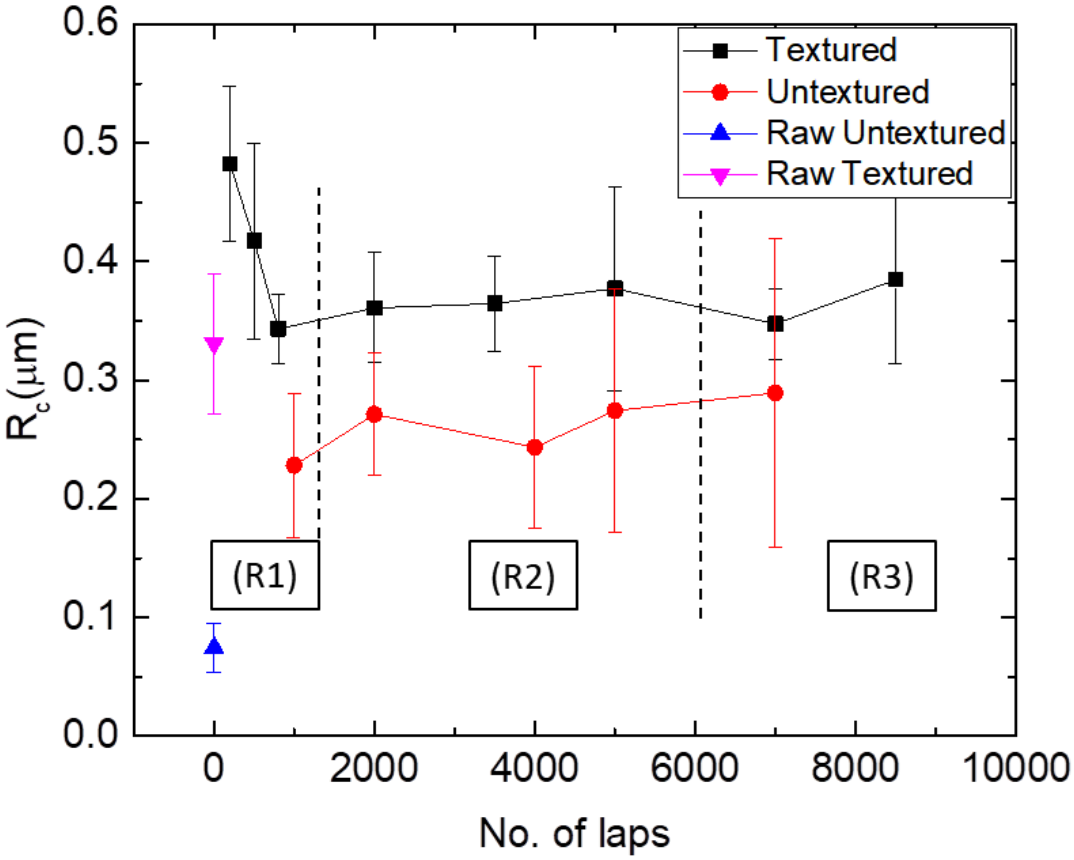

Figure 6.13 Variation in the mean height of profile elements (R_c) for textured and untextured discs.

For untextured discs, the initial increase in the mean height of features could be attributed to the re-organization and re-alignment of features and the creation of directionally aligned peaks and valleys as noted before. The change in R_c values in R2 and R3 could be attributed to the creation and evolution of directional texture as previously discussed with areal texture parameters.

Furthermore, under the assumption that changes in surface texture during re-organization primarily affected the sharp peaks and did not affect the deeper valleys (as characterized by S_{vk}

and V_{vv} above for raw discs), higher R_c values for textured discs indicated the presence of deeper valleys available for lubricant storage at all time intervals.

Mean width of profile elements (R_{sm})

The average periodicity of peaks and valleys across the wear track was gauged by studying the evolution of R_{sm} values. The evolution of R_{sm} values for textured and untextured discs is shown in Figure 6.14. As previously noted, the data point for raw untextured disc is not shown as it did not carry meaningful information. The R_{sm} values for the raw textured discs showed almost 15% variation from the mean value indicating variability in directional texturing (locally random asperities) performed by P1200 grit size paper and confirming previous observations.

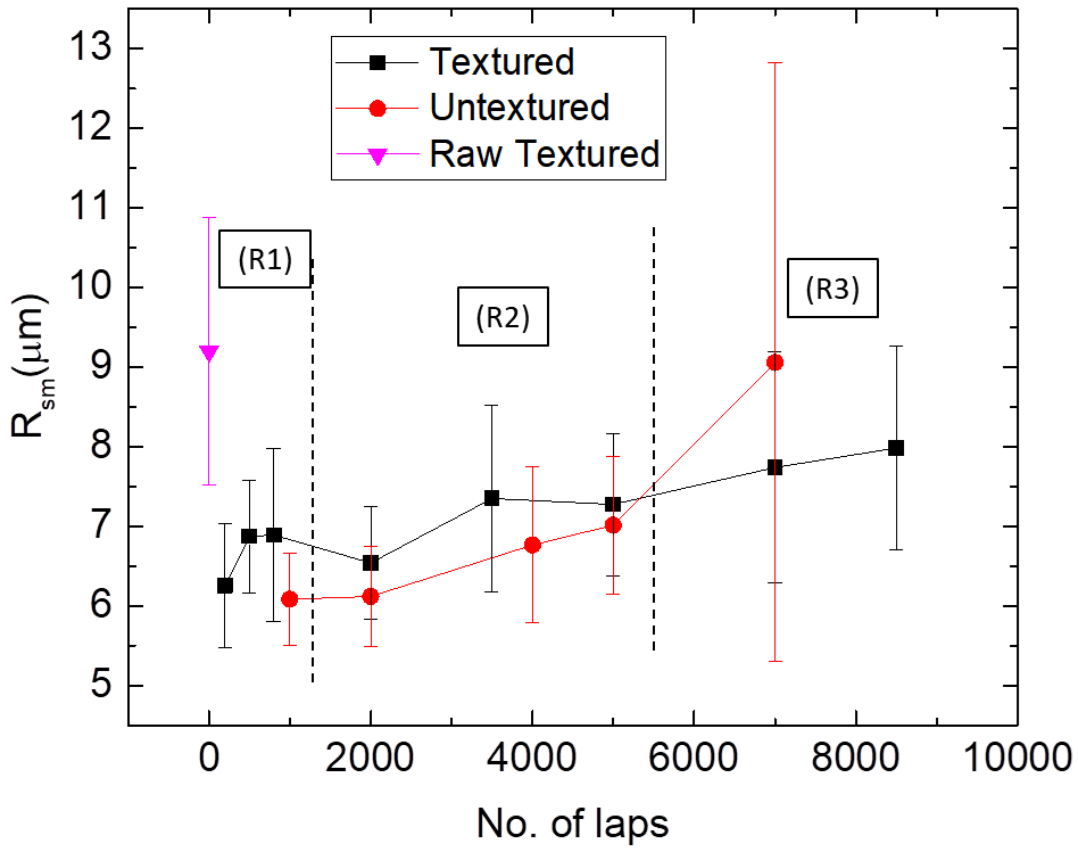

Figure 6.14 Variation in the mean width of profile elements (R_{sm}) for textured and untextured discs.

As shown in the plot, for textured discs, the re-alignment of asperities into directional texture and re-arrangement primarily occured during the break-in stage and early part of the development stage (up to 3500 laps time interval). The overall width of directional features increased slightly over time as surface features dynamically evolved synergistically with development and stabilization of tribofilm in R2 and R3.

For untextured discs, where the initial arrangement of asperities was isotropic, the creation of directional features leads to an increase in R_{sm} values. The directional texture continued to evolve during R2 and R3 as previously discussed and was reflected by a steady increase in R_{sm} values. These observations are consistent with the previous results discussed for untextured discs from SEM images and areal surface texture characterization.

The shift to longer wavelengths over time (for both textured and untextured discs) suggests that texture stabilization occurs by formation of wider grooves. This possibly happened by dissolution of small closely spaced peaks and valleys into larger directional features and highlights the dynamic nature of surface texture at the sub-microscopic scale. This re-arrangement might be beneficial for effective lubricant storage while delivering tribofilm to adjacent peaks and for effective load distribution.

However, it should be noted that those values were measured across the width of the wear track. As seen from optical micrographs, the width of the wear track increased with time. Hence, in order to compare the overall trend in evolution, R_{sm} values were normalized with the wear track widths and are shown in Figure 6.15. As seen from the figure, the normalized R_{sm} values stabilized early for textured discs as compared to untextured discs. The overall trend in the normalized R_{sm} values was also consistent with the fact that texture, tribofilm, and the COF evolved during R1 and R2 before reaching the steady-state (R3).

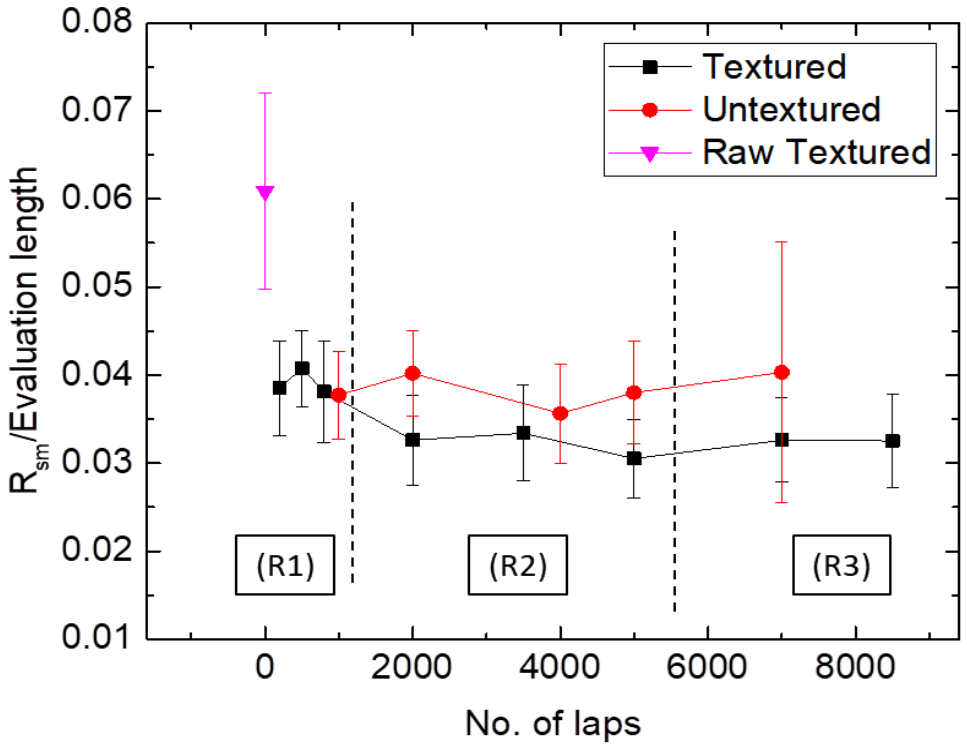

Figure 6.15 Variation in normalized R_{sm} for textured and untextured discs.

From the surface texture analysis of textured and untextured discs it can be concluded that the addition of macroscopic directional texture led to an early onset of tribo-chemical reactions and steady-state. The textured discs provided more volume for lubricant storage compared to the untextured discs and manipulated the tribofilm dynamics in the break-in period leading to stable steady-state COF values. The chemical analysis of tribofilm and the interaction of lubricant particles with surface asperities is explored further in the following discussion using Raman and cross-sectional TEM techniques.

D. Chemical Analysis: Raman Spectroscopy and FIB/TEM

This section details the analysis of tribofilm chemistry and morphology characterized with Raman and cross-sectional TEM. The measurements were performed following the process methodology described in Chapter 3 and discussed in Section 5-D. Three representative discs (800 laps - R1, 3500 laps - R2 and 7000 laps - R3) were chosen from each stage of lubrication

for TEM analysis. Also, as previously discussed in Section 5-D, the physisorbed lubricant was removed from the wear track using a cotton tip applicator before measurements.

I. Raman measurements

Raman measurements were performed under the same measurement settings described in Section 5-D.I (20X lens magnification, 20% laser power and three cumulative acquisitions with 60 sec acquisition time). Measurements were performed at three locations (similar to locations shown in Figure 5.15) across the wear track on representative sample discs and averaged data is presented. A background scan was performed on the raw textured disc using the same scan settings and subtracted to get corrected Raman spectra. Figure 6.16 shows the averaged corrected Raman spectra for the three stages of lubrication with 800 laps (R1), 3500 laps (R2), and 7000 laps (R3) time interval samples.

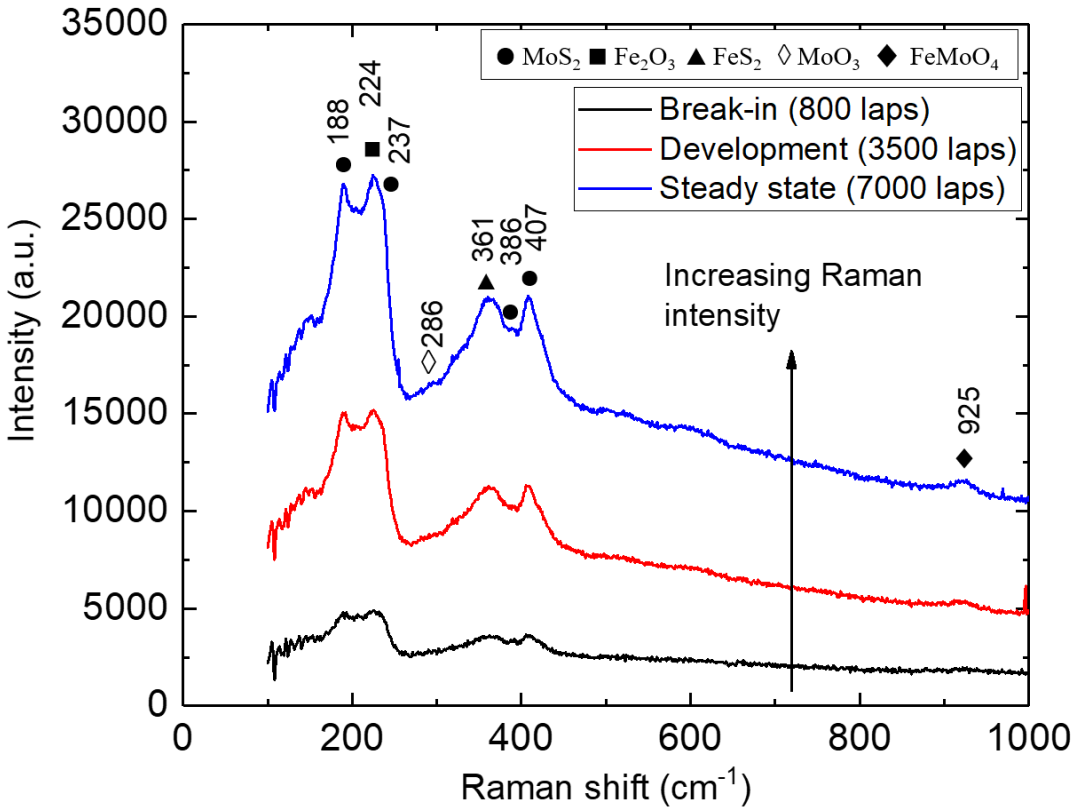

Figure 6.16 Averaged Raman spectra for the three stages of lubrication.

Like the results obtained for untextured discs, the Raman signal confirmed the presence of tribo-active elements and tribo-chemical compounds on the wear track. The peak intensity increased with time and peaks became sharper and more well defined, indicating increasing tribofilm coverage/ thickness and progression of chemical reactions between the substrate and functional lubricant additives. The Raman spectra showed peaks previously identified (Section 5-D.I) as MoS_2 tribofilm (primary modes E^1_{2g} at 386 cm^{-1}, A_{1g} at 407 cm^{-1} and secondary modes at 188 cm^{-1}, 237 cm^{-1}). Additional peaks corresponding to different lubricious compounds — Fe_2O_3 (224 cm^{-1}), FeS_2 at (361 cm^{-1}), molybdate $FeMoO_4$ (925 cm^{-1}) and weak signature of MoO_3 (286 cm^{-1}) — were also identified from the Raman spectra. Overall, the intensity of peaks increased with time with clear signatures of tribo-active elements and tribo-chemically formed compounds.

Similar to untextured discs, the peak at 925 cm^{-1} (molybdate) became more prominent with time indicating progression and evolution of complex compounds formed under harsh conditions because of tribo-chemical reactions. The intensity of the primary MoS_2 peaks at 7000 laps (steady-state) was comparable (around 21000 for 407 cm^{-1} peak) for both textured and untextured discs (Figure 5.16). This suggests that under steady-state conditions, the tribo-chemical reactions result in formation of lamellar MoS_2-based (as seen from TEM images) tribofilm with comparable tribofilm thickness and coverage for both textured and untextured discs. A similar comparison of peak intensities during the development stage (R2) showed higher Raman signal intensity for the textured discs (at 3500 laps) than untextured discs (at 4000 laps). Additionally, the presence of a $FeMoO_4$ peak at 925 cm^{-1} (indicative of progression of tribo-chemical reactions) was observed for the 3500 laps sample in Figure 6.16. This confirmed the early onset and stabilization of tribo-chemical reactions for textured discs. The MoS_2 peak at 237 cm^{-1} for textured disc was weaker than observed in the case of untextured discs. This was

possibly because of the stronger contribution of Fe_2O_3 peak at 224 cm^{-1} due to a higher asperity-to-asperity contact resulting in surface oxidation of asperities.

II. FIB/TEM measurements

The interaction between the surface asperities and lubricant particles and tribofilm was studied using cross-sectional TEM. As mentioned above, representative samples were chosen to analyze all three stages of lubrication from the tested time intervals. 800 laps (R1), 3500 laps (R2), and 7000 laps (R3) samples were used for cross-sectional analysis. On each sample, a representative area was identified by elemental mapping using EDS tool as shown in Figure 6.17.

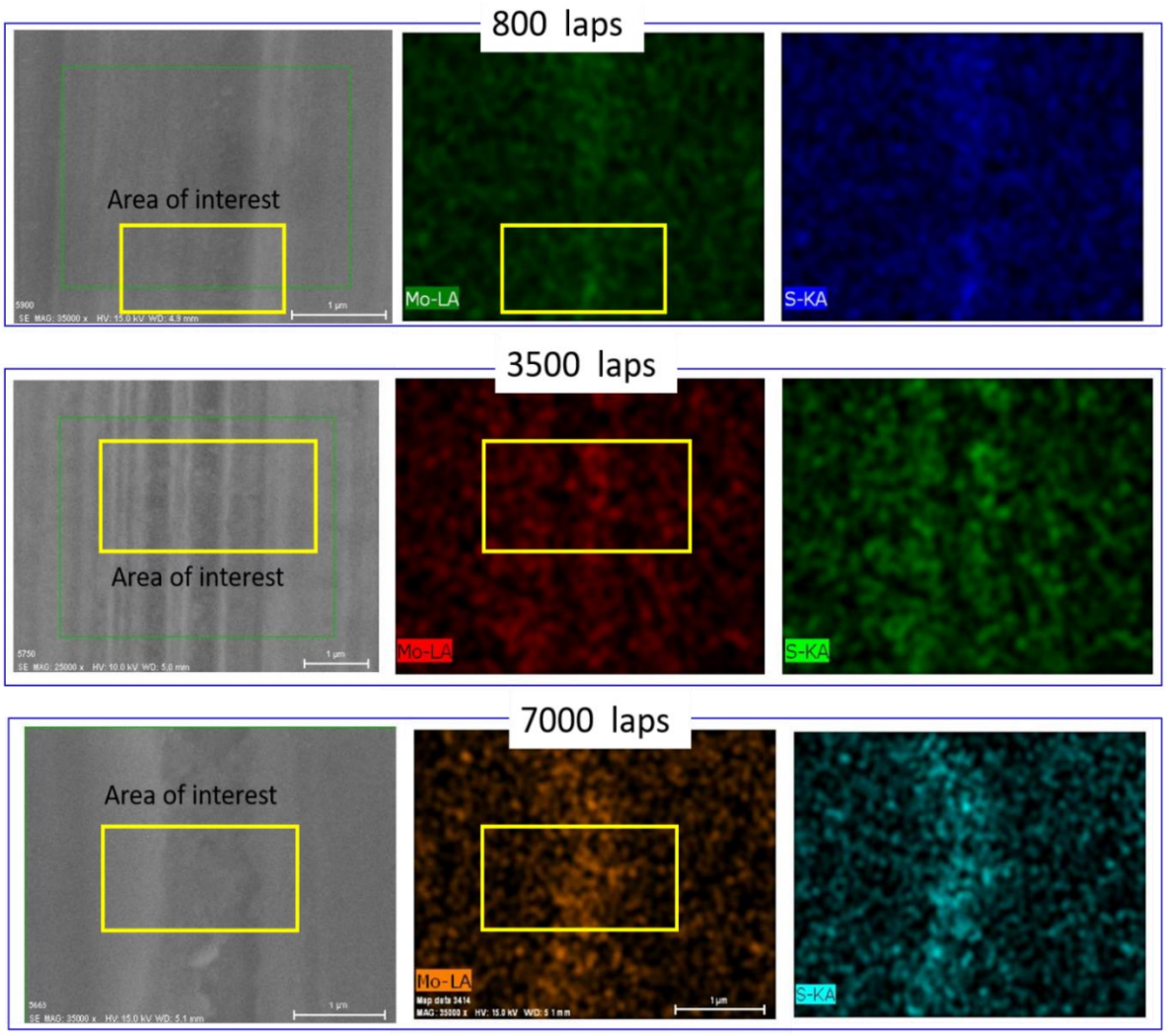

Figure 6.17 Selected areas of interest for FIB sample preparation.

The TEM samples were then prepared by using the process protocol described in Section 3-A.III. The area of interest was first protected with a platinum layer to avoid damage to the underlying tribofilm surface. The final polishing step to reduce the cross-section thickness was performed at low ion beam current (30 pA) to minimize damage to the sample due to high energy ions. The cross-section was cut on the textured disc surface to include at least one valley on the finished sample that was imaged using the TEM. This allowed monitoring of interaction between individual surface asperity and lubricant particles by high resolution TEM imaging. The cut cross-section was then mounted on a TEM grid and analyzed using high-resolution TEM and EDS line scans. Also, as seen in Figure 6.17, that the intensity of Mo and S signal in the EDS maps progressively increased and became more prominent from 800 laps to 7000 laps. This observation was consistent with the previous results of Raman measurements where it was noted that chemically reacted tribofilm increases in thickness and overall coverage with time.

The results of TEM measurements are shown below. Figure 6.18 and Figure 6.19 show TEM images and EDS scans for the 800 laps (R1) sample, Figure 6.20 and Figure 6.21 show TEM images and EDS scans for the 3500 laps (R2) sample, while TEM images and EDS scans for the 7000 laps (R3) sample are shown in Figure 6.22 and Figure 6.23, respectively. For TEM images, a low magnification image (top image in Figure 6.18 and top left images in Figure 6.20, Figure 6.22) showed a peak-valley region of interest followed by high magnification images at various points along the asperity peak and valley region. EDS line scans were taken in the peak and valley regions for all the samples to identify the interfacial chemistries. Since the total number of compiled images was large along with the individual TEM image size (for better resolution), all the results are first presented on following pages (page numbers 116-121). A collective analysis from all TEM images from three stages of lubrication is discussed next.

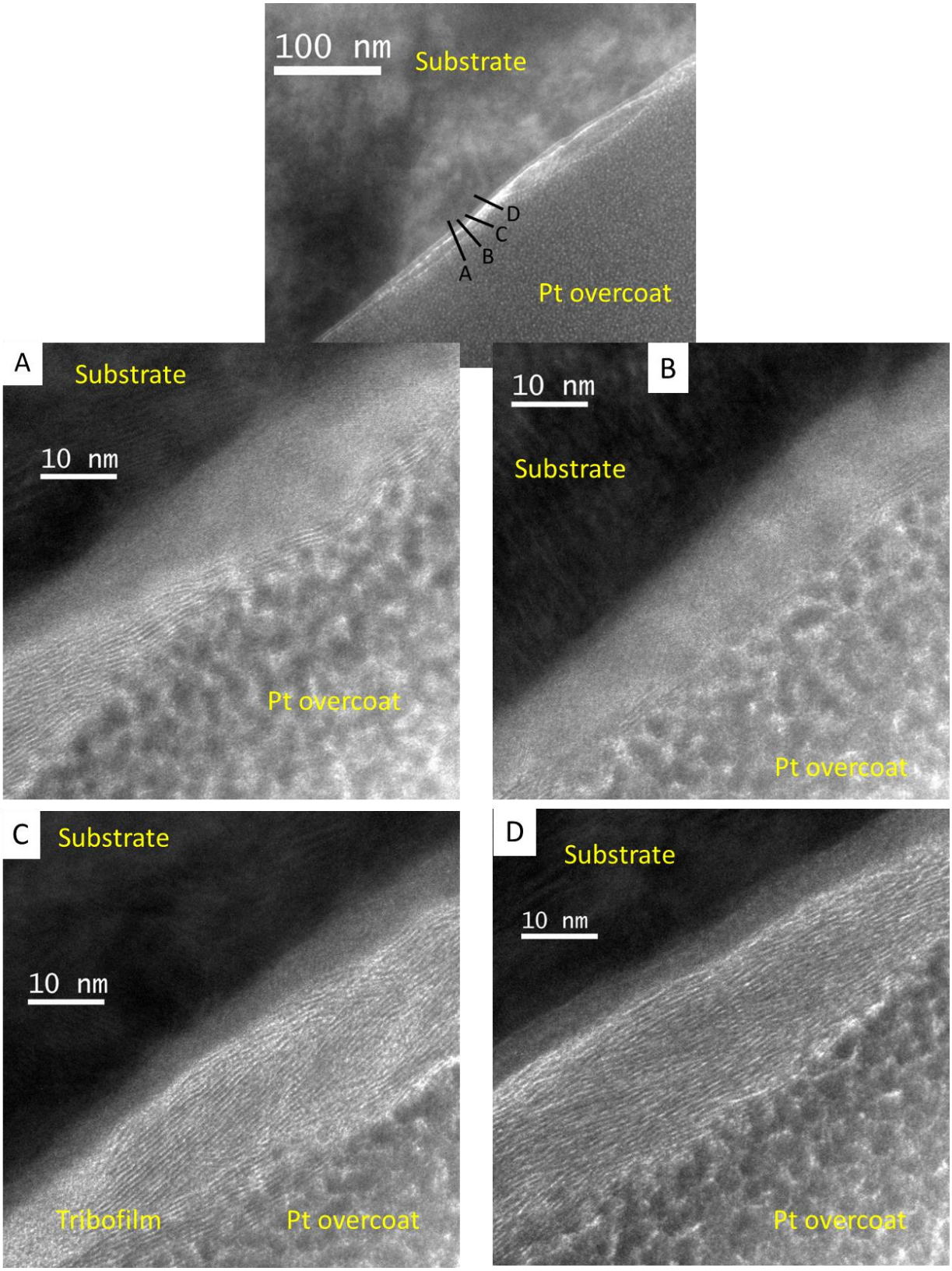

Figure 6.18 Cross-sectional TEM images of 800 laps (R1) sample.

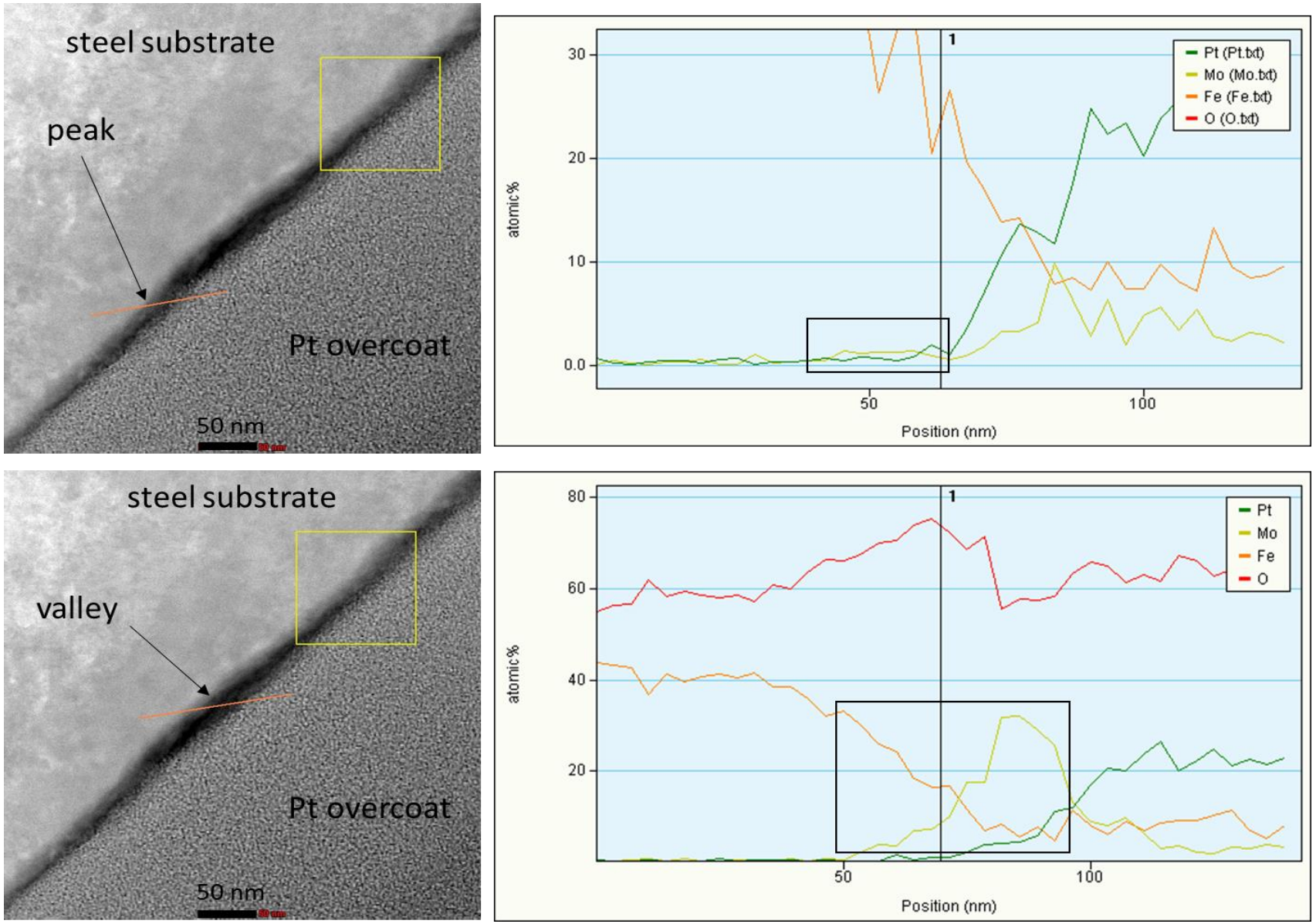

Figure 6.19 EDS line scans near peak and valley for 800 laps (R1) sample.

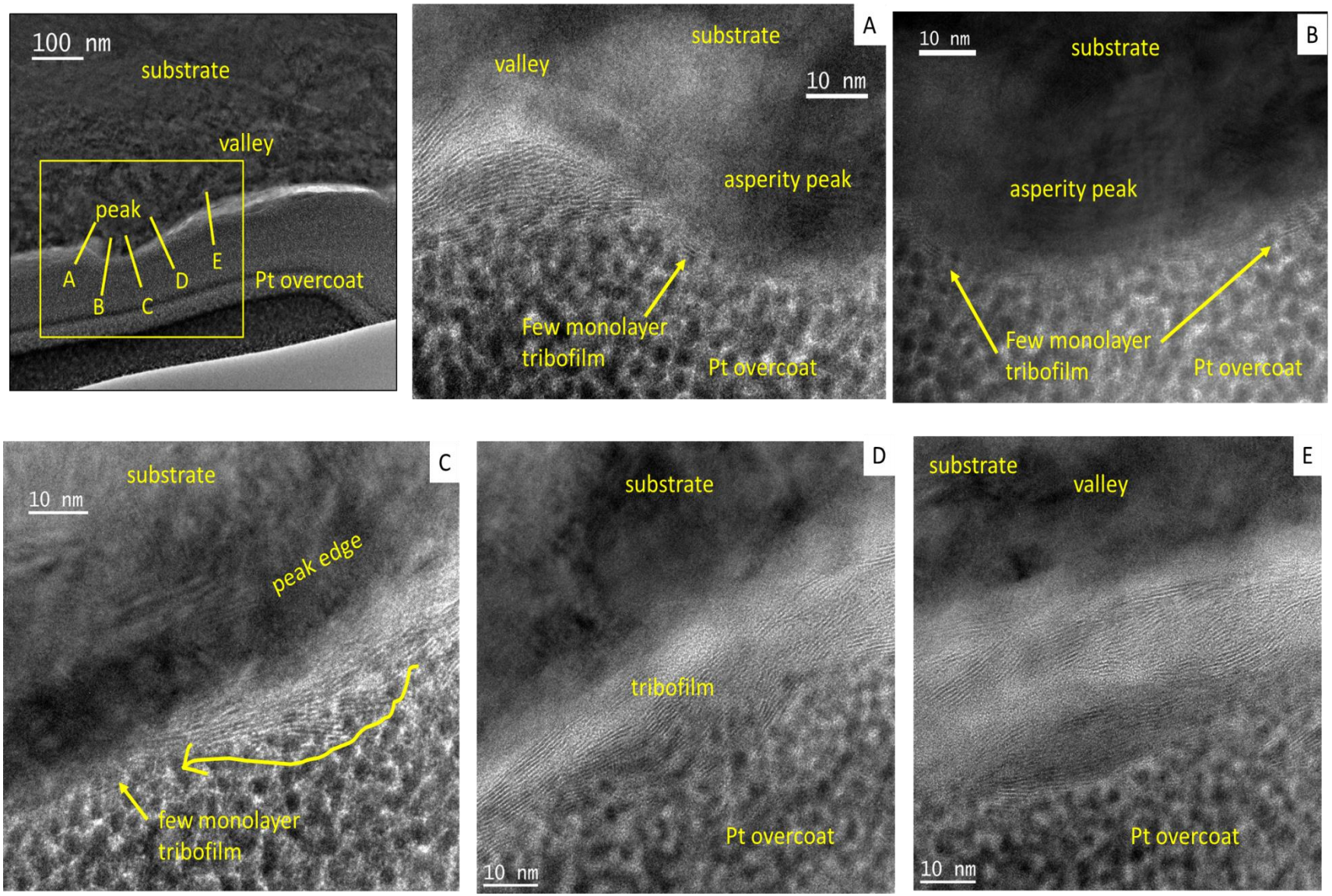

Figure 6.20 Cross-sectional TEM images of 3500 laps (R2) sample.

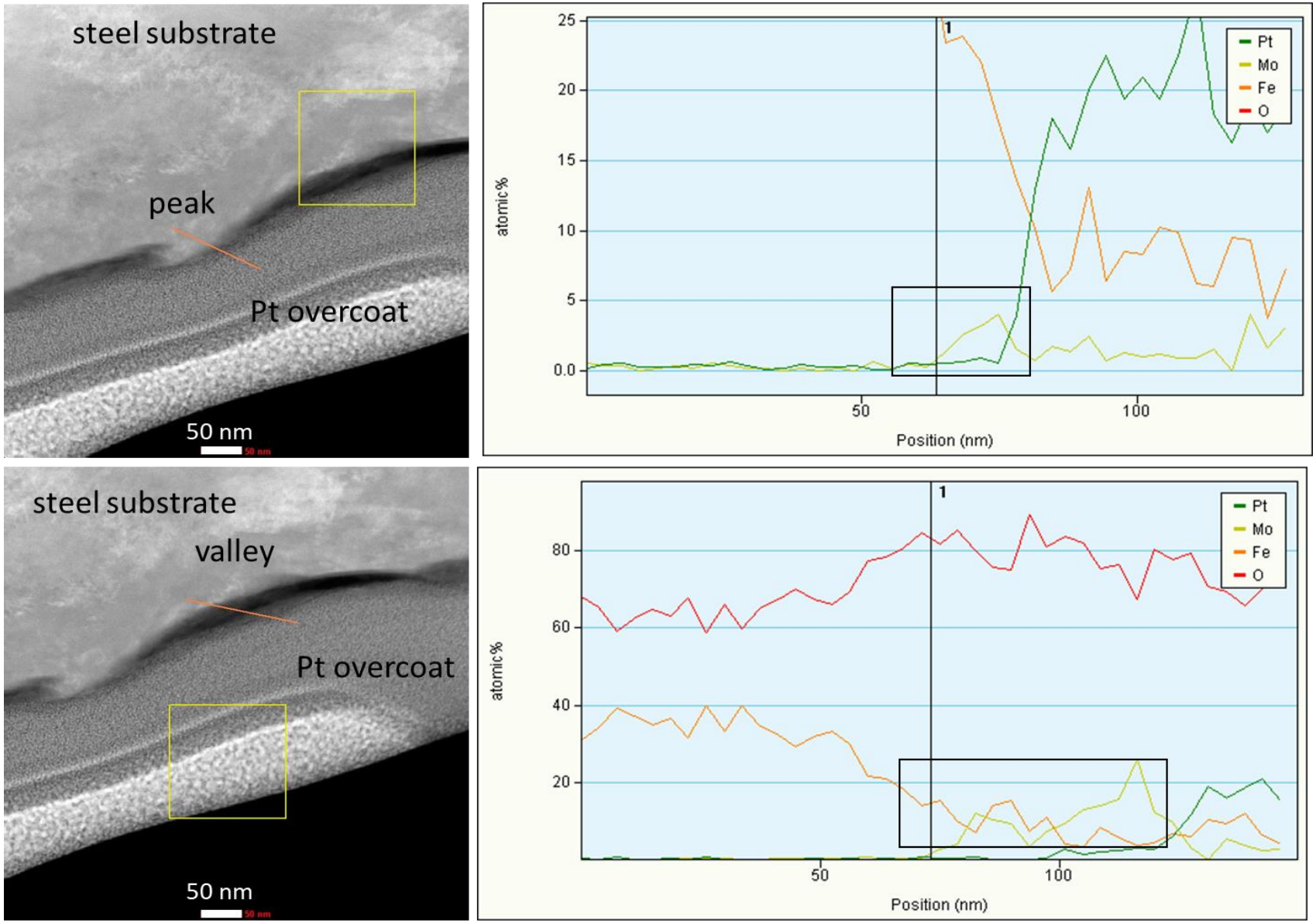

Figure 6.21 EDS line scans near peak and valley for 3500 laps (R2) sample.

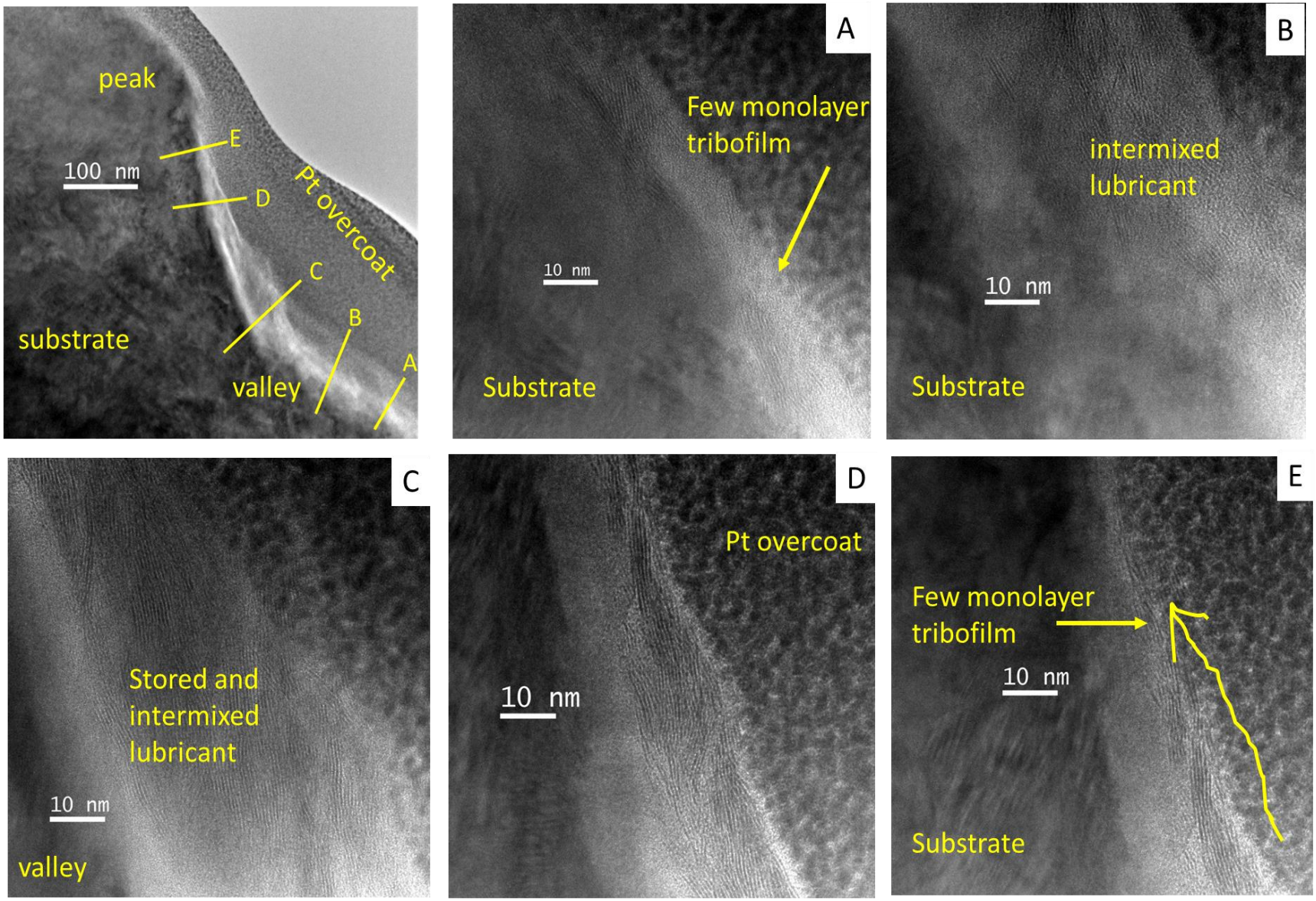

Figure 6.22 Cross-sectional TEM images of 7000 laps (R3) sample.

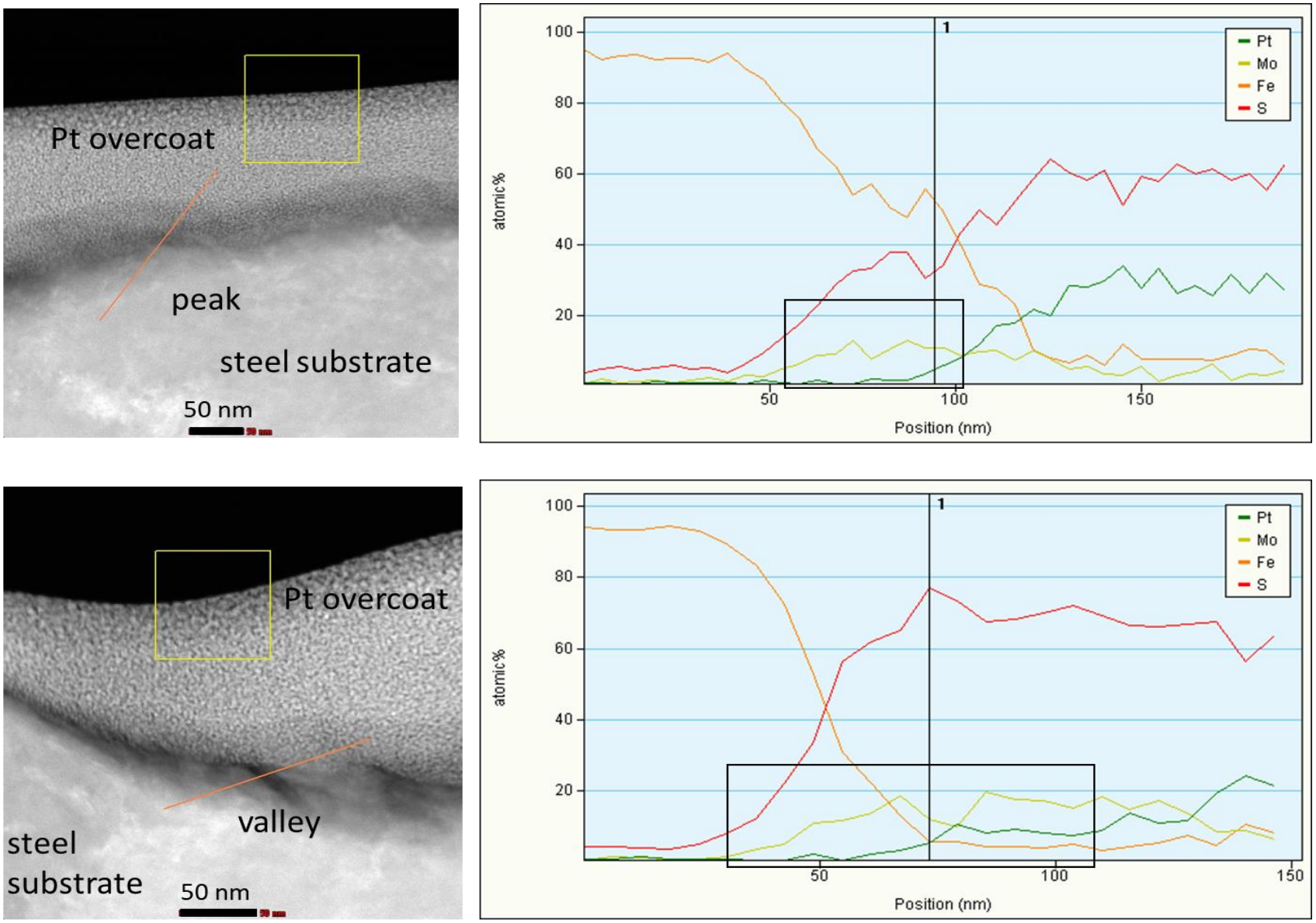

Figure 6.23 EDS line scans near peak and valley for 7000 laps (R3) sample.

The TEM images shown above confirm the lubrication mechanism proposed in Chapter 5 where the lubricant was stored in the valleys while delivering the tribofilm on the adjacent peaks as seen in Figure 6.18, Figure 6.20 and Figure 6.22. Few monolayers thick MoS_2 tribo-layers were observed near the asperity peaks confirming the surface protection offered by lamellar solid lubricant. Additionally, the conformal alignment of the lubricant layers with respect to the asperity edge angle could be seen (Figure 6.20-D and Figure 6.22-D) which was consistent with previous observations on untextured discs. These observations also indicated the self-assembly of lubricant layers with respect to the contours of underlying surface to provide better protection. The shearing and exfoliation of layers near the edge of the asperities to deliver protective layers was observed and is highlighted by arrows in Figure 6.20-C and Figure 6.22-E.

Corresponding EDS line scans confirmed the presence of tribo-active elements in the valleys at all three time durations as denoted by the black box in bottom portions of Figure 6.19, Figure 6.21 and Figure 6.23. This confirmed the storage of lubricant in valleys consistent with previous interpretations. The overall width of the black box also increased from 800 to 7000 laps consistent with the increasing tribofilm thickness and was also verified from high resolution TEM images presented in Figure 6.24 below.

While in the case of line scans near the peak region, the presence of Mo near the peak region became more distinguishable from the platinum signal (from the protective layer) as time increased from 800 laps to 7000 laps as indicated by the black box in the top portions of Figure 6.19, Figure 6.21, and Figure 6.23. This indicated the progression of tribo-chemical reactions and the effective delivery (better protection) of tribo-layers onto surface asperities with time.

A compiled series of selected images in the valley region is presented in Figure 6.24 for comparative evaluation. The thickness of MoS_2 layers stored within the valleys increased with

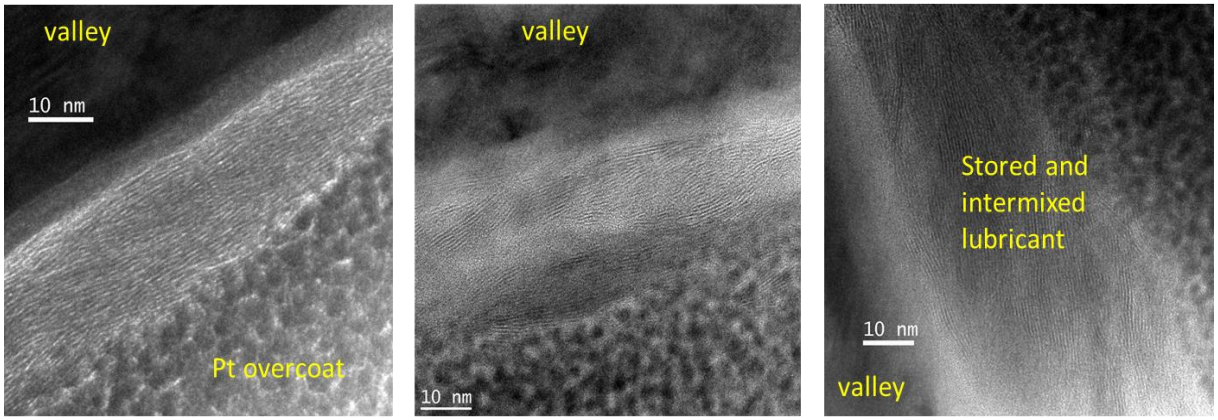

Figure 6.24 Evolution of stored tribo-layers within the surface valleys.

time from 800 laps to 7000 laps consistent with the observations made during the Raman measurements and similar to the previous observations on untextured discs. The degree on intermixing between the individual nanoparticle layers, as well as exfoliation of nanoparticles, also increased with time as seen from the images. This suggests that the individual nanoparticles were sheared at the mating contact points (asperities) leading to exfoliation and delivery of lamellar tribo-layers. This process repeated itself under continuous interaction between surface asperities and lubricant under the applied load resulting in consumption, exfoliation, and intermixing of lubricant particles over time. These intermixed and exfoliated layers were stored in the reservoir valleys as shown in Figure 6.24 . This observation proved the lubrication mechanism proposed earlier in Chapter 5 consistent with hypothesis in previous reported literature. [128]

E. Discussion of Lubrication Mechanism

Based on above results and analysis presented above, the following lubrication mechanism was proposed:

i. In the break-in stage (R1), lubrication is dominated by direct asperity-to-asperity contact

leading to the re-alignment and re-organization of surface asperities along the direction of motion within the wear track. Thus, effect of hierarchical texture features was observed in the break-in stage. The directional features on microscopic scales provide a template while the sub-microscopic asperities are re-aligned and re-organized. Textured discs show higher initial peak volume and reduced peak heights as compared to untextured discs. This leads to high starting COF and WSD values and more energy dissipation in the break-in stage. The presence of partially broken-in and partially directional asperities for textured discs along with higher peak volume leads to early onset of tribo-chemical reactions. Textured discs also have higher valley volume as compared to untextured discs helping the lubricant storage, retention and delivery.

ii. In the development stage (R2) and steady-state (R3), surface texture evolves and stabilizes along with the tribofilm resulting in a directionally aligned spatial arrangement of peaks and valleys across the wear track. The peaks are protected by sheared and exfoliated lubricant layers. The unreacted lubricant particles as well as sheared, intermixed and exfoliated layers are stored in the adjacent valleys as confirmed by TEM images. As time increases, more and more lubricant particles are sheared and react resulting in better tribofilm coverage and an increase in tribofilm thickness in stored valleys. The process of shearing, reacting and exfoliation is repeated during the continuous interaction between the mating surfaces and lubricant. The stored lubricant layers are conformally aligned with respect to the asperity angle suggesting that these layers are sheared along the asperity edge under the application of applied load while delivering a few monolayer thick tribofilm on asperity peaks as shown in Figure 6.25 below. Thus, stored lubricant layers and coated asperities together support the contact

load leading to a stable, steady-state friction consistent with previously proposed lubrication mechanisms for lamellar solid lubricants. [28], [128], [129]

F. Conclusion

A directional concentric texture was applied to the steel discs by polishing with SiC abrasive paper. The texture was directional on a larger scale yet remained locally random at the micron and sub-micron scales as a result of the selected fabrication process. This led to a re-alignment of surface asperities and an increased surface roughness during the early part of break-in stage. The textured discs also had higher valley depths (and volume) compared to untextured discs, resulting in effective lubricant storage and retention. It was found that the addition of directional roughness triggered an early onset and stabilization of tribofilm, delivering the desired frictional response. The analysis discovered for the first time (as shown in Figure 6.25) the presence of stored lubricant in valleys while delivering a lamellar MoS_2 tribo-layer (few monolayers) on nearby asperities.

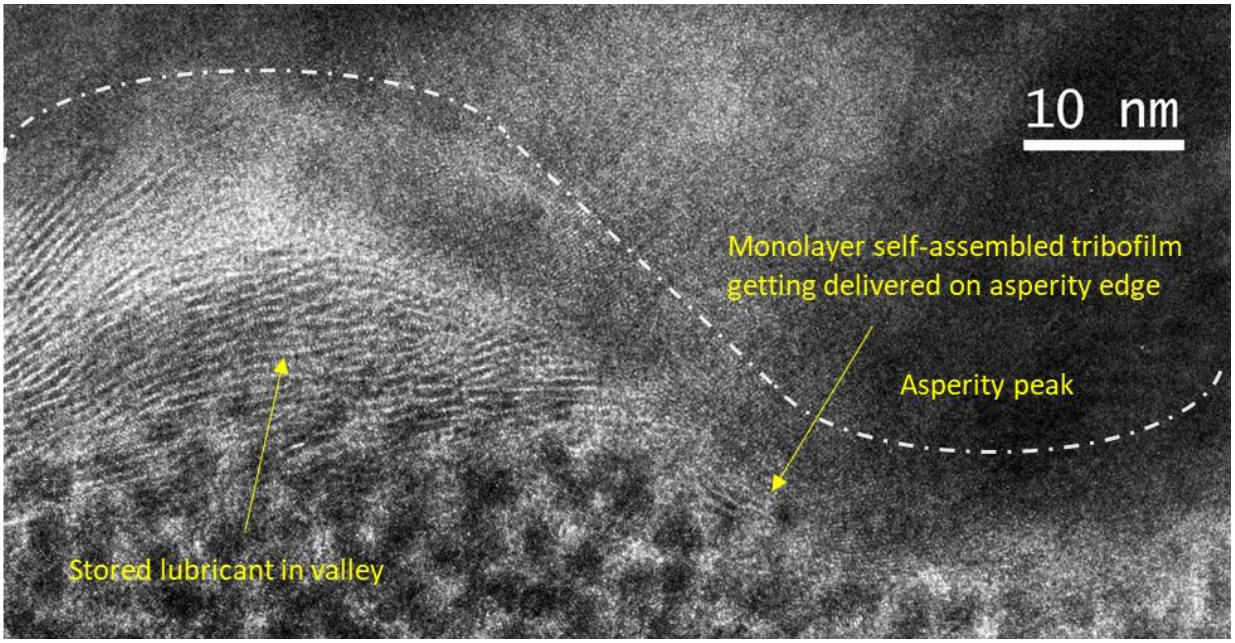

Figure 6.25 TEM micrograph of individual peak and adjacent valley showing behavior of stored lubricant and tribofilm.

Overall, it can be concluded that hierarchical texture features play a role in governing the tribo-chemical reactions and the dynamics of surface re-organization during break-in stage and thereafter. Initial re-alignment and re-organization of surface asperities in the direction of relative motion is expected because of direct asperity-to-asperity contact under boundary lubrication during the break-in stage before the activation of tribofilm. Since the onset of tribo-chemical reactions is a result of interaction between mating surfaces and energy dissipation, it requires finite time before activation. Thus, it is concluded that break-in and re-organization of surface asperities is a fundamental event at sub-microscopic scales and should be accounted for while designing textures for tribological applications.

7. FUTURE DIRECTIONS FOR RESEARCH

The work presented in this research identified the three stages of lubrication and synergistic progression of texture and tribofilm. The simple texturing technique was utilized to study the effect of intentionally fabricated peaks and valleys on tribofilm formation, delivery, and evolution. Investigating the effect of deterministic textures on tribofilm formation and evolution would be a promising next step for this research. In addition to textured surfaces, the testing setup and variables such as lubricant chemistry and concentration can be varied to further explore the effect of surface texture on manipulating frictional response. This section presents a very brief outlook of potential future directions of this research.

i. Different textures and texturing techniques:

As discussed before, the textures studied during this research were directional at the macroscopic scale and stochastic at micron and sub-micron scales. Different texturing techniques including laser texturing (with optimized texture design) and electro-chemical machining should be explored to fabricate more deterministic textures for further study. Insights gained from tribological tests on LST disc and recommendations for further optimization of texture design are presented in Appendix C. Additionally, bio-inspired directional textures such a snake skin and shark skin can also be studied.

ii. Tribo-testing setup and lubrication conditions:

Different tribological testing setups such as 4-ball wear can be explored to study effect of contact mechanics on evolution of surface texture. Furthermore, effect of lubricant starvation should be studied under appropriate time intervals and testing conditions.

iii. Different material choices:

During this research, steel was used as a material of interest because of its wide

application in industry. However, semiconductors (for MEMS/NEMS devices) and ceramic/polymeric materials (for magnetic storage media and lubrication) and functional coatings could also potentially benefit from this research and should be explored further.

iv. In-situ measurements:

If possible, in-situ measurements of surface texture would be extremely beneficial to capture the dynamic events during a tribological tests and its feasibility should be explored for real-time monitoring of surface features of interest. This might also allow for the use of functional volume parameters from the ISO 25178 set to gain more information on the evolution of texture.

v. Simulation and modeling:

The effect of surface roughness on the energy dissipation and tribo-chemical reactions should be further explored by theoretical simulation studies. Modeling the changes in surface roughness as from a theoretical thermodynamic point of view will be beneficial considering the surface energy changes associated with the evolution of textural features as well as for considering the tribo-chemical reactions.

REFERENCES

[1] A. Verma, “Fundamental Understanding of the Synthesis and Tribological Behavior of Organic-inorganic Nanoparticles,” University of Arkansas, 2008.

[2] P. Kalita, “Design and fundamental understanding of minimum quantity lubrication (MQL) assisted grinding using advanced nanolubricants,” University of Arkansas, 2013.

[3] W. Zhang, “Fundamental Understanding of Evolution of Tribofilms under Boundary Lubrication during Nanolubrication,” University of Arkansas, 2016.

[4] K. Holmberg, P. Andersson, and A. Erdemir, “Global energy consumption due to friction in passenger cars,” *Tribol. Int.*, vol. 47, pp. 221–234, Mar. 2012.

[5] K. Holmberg, P. Kivikytö-Reponen, P. Härkisaari, K. Valtonen, and A. Erdemir, “Global energy consumption due to friction and wear in the mining industry,” *Tribol. Int.*, vol. 115, pp. 116–139, Nov. 2017.

[6] K. Holmberg and A. Erdemir, “Influence of tribology on global energy consumption, costs and emissions,” *Friction*, vol. 5, no. 3, pp. 263–284, Sep. 2017.

[7] B. A. W. Stachowiak Gwidon W., “Introduction,” in *Engineering Tribology*, Elsevier, 2014, pp. 1–10.

[8] “Lubrication regimes [SubsTech].” [Online]. Available: http://www.substech.com/dokuwiki/doku.php?id=lubrication_regimes. [Accessed: 08-Mar-2018].

[9] “Hydrodynamic Lubrication,” in *Encyclopedia of Tribology*, Boston, MA: Springer US, 2013, pp. 1748–1748.

[10] C. M. Mate, “Lubrication in tight spots,” in *Tribology on the Small Scale*, Oxford University Press, 2007, pp. 246–283.

[11] B. Bhushan, “Boundary Lubrication and Lubricants,” in *Introduction to Tribology*, John Wiley & Sons, Ltd, 2013, pp. 501–523.

[12] S. M. Hsu, “Boundary lubrication: current understanding,” *Tribol. Lett.*, vol. 3, no. 1, pp. 1–11, 1997.

[13] S. Hironaka, “Boundary lubrication and lubricants,” *Three Bond Tech. News*, vol. 9, pp. 1–8, 1984.

[14] S. M. Hsu, “Molecular basis of lubrication,” *Tribol. Int.*, vol. 37, no. 7, pp. 553–559, 2004.

[15] B. A. W. Stachowiak Gwidon W., “Boundary and Extreme Pressure Lubrication,” in *Engineering Tribology*, Elsevier, 2014, pp. 371–428.

[16] J. Williams, “Boundary lubrication and friction,” in *Engineering Tribology*, Cambridge University Press, 2005, pp. 348–380.

[17] S. M. Hsu, “Nano-lubrication: concept and design,” *Tribol. Int.*, vol. 37, no. 7, pp. 537–545, Jul. 2004.

[18] S. Jacobson and S. Hogmark, “Surface modifications in tribological contacts,” *Wear*, vol. 266, no. 3–4, pp. 370–378, Feb. 2009.

[19] W. Zhang, M. P. Jahan, and A. P. Malshe, “Chemical Understanding of Friction Polymer Based Tribo-Chemical Films Derived From Nanolubricant,” in *ASME/STLE 2012 International Joint Tribology Conference*, 2012, pp. 13–15.

[20] N. K. Myshkin, A. Y. Grigoriev, S. A. Chizhik, K. Y. Choi, and M. I. Petrokovets, “Surface roughness and texture analysis in microscale,” *Wear*, vol. 254, no. 10, pp. 1001–1009, 2003.

[21] R. Leach, “CIRP Encyclopedia of Production Engineering,” The International Academy for Produ, Ed. Springer Berlin Heidelberg, 2018, pp. 2–5.

[22] A. Malshe, K. Rajurkar, A. Samant, H. N. Hansen, S. Bapat, and W. Jiang, “Bio-inspired functional surfaces for advanced applications,” *CIRP Ann. - Manuf. Technol.*, vol. 62, no. 2, pp. 607–628, 2013.

[23] B. Bhushan, “Biomimetics: lessons from nature--an overview,” *Philos. Trans. A. Math. Phys. Eng. Sci.*, vol. 367, no. 1893, pp. 1445–86, 2009.

[24] K. Liu and L. Jiang, “Bio-inspired design of multiscale structures for function integration,” *Nano Today*, vol. 6, no. 2, pp. 155–175, Apr. 2011.

[25] A. R. Parker and C. R. Lawrence, “Water capture by a desert beetle,” *Nature*, vol. 414, no. 6859, pp. 33–34, Nov. 2001.

[26] R. K. Leach, “Surface topography measurement instrumentation,” in *Fundamental Principles of Engineering Nanometrology*, Oxford; Amsterdam: Elsevier, 2010, pp. 115–175.

[27] “Geometrical product specifications (GPS) -- Surface texture: Areal -- Part 2: Terms, definitions and surface texture parameters,” in *ISO 25178*, International Organization for Standardization, 2012.

[28] A. Verma, W. Jiang, H. H. Abu Safe, W. D. Brown, and A. P. Malshe, “Tribological Behavior of Deagglomerated Active Inorganic Nanoparticles for Advanced Lubrication,” *Tribol. Trans.*, vol. 51, no. 5, pp. 673–678, 2008.

[29] P. Kalita, A. P. Malshe, and K. P. Rajurkar, “Study of tribo-chemical lubricant film formation during application of nanolubricants in minimum quantity lubrication (MQL) grinding,” *CIRP Ann.*, vol. 61, no. 1, pp. 327–330, 2012.

[30] W. Zhang, S. Bapat, A. P. Malshe, and K. P. Rajurkar, “Understanding evolution of tribo-chemical interfaces during boundary lubrication in manufacturing,” *CIRP Ann.*, vol. 66, no. 1, pp. 555–558, 2017.

[31] N. Talib, R. M. Nasir, and E. A. Rahim, “Tribological behaviour of modified jatropha oil by mixing hexagonal boron nitride nanoparticles as a bio-based lubricant for machining processes,” *J. Clean. Prod.*, vol. 147, pp. 360–378, 2017.

[32] Q. Wan, Y. Jin, P. Sun, and Y. Ding, “Tribological Behaviour of a Lubricant Oil Containing Boron Nitride Nanoparticles,” *Procedia Eng.*, vol. 102, pp. 1038–1045, 2015.

[33] J. Kogovšek and M. Kalin, “Various MoS_2-, WS_2- and C-based micro- and nanoparticles in boundary lubrication,” *Tribol. Lett.*, vol. 53, no. 3, pp. 585–597, 2014.

[34] Y. Zhang, Y. Xu, Y. Yang, S. Zhang, P. Zhang, and Z. Zhang, “Synthesis and tribological properties of oil-soluble copper nanoparticles as environmentally friendly lubricating oil additives,” *Ind. Lubr. Tribol.*, vol. 67, no. 3, pp. 227–232, Apr. 2015.

[35] C. Kumara, H. Luo, D. N. Leonard, H. M. Meyer, and J. Qu, “Organic-Modified Silver Nanoparticles as Lubricant Additives,” *ACS Appl. Mater. Interfaces*, vol. 9, no. 42, pp. 37227–37237, 2017.

[36] W. Zhang, D. Demydov, M. P. Jahan, K. Mistry, A. Erdemir, and A. P. Malshe, “Fundamental understanding of the tribological and thermal behavior of Ag–MoS_2 nanoparticle-based multi-component lubricating system,” *Wear*, vol. 288, pp. 9–16, May 2012.

[37] H. Ghaednia, R. L. Jackson, and J. M. Khodadadi, “Experimental analysis of stable CuO nanoparticle enhanced lubricants,” *J. Exp. Nanosci.*, vol. 10, no. 1, pp. 1–18, Jan. 2015.

[38] S. Ingole, A. Charanpahari, A. Kakade, S. S. Umare, D. V. Bhatt, and J. Menghani, “Tribological behavior of nano TiO_2 as an additive in base oil,” *Wear*, 2013.

[39] H. Wu, J. Zhao, X. Cheng, W. Xia, A. He, J.-H. Yun, S. Huang, L. Wang, H. Huang, S. Jiao, and Z. Jiang, “Friction and wear characteristics of TiO_2 nano-additive water-based lubricant on ferritic stainless steel,” *Tribol. Int.*, vol. 117, no. August 2017, pp. 24–38, 2018.

[40] S. M. Alves, B. S. Barros, M. F. Trajano, K. S. B. Ribeiro, and E. Moura, “Tribological behavior of vegetable oil-based lubricants with nanoparticles of oxides in boundary lubrication conditions,” *Tribol. Int.*, vol. 65, pp. 28–36, 2013.

[41] M. Akbulut, “Nanoparticle-Based Lubrication Systems,” *J. Powder Metall. Min.*, vol. 1, no. 1, pp. 1–3, 2012.

[42] A. K. Rasheed, M. Khalid, W. Rashmi, T. C. S. M. Gupta, and A. Chan, “Graphene based nanofluids and nanolubricants – Review of recent developments,” *Renew. Sustain. Energy Rev.*, vol. 63, pp. 346–362, 2016.

[43] T. W. Scharf and S. V. Prasad, “Solid lubricants: A review,” *Journal of Materials Science*. 2013.

[44] S. Shahnazar, S. Bagheri, and S. B. Abd Hamid, “Enhancing lubricant properties by nanoparticle additives,” *Int. J. Hydrogen Energy*, vol. 41, no. 4, pp. 3153–3170, Jan. 2016.

[45] W. Dai, B. Kheireddin, H. Gao, and H. Liang, “Roles of nanoparticles in oil lubrication,” *Tribol. Int.*, vol. 102, pp. 88–98, 2016.

[46] M. Gulzar, H. H. Masjuki, M. A. Kalam, M. Varman, N. W. M. Zulkifli, R. A. Mufti, and R. Zahid, “Tribological performance of nanoparticles as lubricating oil additives,” *J. Nanoparticle Res.*, vol. 18, no. 8, pp. 1–25, 2016.

[47] C. Gachot, A. Rosenkranz, S. M. Hsu, and H. L. Costa, “A critical assessment of surface texturing for friction and wear improvement,” *Wear*, vol. 372–373, pp. 21–41, Feb. 2017.

[48] M. Scaraggi, F. P. Mezzapesa, G. Carbone, A. Ancona, and L. Tricarico, “Friction properties of lubricated laser-micro-textured-surfaces: An experimental study from boundary to hydrodynamic lubrication,” *Tribol. Lett.*, vol. 49, no. 1, pp. 117–125, 2013.

[49] I. Etsion, “Modeling of surface texturing in hydrodynamic lubrication,” *Friction*, vol. 1, no. 3, pp. 195–209, 2013.

[50] S. Kango, D. Singh, and R. K. Sharma, “Numerical investigation on the influence of surface texture on the performance of hydrodynamic journal bearing,” *Meccanica*, vol. 47, no. 1, pp. 469–482, 2011.

[51] Q. Liu, N. Lin, J. Zou, J. Guo, D. Li, S. Yuan, R. Xie, Z. Wang, Y. Ma, Z. Wang, and B. Tang, “Research Progress in Improving Tribological Behaviors of Iron and Steel Materials Via surface Texturing in China: A literature Review,” *Rev. Adv. Mater. Sci.*, vol. 49, no. 2, pp. 171–188, 2017.

[52] Z. Wu, J. Deng, H. Zhang, Y. Lian, and J. Zhao, “Tribological behavior of textured cemented carbide filled with solid lubricants in dry sliding with titanium alloys,” *Wear*, 2012.

[53] Y. Xing, J. Deng, Z. Wu, and H. Cheng, “Effect of regular surface textures generated by laser on tribological behavior of Si_3N_4/TiC ceramic,” *Appl. Surf. Sci.*, 2013.

[54] X. Hua, X. Xie, B. Yin, P. Zhang, J. Ji, H. Wang, and Y. Fu, “Tribological performance and self-lubricating mechanism of the laser-textured surface filled with solid lubricant in rolling friction pair,” *Ind. Lubr. Tribol.*, vol. 70, no. 2, pp. 371–384, Mar. 2018.

[55] T. Hu, Y. Zhang, and L. Hu, “Tribological investigation of MoS_2 coatings deposited on the laser textured surface,” *Wear*, vol. 278–279, pp. 77–82, Mar. 2012.

[56] L. Rapoport, A. Moshkovich, V. Perfilyev, I. Lapsker, G. Halperin, Y. Itovich, and I. Etsion, “Friction and wear of MoS_2 films on laser textured steel surfaces,” *Surf. Coatings Technol.*, vol. 202, no. 14, pp. 3332–3340, Apr. 2008.

[57] J. H. Wu, B. S. Phillips, W. Jiang, J. H. Sanders, J. S. Zabinski, and a. P. Malshe, “Bio-inspired surface engineering and tribology of MoS_2 overcoated cBN-TiN composite coating,” *Wear*, vol. 261, no. 5–6, pp. 592–599, 2006.

[58] A. Kovalchenko, O. Ajayi, A. Erdemir, G. Fenske, and I. Etsion, “The effect of laser surface texturing on transitions in lubrication regimes during unidirectional sliding contact,” vol. 38, no. 3, pp. 219–225, 2005.

[59] A. M. Kovalchenko, A. Erdemir, O. O. Ajayi, and I. Etsion, “Tribological Behavior of Oil-Lubricated Laser Textured Steel Surfaces in Conformal Flat and Non-Conformal Contacts,” *Mater. Perform. Charact.*, vol. 6, no. 2, p. MPC20160013, 2017.

[60] D. Zenebe Segu and P. Hwang, “Friction control by multi-shape textured surface under pin-on-disc test,” *Tribol. Int.*, vol. 91, pp. 111–117, 2015.

[61] D. Z. Segu and P. Hwang, “Effectiveness of multi-shape laser surface texturing in the reduction of friction under lubrication regime,” *Ind. Lubr. Tribol.*, vol. 68, no. 1, pp. 116–124, 2016.

[62] D. Z. Segu, S. G. Choi, J. H. Choi, and S. S. Kim, “The effect of multi-scale laser textured surface on lubrication regime,” *Appl. Surf. Sci.*, vol. 270, pp. 58–63, Apr. 2013.

[63] B. Podgornik, L. M. Vilhena, M. Sedlaček, Z. Rek, and I. Žun, “Effectiveness and design of surface texturing for different lubrication regimes,” *Meccanica*, vol. 47, no. 7, pp. 1613–1622, 2012.

[64] A. Rosenkranz, A. Szurdak, C. Gachot, G. Hirt, and F. Mücklich, “Friction reduction under mixed and full film EHL induced by hot micro-coined surface patterns,” *Tribol. Int.*, vol. 95, pp. 290–297, Mar. 2016.

[65] A. Rosenkranz, S. A. Khan, A. Szurdak, G. Hirt, and C. Gachot, “Wear behavior of micro-coined steel surfaces under mixed lubrication,” *Ind. Lubr. Tribol.*, vol. 69, no. 6, pp. 1033–1039, Nov. 2017.

[66] J. Schneider, D. Braun, and C. Greiner, “Laser Textured Surfaces for Mixed Lubrication: Influence of Aspect Ratio, Textured Area and Dimple Arrangement,” *Lubricants*, vol. 5, no. 3, p. 32, 2017.

[67] F. Saeidi, B. Meylan, P. Hoffmann, and K. Wasmer, “Effect of surface texturing on cast iron reciprocating against steel under starved lubrication conditions: A parametric study,” *Wear*, vol. 348–349, pp. 17–26, 2016.

[68] N. Saurín, I. Minami, J. Sanes, and M. D. Bermúdez, “Study of the effect of tribo-materials and surface finish on the lubricant performance of new halogen-free room temperature ionic liquids,” *Appl. Surf. Sci.*, vol. 366, pp. 464–474, 2016.

[69] S. M. Hsu, Y. Jing, and F. Zhao, “Self-adaptive surface texture design for friction reduction across the lubrication regimes,” *Surf. Topogr. Metrol. Prop.*, vol. 4, no. 1, p. 14004, Nov. 2015.

[70] P. J. Blau, “Use of Textured Surfaces to Mitigate Sliding Friction and Wear of Lubricated and Non-Lubricated Contacts,” Oak Ridge National Laboratory, TN (United States), Mar. 2012.

[71] L. Bai, Y. Meng, Z. A. Khan, and V. Zhang, “The Synergetic Effects of Surface Texturing and MoDDP Additive Applied to Ball-on-Disk Friction Subject to Both Flooded and Starved Lubrication Conditions,” *Tribol. Lett.*, vol. 65, no. 4, pp. 1–18, 2017.

[72] P. L. Menezes, “Surface texturing to control friction and wear for energy efficiency and sustainability,” *Int. J. Adv. Manuf. Technol.*, vol. 85, no. 5–8, pp. 1385–1394, Jul. 2016.

[73] S. Yuan, W. Huang, and X. Wang, “Orientation effects of micro-grooves on sliding surfaces,” *Tribol. Int.*, vol. 44, no. 9, pp. 1047–1054, 2011.

[74] J. Keller, V. Fridrici, P. Kapsa, and J. F. Huard, “Surface topography and tribology of cast iron in boundary lubrication,” *Tribol. Int.*, vol. 42, no. 6, pp. 1011–1018, Jun. 2009.

[75] B. Olofinjana, C. Lorenzo-Martin, O. O. Ajayi, and E. O. Ajayi, “Effect of laser surface texturing (LST) on tribochemical films dynamics and friction and wear performance,” *Wear*, vol. 332–333, pp. 1225–1230, May 2015.

[76] N. G. Demas, E. V. Timofeeva, J. L. Routbort, and G. R. Fenske, “Tribological Effects of BN and MoS_2 Nanoparticles Added to Polyalphaolefin Oil in Piston Skirt/Cylinder Liner Tests,” *Tribol. Lett.*, vol. 47, no. 1, pp. 91–102, Jul. 2012.

[77] J.-F. Peng, M.-X. Shen, and Z.-B. Cai, “Nano Diesel Soot Particles Reduce Wear and Friction Performance Using an Oil Additive on a Laser Textured Surface,” *Coatings*, vol. 8, no. 3, p. 89, 2018.

[78] L. Peña-Parás, H. Gao, D. Maldonado-Cortés, A. Vellore, P. García-Pineda, O. E. Montemayor, K. L. Nava, and A. Martini, “Effects of substrate surface roughness and nano/micro particle additive size on friction and wear in lubricated sliding,” *Tribol. Int.*, vol. 119, no. February 2017, pp. 88–98, 2018.

[79] V. Narayanunni, B. A. Kheireddin, and M. Akbulut, “Influence of surface topography on frictional properties of Cu surfaces under different lubrication conditions: Comparison of dry, base oil, and ZnS nanowire-based lubrication system,” *Tribol. Int.*, vol. 44, no. 12, pp. 1720–1725, Nov. 2011.

[80] R. R. Sahoo and S. K. Biswas, “Microtribology and friction-induced material transfer in layered MoS_2 nanoparticles sprayed on a steel surface,” *Tribol. Lett.*, vol. 37, no. 2, pp. 313–326, 2010.

[81] G. Morales-Espejel, V. Brizmer, and E. Piras, “Roughness evolution in mixed lubrication condition due to mild wear,” *Proc. Inst. Mech. Eng. Part J J. Eng. Tribol.*, vol. 229, no. 11, pp. 1330–1346, Nov. 2015.

[82] A. D. Jenson, S. Roy, and S. Sundararajan, “The evolution of hardness and tribofilm growth during running-in of case carburized steel under boundary lubrication,” *Tribol. Int.*, vol. 118, no. May 2017, pp. 1–10, 2018.

[83] J. J. Wagner, A. D. Jenson, and S. Sundararajan, “The effect of contact pressure and surface texture on running-in behavior of case carburized steel under boundary lubrication,” *Wear*, vol. 376–377, pp. 851–857, 2017.

[84] C. Q. Yuan, Z. Peng, X. P. Yan, and X. C. Zhou, “Surface roughness evolutions in sliding wear process,” *Wear*, vol. 265, no. 3–4, pp. 341–348, Jul. 2008.

[85] K. J. Kubiak, M. Bigerelle, T. G. Mathia, A. Dubois, and L. Dubar, “Dynamic evolution of interface roughness during friction and wear processes,” *Scanning*, vol. 36, no. 1, pp. 30–38, Jan. 2014.

[86] “Geometrical product specifications (GPS) -- Surface texture: Areal -- Part 3: Specification operators,” in *ISO 25178*, International Organization for Standardization, 2012.

[87] “Geometrical product specifications (GPS) -- Surface texture: Profile method -- Rules and procedures for the assessment of surface texture,” in *ISO 4288*, International Organization for Standardization, 1996.

[88] “Keyence VK-X 250 laser microscope.” [Online]. Available: https://www.keyence.com/landing/microscope/lp_vk250_micro.jsp. [Accessed: 01-May-2018].

[89] “Pin-on-disc tribometer.” [Online]. Available: https://www.anton-paar.com/us-en/products/details/pin-on-disk-tribometer-trb/. [Accessed: 01-May-2018].

[90] “Bruker - EDS.” [Online]. Available: https://www.bruker.com/products/x-ray-diffraction-and-elemental-analysis/eds-wds-ebsd-sem-micro-xrf-and-sem-micro-ct.html. [Accessed: 01-May-2018].

[91] “FEI Nova Nanolab.” [Online]. Available: https://microscopy.uark.edu/nova-nanolab/. [Accessed: 01-May-2018].

[92] “Omniprobe 100.” [Online]. Available: https://www.oxford-instruments.com/products/nanomanipulation/nanomanipulator/omniprobe-100/omniprobe-100-brochure. [Accessed: 01-May-2018].

[93] “Esprit Sorftware.” [Online]. Available: https://www.bruker.com/products/x-ray-diffraction-and-elemental-analysis/eds-wds-ebsd-sem-micro-xrf-and-sem-micro-ct/esprit-2.html. [Accessed: 01-May-2018].

[94] “Titan 80-3000.” [Online]. Available: https://microscopy.uark.edu/titan-80-3000/. [Accessed: 22-Mar-2018].

[95] “Renishaw inVia Raman microscope.” [Online]. Available: http://www.renishaw.com/en/invia-confocal-raman-microscope--6260. [Accessed: 01-May-2018].

[96] *VK-X250 User Manual*. Keyence Corporation, 2013.

[97] “Line roughness parameters.” [Online]. Available: https://www.keyence.eu/ss/products/microscope/roughness/line/parameters.jsp. [Accessed: 22-Mar-2018].

[98] “Mean Height Of Profile Elements (Rc, Pc, Wc) Surface Roughness Parameters Introduction To Roughness,” *Keyence Corporation America*. [Online]. Available: https://www.keyence.com/ss/products/microscope/roughness/line/mean-height-of-profile-elements.jsp. [Accessed: 30-Mar-2018].

[99] “Mean Width Of The Profile Elements (Rsm, Psm, Wsm) Surface Roughness Parameters Introduction To Roughness,” *Keyence Corporation America*. [Online]. Available: https://www.keyence.com/ss/products/microscope/roughness/line/RSm-PSm-WSm.jsp. [Accessed: 30-Mar-2018].

[100] “Area roughness parameters.” [Online]. Available: https://www.keyence.eu/ss/products/microscope/roughness/surface/parameters.jsp. [Accessed: 22-Mar-2018].

[101] “Sq (Root Mean Square Height) Area Roughness Parameters,” *Keyence Corporation America*. [Online]. Available: https://www.keyence.com/ss/products/microscope/roughness/surface/sq-root-mean-square-height.jsp. [Accessed: 30-Mar-2018].

[102] “Spd - Density of peaks,” *Keyence Corporation America*. [Online]. Available: https://www.keyence.com/ss/products/microscope/roughness/surface/spd-density-of-peaks.jsp. [Accessed: 31-Mar-2018].

[103] “Spc- Arithmatic mean peak curvature,” *Keyence Corporation America*. [Online]. Available: https://www.keyence.com/ss/products/microscope/roughness/surface/spc-arithmetic-mean-peak-curvature.jsp. [Accessed: 31-Mar-2018].

[104] Don Cohen, “Surface Texture Parameters Glossary,” 2014. [Online]. Available: https://www.michmet.com/Texture_parameters.htm. [Accessed: 23-Mar-2018].

[105] *VK-X250K MultiFileAnalyzer Reference Manual*. Keyence Corporation, 2014.

[106] F. Blateyron, “The Areal Field Parameters,” in *Characterisation of Areal Surface Texture*, R. Leach, Ed. Springer Berlin Heidelberg, 2013, pp. 15–43.

[107] “Spk (Reduced Peak Height) Area Roughness Parameters Introduction To Roughness,” *Keyence Corporation America*. [Online]. Available: https://www.keyence.com/ss/products/microscope/roughness/surface/spk-reduced-peak-height.jsp. [Accessed: 30-Mar-2018].

[108] “Svk (Reduced Dale Height, Reduced Valley Depth) Area Roughness Parameters Introduction To Roughness,” *Keyence Corporation America*. [Online]. Available: https://www.keyence.com/ss/products/microscope/roughness/surface/svk-reduced-dale-height.jsp. [Accessed: 01-May-2018].

[109] “Vvv (Dale Void Volume) Area Roughness Parameters Introduction To Roughness,” *Keyence Corporation America*. [Online]. Available: https://www.keyence.com/ss/products/microscope/roughness/surface/vvv-dale-void-volume.jsp. [Accessed: 30-Mar-2018].

[110] “Vmp (Peak Material Volume) Area Roughness Parameters Introduction To Roughness,” *Keyence Corporation America*. [Online]. Available: https://www.keyence.com/ss/products/microscope/roughness/surface/vmp-peak-material-volume.jsp. [Accessed: 30-Mar-2018].

[111] “52100 alloy steel.” [Online]. Available: http://amsresources.com/52100-alloy-steel/. [Accessed: 04-Apr-2018].

[112] A. F. Shamsul Baharin, M. J. Ghazali, and J. A Wahab, “Laser surface texturing and its contribution to friction and wear reduction: a brief review,” *Ind. Lubr. Tribol.*, vol. 68, no. 1, pp. 57–66, 2016.

[113] T. Ibatan, M. S. Uddin, and M. A. K. Chowdhury, “Recent development on surface texturing in enhancing tribological performance of bearing sliders,” *Surf. Coatings Technol.*, vol. 272, pp. 102–120, 2015.

[114] I. Etsion, “State of the Art in Laser Surface Texturing,” *J. Tribol.*, vol. 127, no. 1, p. 248, 2005.

[115] R. Bathe, V. Sai Krishna, S. K. Nikumb, and G. Padmanabham, “Laser surface texturing of gray cast iron for improving tribological behavior,” *Appl. Phys. A*, vol. 117, no. 1, pp. 117–123, 2014.

[116] L. Yang, Y. Ding, B. Cheng, J. He, G. Wang, and Y. Wang, “Investigations on femtosecond laser modified micro-textured surface with anti-friction property on bearing steel GCr15,” *Appl. Surf. Sci.*, vol. 434, pp. 831–842, 2018.

[117] “Buehler Ecomet 300.” [Online]. Available: https://www.buehler.com/ecoMet-300-grinder-polisher.php. [Accessed: 01-May-2018].

[118] “Silicon carbide paper - Buehler CarbiMet.” [Online]. Available: https://shop.buehler.com/silicon-carbide-paper. [Accessed: 01-May-2018].

[119] P. J. Blau, “On the nature of running-in,” *Tribol. Int.*, vol. 38, no. 11–12, pp. 1007–1012, Nov. 2005.

[120] G. C. Barber and K. C. Ludema, “The break-in stage of cylinder-ring wear: A correlation between fired engines and a laboratory simulator,” *Wear*, vol. 118, no. 1, pp. 57–75, Jul. 1987.

[121] “Profile Parameters.” [Online]. Available: http://www.digitalsurf.fr/en/guide-profile-parameters.html. [Accessed: 05-Apr-2018].

[122] M. Yi and C. Zhang, “The synthesis of MoS_2 particles with different morphologies for tribological applications,” *Tribol. Int.*, vol. 116, no. July, pp. 285–294, Dec. 2017.

[123] M. Miyajima, K. Kitamura, and K. Matsumoto, “Characterization of Tribofilm with the Remaining Lubricating Oil by Raman Spectroscopy,” *Tribol. Online*, vol. 10, no. 3, pp. 225–231, 2015.

[124] D. N. Khaemba, A. Neville, and A. Morina, “New insights on the decomposition mechanism of Molybdenum DialkyldiThioCarbamate (MoDTC): a Raman spectroscopic study,” *RSC Adv.*, vol. 6, no. 45, pp. 38637–38646, 2016.

[125] V. N. Bakunin, A. Y. Suslov, G. N. Kuzmina, O. P. Parenago, and A. V. Topchiev, “Synthesis and Application of Inorganic Nanoparticles as Lubricant Components – a Review,” *J. Nanoparticle Res.*, vol. 6, no. 2/3, pp. 273–284, Jun. 2004.

[126] Z. Chen, Y. Liu, S. Gunsel, and J. Luo, “Mechanism of Antiwear Property Under High Pressure of Synthetic Oil-Soluble Ultrathin MoS_2 Sheets as Lubricant Additives,” *Langmuir*, vol. 34, no. 4, pp. 1635–1644, Jan. 2018.

[127] J. Tannous, F. Dassenoy, I. Lahouij, T. Le Mogne, B. Vacher, A. Bruhács, and W. Tremel, “Understanding the Tribochemical Mechanisms of IF-MoS_2 Nanoparticles Under Boundary Lubrication,” *Tribol. Lett.*, vol. 41, no. 1, pp. 55–64, Jan. 2011.

[128] M. Kalin, J. Kogovšek, and M. Remškar, “Mechanisms and improvements in the friction and wear behavior using MoS_2 nanotubes as potential oil additives,” *Wear*, vol. 280–281, pp. 36–45, Mar. 2012.

[129] J. Kogovšek, M. Remškar, A. Mrzel, and M. Kalin, “Influence of surface roughness and running-in on the lubrication of steel surfaces with oil containing MoS_2 nanotubes in all lubrication regimes,” *Tribol. Int.*, vol. 61, pp. 40–47, May 2013.

Appendix A: Reciprocating Vs Rotational Tribotesting Setup

Both reciprocating and rotational tribological tests were conducted during the initial planning experiments. A brief comparison of two modes of testing is presented below in Figure A.1.

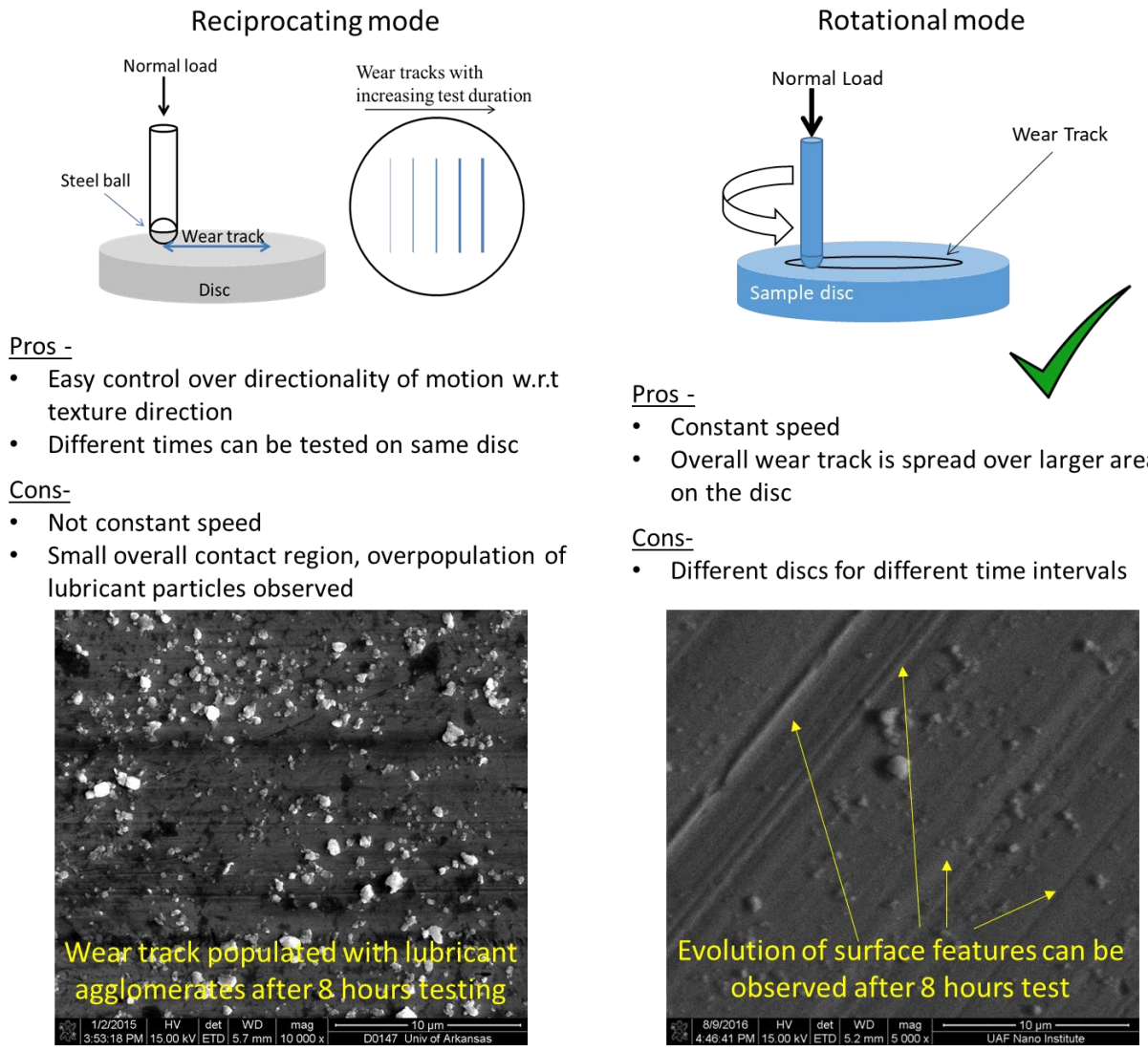

Figure A.1 Comparison of rotating Vs reciprocating tribotest.

Reciprocating tests offer the advantage of controlling the direction of motion with respect to texture direction (e.g. parallel to lay or perpendicular to lay direction). Additionally, different time intervals can be tested on the same disc reducing the total number of discs to be used for

particular set of experiments and reducing the equipment setup time for experiments and characterization. However, the speed of linear movement in a reciprocating setup is not constant as pin goes to acceleration and deceleration during each back and forth longitudinal cycle. This adds to the complexity of experimental characterization and subsequent analysis as each point along the wear track experiences different relative speed of motion. Also, the overall length of wear track is smaller in a reciprocating setup as compared to rotational setup making the lubricant stay in contact region rather than getting distributed along a longer circular track over the test disc. As a result, the contact region was found to be overpopulated with lubricant in reciprocating setup as compared to rotational setup as shown in Figure A.1. For these reasons, for the purpose of studying the evolution of surface features under constant speed, rotational testing setup was chosen for experiments.

Appendix B: Materials Ratio Curve

ISO also defines volume parameters those are extracted from area materials ratio curve or also known as area bearing curve. [1] A material ratio (mr) is defined as a percentage of material area on an intersecting plane at a given height Z. A material ratio curve is created by calculating material ratios at different heights starting from the tallest peak (where mr is 0) to the lowest valley (where mr is 1). Calculation of mr and a typical material ratio curve plot is shown in Figure B.1 as an illustration for an arbitrary surface profile.

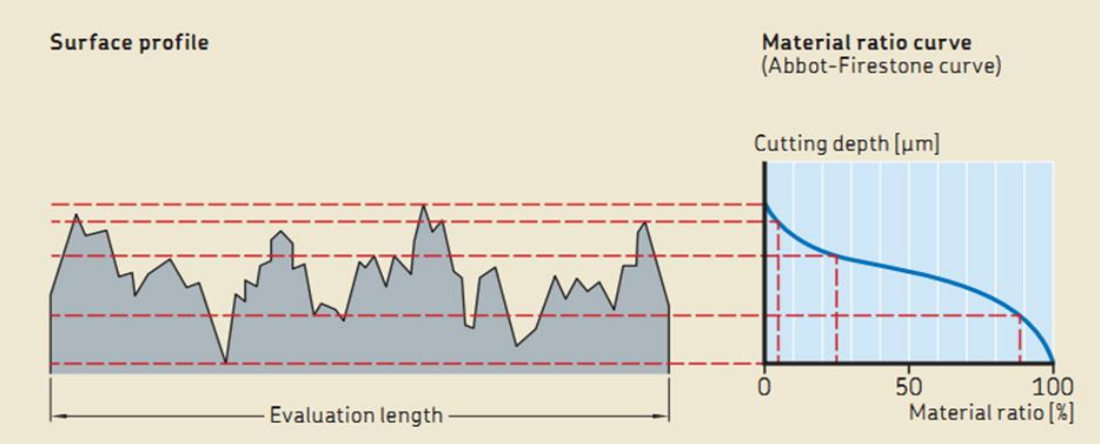

Figure B.1 Illustration of materials ratio curve for an arbitrary surface profile (Image from [2]).

Volume parameters described in Table 3.3 are calculated on from the material ratio curve generated on each individual surface measurement area and thus may not provide an accurate comparison between two different samples at two different time intervals that are expected to have different arrangement of features due to the texture evolution.

References:

[1] "Geometrical product specifications (GPS) -- Surface texture: Areal -- Part 2: Terms, definitions and surface texture parameters," in *ISO 25178*, International Organization for Standardization, 2012.

[2] "EcoSeal: Hydraulic seals - General technical information." [Online]. Available: http://www.ecosealthailand.com/Ecoseal2016/index.php/10-products/hydraulic-seal/11-hydraulic-seal. [Accessed: 28-Mar-2018].

Appendix C: Results of Tribological Control Test with Laser Textured Disc

Figure C.1 shows the optical images of the wear track and wear scar diameter after the control test on a laser textured disc (COF plot shown Figure 4.8). The high values of COF suggest that the nano-engineered lubricant did not work effectively. The wear scar images confirm that the lubricant failed to provide efficient lubrication. Traces of ball were seen on the wear track suggesting high degree of adhesive wear and stiction. Additionally, the periodicity of features on the disc is replicated on the ball as seen in the picture. Both these observations indicate that there was direct contact between the textured disc surface and the ball without any lubrication.

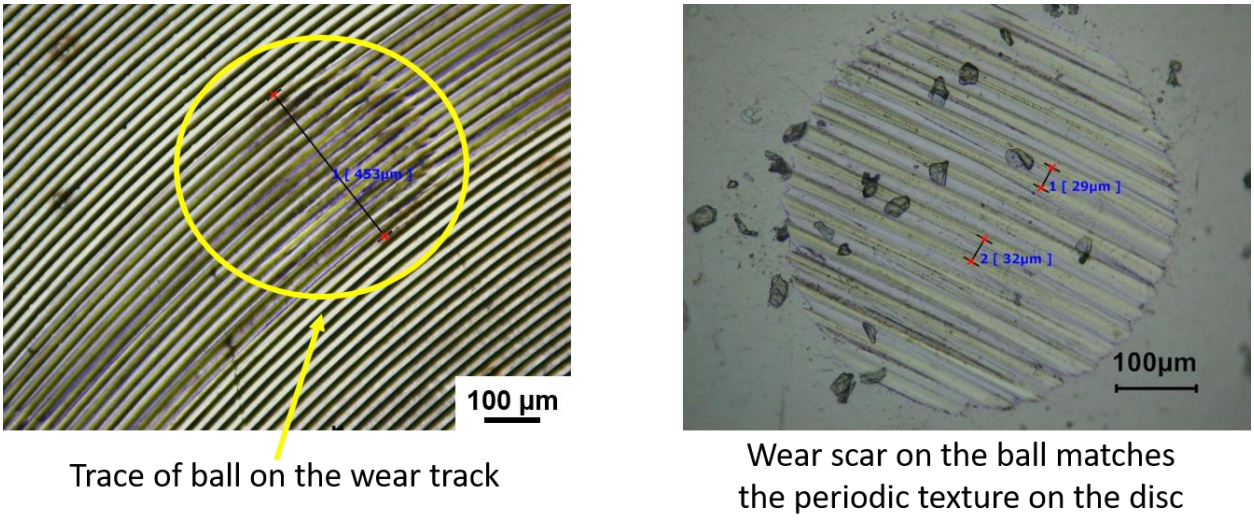

Figure C.1 Images of wear track and wear scar diameter for a laser-textured disc after 10000 laps control experiment.

From the images, it was concluded that without proper lubrication, the disc and ball cut into each other like a machining operation. The improper lubrication can be attributed to lack of nanoparticles into contact area and also due to effective high loads getting applied on to small number of peaks. It was concluded that the texture design had valleys too deep (10 µm depth) and too wide (20 µm width). Ill-effects of deep reservoirs have been previously described using a

model for DLC coated surface and these results are consistent with the observations. [1]

A possible design that can be used for future optimization with texture will be to use shallow (1-2 μm depth) grooves with narrow widths (5-10 μm) as a part of recommended future work described in Chapter 7.

References:

[1] J. Kogovšek, M. Remškar, and M. Kalin, “Lubrication of DLC-coated surfaces with MoS2nanotubes in all lubrication regimes: Surface roughness and running-in effects,” *Wear*, vol. 303, no. 1–2, pp. 361–370, 2013.

Appendix D: Description of Research for Popular Publication

Self-adjusting nanoparticle lubricant layers for friction reduction

By Salil Bapat

Over the last few decades, the trend in industry and manufacturing is to move toward more environmentally conscious and sustainable methods. 'Using less to deliver more' has been a commonly adopted design principle to conserve material and energy resources. On the parallel side, researchers are looking to develop smart solutions by learning from nature. These bio-inspired strategies have one thing in common — the use of surface textures or surface patterns. From superhydrophobic lotus leaves, to anti-reflective moth-eyes, to drag reducing shark skin, this bio-inspired approach has resulted in many commercial applications involving energy harvesting, displays, solar cells, robots, security, and many more. However, unlike their natural counterparts, many of these strategies fail to account for change in texture due to wear and tear during product application. Mr. Salil Bapat, PhD student of the Microelectronics-Photonics program at the University of Arkansas has studied this under Dr. Ajay P. Malshe, Professor in Mechanical Engineering at the University of Arkansas.

Dr. Malshe states that texture or topography is very fundamental to the many natural and artificial systems. From protrusions of the size of human hair on a waxy lotus leaf, or dimples on the golf balls, and even the pattern found on rocks in the Grand Canyon, texture patterns are around us at every possible length scale. Oddly though, when it comes to engineering texture designs, the change in the topography over time is largely ignored.

Mr. Bapat noted that the textured surfaces have been used to control friction and lubrication for quite some time and yet the changes in texture over time were never systematically studied. Dr. Malshe says, "When you buy a truck you keep it running in idle for

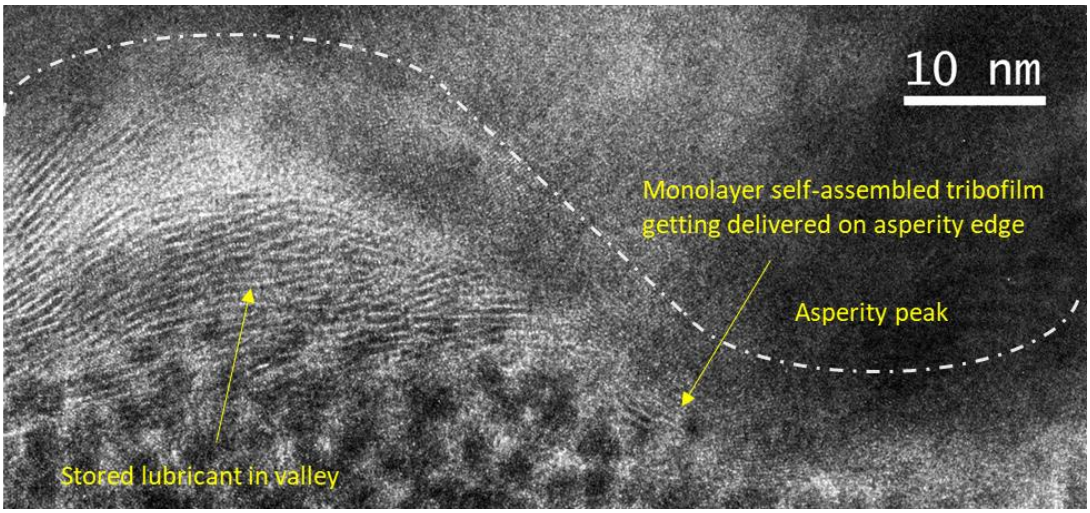

few hundred miles to break-in the new engine. What happens during the break-in is that the two interacting surfaces rub-off against each other to form a suitable texture pattern where the stable oil film can now form and provide good lubrication. We know that texture changes; it is so obvious that it is almost taken for granted. Nobody has studied the fundamental aspect of texture evolution at microscopic length scale"

For this research, the researchers used a unique nanoparticle-based lubricant. These nanoparticles have a layered slippery structure (like slipping on banana peel), which reduces the friction. Additionally, under the application of load, these layers get exfoliated and react with the surface to form a protective film. The effect of surface texture on the behavior of lubricant nanoparticles was studied along with the changes in texture.

The findings of this research show that the texture and lubricant film evolve synergistically to deliver superior low frictional properties. The surface asperity peaks act as anchoring and reaction points for the lubricant layer while the valleys are essential for storage of lubricant particles. The self-assembly of lubricant layers along the contours of surface was discovered for the first time at nano-scale as seen in the above image.

Appendix E: Executive Summary of Newly Created Intellectual Property

There was no newly created intellectual property in the course of this research project. This research was fundamental and scientific understanding/discovery of role of surface texture under boundary lubrication.

Appendix F: Potential Patent and Commercialization Aspects of Listed Intellectual Property Items

There was no newly created intellectual property in the course of this research project. This research was fundamental and scientific understanding/discovery of role of surface texture under boundary lubrication.

Appendix G: Broader Impact of Research

G.1 Applicability of Research Methods to Other Problems

This research was focused on fundamental understanding of the events at the micron and submicron scales in a tribological system and the role of surface texture in managing and manipulating the friction. Surface texture is a very fundamental design parameter and is widely used in several natural and engineered surfaces delivering different functionalities. The methodology of studying the evolution of surface texture for delivering a desired functionality can certainly be used to investigate other problems/design strategies. For example, 1) textured biological implants that promote osteointegration, 2) textured surfaces for controlled wettability (superhydrophobic, superhydrophilic etc.), 3) textured adhesive pads used for robotic locomotion and space grippers and many more. However, the time intervals and nature of interaction would have to be optimized for each individual problem owing to the dynamic and statistical nature of events.

G.2 Impact of Research Results on U.S. and Global Society

The economic development in the United States over the past few years and in the immediate future will be controlled by the manufacturing sector. Surface texture is one of the very fundamental design tools that Nature has used to realize some of the most highly engineered multi-functional surfaces with elegant aesthetics. Researchers have mimicked such textures in recent times to for coating, lubrication, and energy harvesting solutions. In conjunction with the societal demand for developing effective strategies for lubrication in numerous commonly used machines, this research serves as a bridging link between the fundamental science, biomimetic technology, and global obligation. Fields such as biomedical, aerospace, automotive, wind and hydro-turbines and others will be benefitted using findings of this research.

G.3 Impact of Research Results on the Environment

Environmental concerns and efficient use of the natural resources is a global driver for research in the field of tribology. Material and energy losses because of improper lubrication cause significant waste of resources, time, and money. By incorporating textured surfaces for delivering advanced lubrication functions, these losses could be minimized. By reducing the friction and thus, the fuel consumption, the energy savings would have positive impact on the depleting non-renewable energy resources.

Appendix H: Microsoft Project for PhD MicroEP Degree Plan

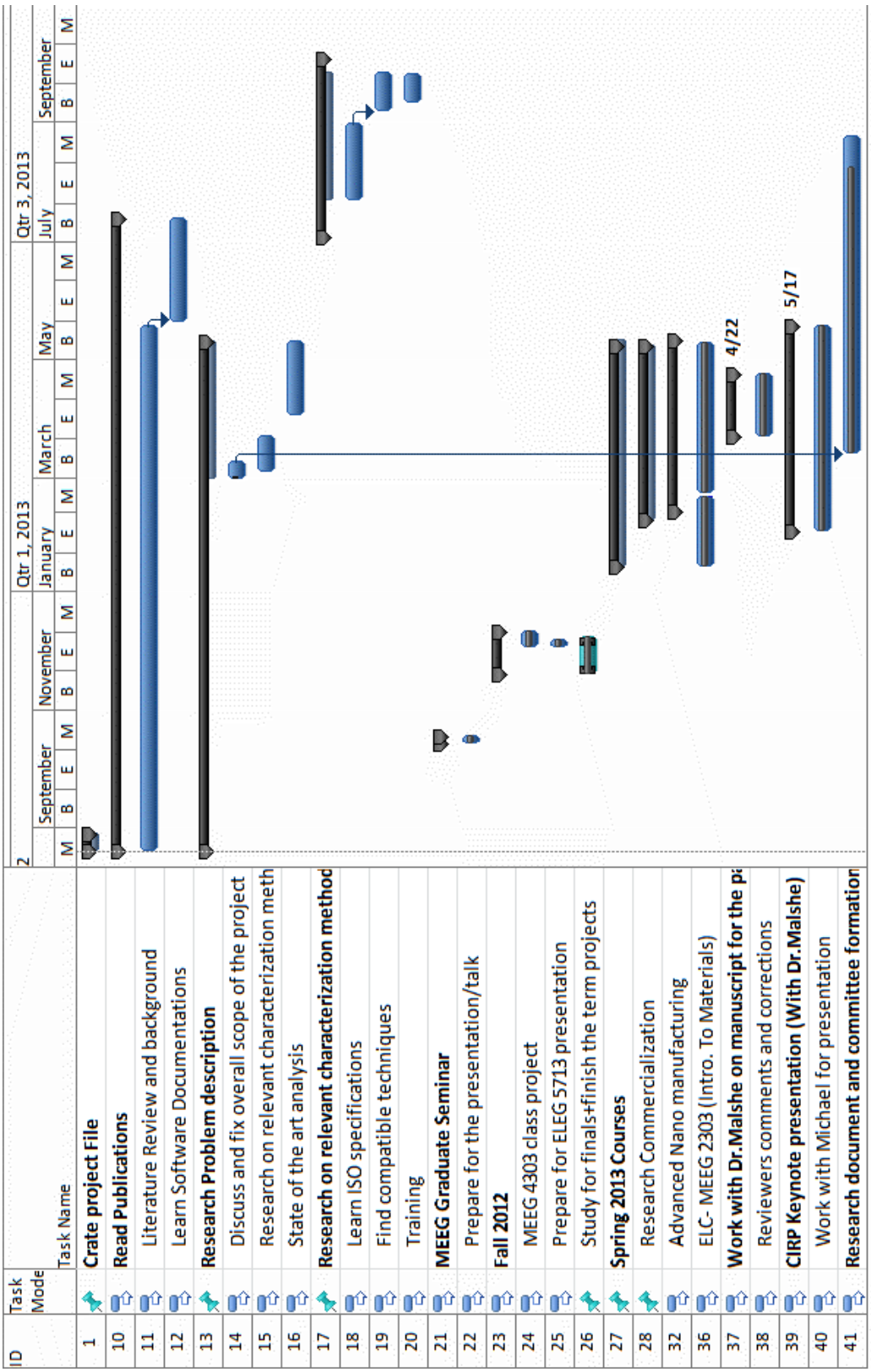

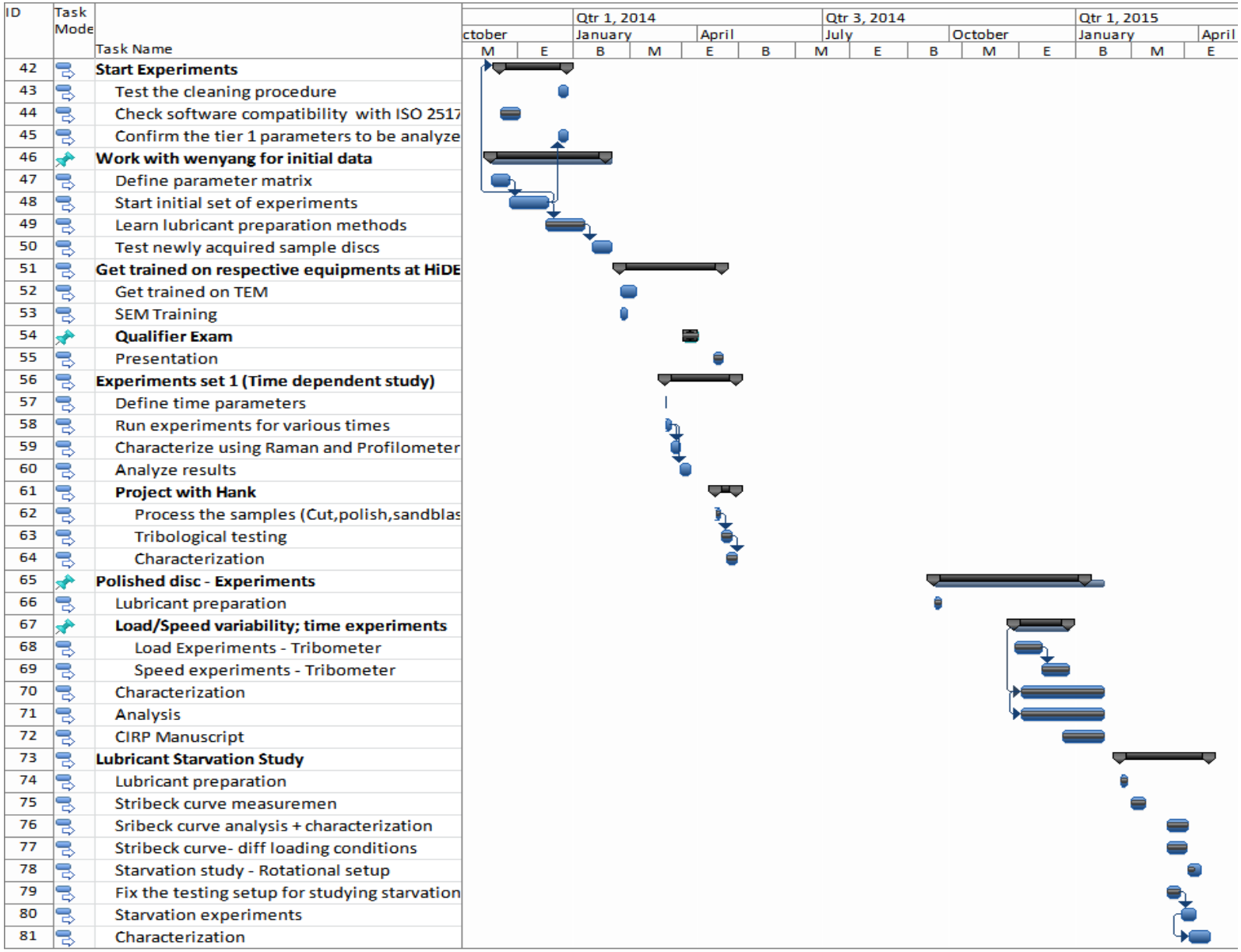
ID
Task Mode
Task Name
Qtr 1, 2014
Qtr 3, 2014
Qtr 1, 2015
ctober
January
April
July
October
January
April
M E B M E B M E B M E B M E B M E
42 Start Experiments
43 Test the cleaning procedure
44 Check software compatibility with ISO 2517
45 Confirm the tier 1 parameters to be analyze
46 Work with wenyang for initial data
47 Define parameter matrix
48 Start initial set of experiments
49 Learn lubricant preparation methods
50 Test newly acquired sample discs
51 Get trained on respective equipments at HiDE
52 Get trained on TEM
53 SEM Training
54 Qualifier Exam
55 Presentation
56 Experiments set 1 (Time dependent study)
57 Define time parameters
58 Run experiments for various times
59 Characterize using Raman and Profilometer
60 Analyze results
61 Project with Hank
62 Process the samples (Cut,polish,sandblas
63 Tribological testing
64 Characterization
65 Polished disc - Experiments
66 Lubricant preparation
67 Load/Speed variability; time experiments
68 Load Experiments - Tribometer
69 Speed experiments - Tribometer
70 Characterization
71 Analysis
72 CIRP Manuscript
73 Lubricant Starvation Study
74 Lubricant preparation
75 Stribeck curve measuremen
76 Sribeck curve analysis + characterization
77 Stribeck curve- diff loading conditions
78 Starvation study - Rotational setup
79 Fix the testing setup for studying starvation
80 Starvation experiments
81 Characterization

ID	Task Mode	Task Name
82		**Gear oil experiments (Summer-REU)**
83		Study starvation
84		Tribotesting
85		SEM characterization
86		Raman
87		Wrap up
88		**Prepare sample discs**
89		**Class Instructor - MEEG 2303 - Fall 2015**
90		**Pace Industries project**
91		Work on tappet cavity cladding
92		Proceed to next simpler cavity
93		Analyze clad portion and repair any poros
94		Repeat the process based
95		**Time evolution experiments**
96		Experimets to define parameters
97		Get trained on VK-150 laser profilometer
98		Assess compatibiity of the sorftware
99		Load speed variation experiments
100		Analyze results
101		Define parameters and run experiments
102		Repeat experiments
103		Compile analyzed data
104		Prepare polished samples

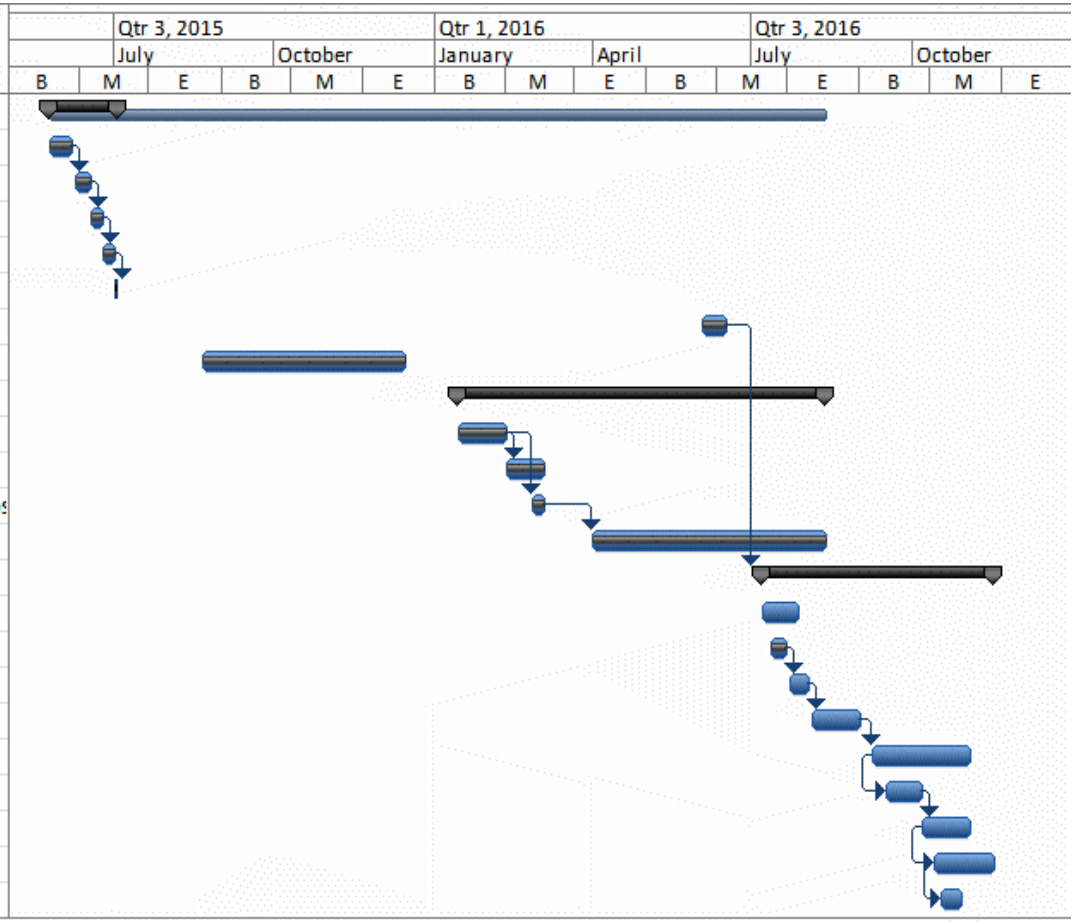

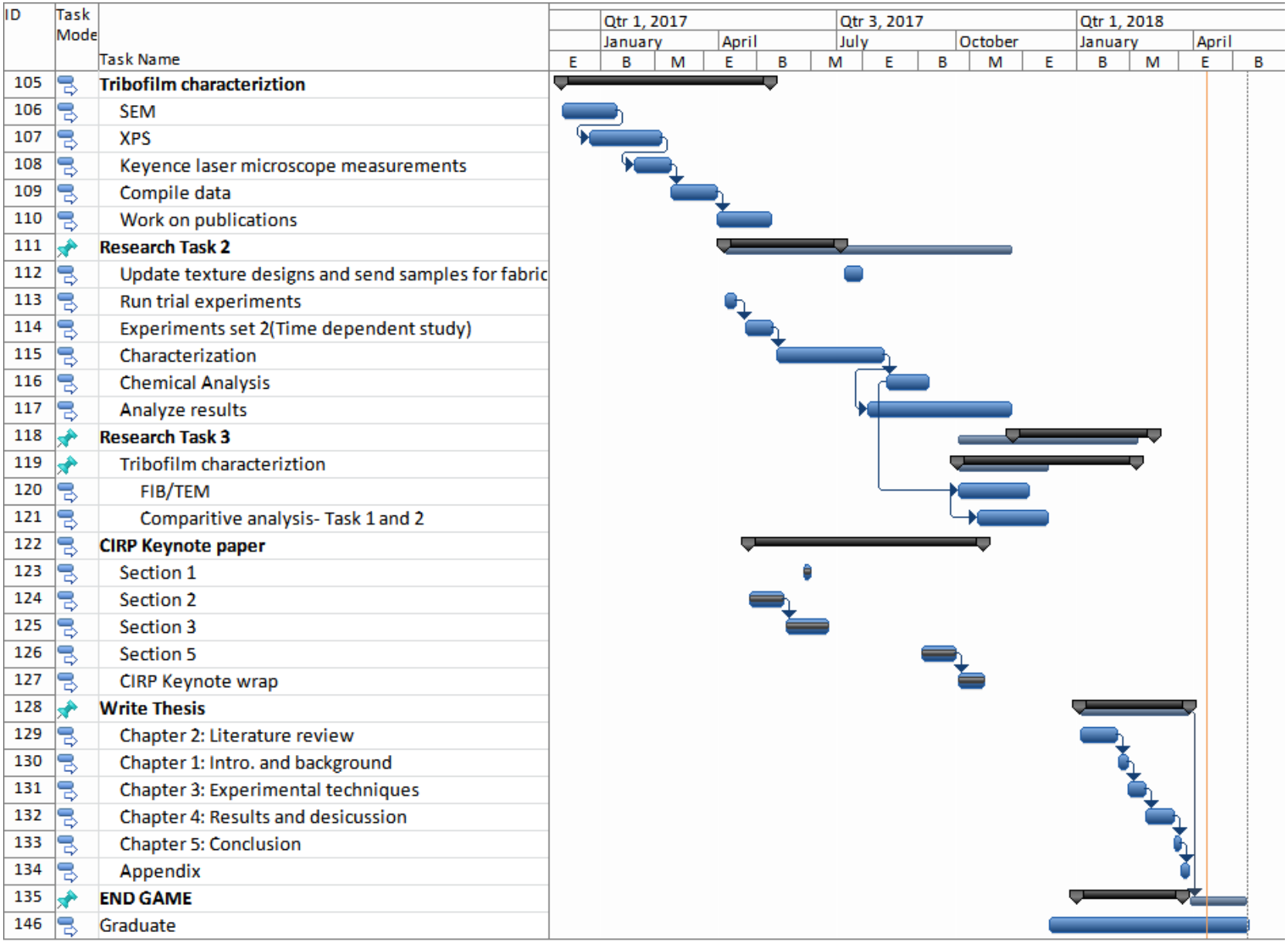
ID
Task Mode
Task Name
105 Tribofilm characteriztion
106 SEM
107 XPS
108 Keyence laser microscope measurements
109 Compile data
110 Work on publications
111 Research Task 2
112 Update texture designs and send samples for fabric
113 Run trial experiments
114 Experiments set 2(Time dependent study)
115 Characterization
116 Chemical Analysis
117 Analyze results
118 Research Task 3
119 Tribofilm characteriztion
120 FIB/TEM
121 Comparitive analysis- Task 1 and 2
122 CIRP Keynote paper
123 Section 1
124 Section 2
125 Section 3
126 Section 5
127 CIRP Keynote wrap
128 Write Thesis
129 Chapter 2: Literature review
130 Chapter 1: Intro. and background
131 Chapter 3: Experimental techniques
132 Chapter 4: Results and desicussion
133 Chapter 5: Conclusion
134 Appendix
135 END GAME
146 Graduate
Qtr 1, 2017
Qtr 3, 2017
Qtr 1, 2018
January
April
July
October
January
April
E B M E B M E B M E B M E B

Appendix I: Identification of All Software Used in Research and Dissertation Generation

Computer# 1: Personal Laptop
Model: Acer Aspire V5-571
Serial number: NXM1JAA002230003ED2000
Owner: Salil Bapat

Software 1:
Name: Microsoft Office Standard 2010
Purchased by: Salil Bapat
License (product) id: 02336-561-9746405-38101

Software 2:
Name: Microsoft Project 2010
Purchased by: Salil Bapat
Free Microsoft software under College of Engineering license, University of Arkansas
License owned by the University of Arkansas

Software 3:
Name: Keyence Multifile Analyzer Version 1.2.6.106
Downloaded by: Salil Bapat
License Number: JA23ETEPG
Copyright 2014 Keyence Corporation
Software provided as a part of Keyence VK- X 250 laser microscope equipment licensed to University of Arkansas

Software 4:
Name: Origin Student Version (2015)
Purchased by: Salil Bapat
License (product) id: GA3S4-6089-7211141

Computer# 2: Personal Laptop
Model: Lenovo ideapad
Serial number: PF0PZ45P
Owner: Salil Bapat

Software 1:
Name: Origin Student Versions (2016, 2017)
Purchased by: Salil Bapat
License (product) ids: GA3S4-6089-7212485 and GA3S4-6089-7611441

Software 2:
Name: Microsoft Office 365 ProPlus
Downloaded by: Salil Bapat
Free Microsoft software under University of Arkansas ProPlus license campus agreement
License owned by the University of Arkansas

Software 3:
Name: Keyence Multifile Analyzer Version 1.2.6.106
Downloaded by: Salil Bapat
License Number: JA23ETEPG
Copyright 2014 Keyence Corporation
Software provided as a part of Keyence VK- X 250 laser microscope equipment licensed to University of Arkansas

Computer# 3:
Model: Dell desktop, Windows XP Professional
Serial number: 249YQ61
Location: Nano 222
Owner: Mechanical Engineering, University of Arkansas

Computer # 4: (For CSM Tribometer)
Model: Dell desktop, Windows XP professional
Serial number: 43B043J
Location: Nano 222
Owner: Mechanical Engineering, University of Arkansas

Software 1:
TriboX (CSM Tribometer)
License owned by: Mechanical Engineering, University of Arkansas

Computer # 5: (For Renishaw InVia Raman Spectrometer)
Model: HP Pavilion, Windows 7
Serial number: 4CE14106ZT
Location: Nano 223
Owner: Mechanical Engineering, University of Arkansas

Software 1:
WiRe3.3 (Renishaw InVia Raman Spectrometer)
License owned by: Mechanical Engineering, University of Arkansas

Appendix J: All Publications Published, Submitted and Planned

1) S. Bapat, W. Zhang, and A. P. Malshe, "Understanding Evolution of Surface Texture under Boundary Lubrication." In preparation.

2) S. Bapat and A. P. Malshe, "Understanding the Mechanism of Tribofilm Formation and Evolution on Directionally Textured Surfaces." In preparation.

3) S. Bapat, W. Zhang, M. Benamara and A. P. Malshe "Characterization of self-assembly and delivery of lamellar tribo-layer and it's interaction with individual surface asperity." In preparation.

4) A. Malshe, S. Bapat, K. Rajurkar and H. Haitjema, "Bio-inspired Textures for Functional Applications,", Submitted for publication in *CIRP Annals-Manufacturing Technology*, 2018, Vol.2.

5) W. Zhang, S. Bapat, A. P. Malshe, and K. P. Rajurkar, "Understanding evolution of tribo-chemical interfaces during boundary lubrication in manufacturing," *CIRP Ann.*, vol. 66, no. 1, pp. 555–558, 2017.

6) A. Malshe, K. Rajurkar, A. Samant, H. N. Hansen, S. Bapat, and W. Jiang, "Bio-inspired functional surfaces for advanced applications," *CIRP Ann.*, vol. 62, no. 2, pp. 607–628, 2013.